REPORT DOCUMENTATION PAGE

AFRL-SR-AR-TR-04-

0021

1. REPORT DATE *(DD-MM-YYYY)*	2. REPORT TYPE	3. DATES COVERED *(From - To)*
	Final Report	Aug 1, 03 - Dec 31, 03

4. TITLE AND SUBTITLE
Feynman Integrals and FOPEN Coding

5a. CONTRACT NUMBER

5b. GRANT NUMBER
F49620-03-1-0414

5c. PROGRAM ELEMENT NUMBER

6. AUTHOR(S)
Dr. Timothy E. Olson

5d. PROJECT NUMBER

5e. TASK NUMBER

5f. WORK UNIT NUMBER

7. PERFORMING ORGANIZATION NAME(S) AND ADDRESS(ES)
Valhalla Technologies, LLC
925 N. San Souci
Deland, FL 32720

8. PERFORMING ORGANIZATION REPORT NUMBER

9. SPONSORING/MONITORING AGENCY NAME(S) AND ADDRESS(ES)
Department of the Air Force
Air Force Office of Scientific Research
4015 Wilson Blvd.
Arlington, VA 22203-1954

10. SPONSOR/MONITOR'S ACRONYM(S)

11. SPONSOR/MONITOR'S REPORT NUMBER(S)

12. DISTRIBUTION/AVAILABILITY STATEMENT

Approved for public release, distribution unlimited.

13. SUPPLEMENTARY NOTES
DODAAD CODE: 3GT63
AFOSR Program Manager: Dr. Arje Nachman

14. ABSTRACT

The goals of this proposal were to address the problems of: a) Developing advanced methods for electromagnetic computation, and b) to develop signal processing methods for finding targets below foliage. We have addressed these problems and have a number of accomplishments to show for our efforts.

1. We have produced the attached paper, "Electromagnetic pulse propagation in passive media", by Sergei Shabanov. This has received a favorable initial review by Applied and Computational Harmonic Analysis, and is under final review.
2. We have produced the attached technical report. "Precursor based HRR for foliage penetration" by Tim Olson. This report demonstrates that precursors yield a 10dB win over standard HRR for foliage penetration.
3. We have produced the attached paper. "Signal Transmission in Passive Media", by John Klauder. This paper demonstrates a new precursor derivation, and has been submitted to IEE Proceedings Radar, Sonar, and Navigation.

15. SUBJECT TERMS

16. SECURITY CLASSIFICATION OF:			17. LIMITATION OF ABSTRACT	18. NUMBER OF PAGES	19a. NAME OF RESPONSIBLE PERSON
a. REPORT	b. ABSTRACT	c. THIS PAGE			Dr. Timothy Olson (386) 740-1212
					19b. TELEPHONE NUMBER *(Include area code)*

Final Report
Friday, November 14, 2003

AFOSR Proposal # AFOSR-49620-03-1-0414
Title: Feynman Integrals and FOPEN Coding
Principal Investigator: Dr. Timothy E. Olson
Duration: August 1, 2003 – December 31, 2003

Major Accomplishments:

The goals of this proposal were to address the problems of: a) Developing advanced methods for electromagnetic computation, and b) to develop signal processing methods for finding targets below foliage. We have addressed these problems and have a number of accomplishments to show for our efforts.

1. We have produced the attached paper, "Electromagnetic pulse propagation in passive media", by Sergei Shabanov. This has received a favorable initial review by Applied and Computational Harmonic Analysis, and is under final review.
2. We have produced the attached technical report, "Precursor based HRR for foliage penetration" by Tim Olson. This report demonstrates that precursors yield a 10 dB win over standard HRR for foliage penetration.
3. We have produced the attached paper, "Signal Transmission in Passive Media", by John Klauder. This paper demonstrates a new precursor derivation, and has been submitted to IEE Proceedings Radar, Sonar, and Navigation.
4. We have refined the attached paper, "Derivation of Precursors via Finite Toeplitz Forms", by Tim Olson. This paper demonstrates that precursors are the dominant singular vector for transmission through foliage like materials.
5. We have produce the attached paper, "Application of the wave packet method to resonant transmission and reflection gratings", by Sergei Shabanov and Andrei Borosov. This paper has been submitted to the Journal of Computational Physics.
6. We have expanded our study to SAR systems, and hope to make gains such as 2 in SAR, as well as HRR. This work, by Sergei Shabanov, was included in the proposal which was recently submitted to this office.

The above works have allowed us to make significant progress on the precursor phenomenon, subsequent to the grant under discussion. Significantly, we have utilized these techniques to construct software showing that precursors can be utilized to greatly improve the resolution of a radar system in a foliage penetration system.

Precursor-Based HRR for Foliage Penetration

Tim Olson
Technical Report
Department of Mathematics
The University of Florida
364 Little Hall
Gainesville, FL 32611-8105

ABSTRACT

We will show that utilizing precursors significantly improves the preformance of an HRR radar system for foliage penetration. We will begin by explaining the many advantages of HRR, and its free-space robustness to noise. We will explain the limitations of this standard system in a highly absorbing and dispersive media such as foliage. We will conclude by outlining the design of a precursor based HRR system which significantly outperforms a standard HRR system in the presence of absorption and dispersion. This new system seems to be viable for foliage penetration.

1. Introduction

Identifying targets under a foliage canopy has proven to be a very difficult problem for the military. The current trend for many radar systems is the design of high frequency systems with high resolution. These systems do not perform in the presence of a highly scattering and absorbing media however. High Range Resolution (HRR) radar systems have many positive characteristics, however. They utilize multiple pulses to significantly improve upon the resultant signal to noise ratio (SNR) of the system. In addition, the mixers in these systems produce constant phase outputs for each pulse returned from a theoretic point target. This constant phase pulse is then integrated over the length of the pulse, additionally increasing the final SNR of the system. The basic design of an HRR system does not account for absorption and dispersion. We will show that the performance of such a system is significantly degraded in a foliage type setting.

The goal of this paper is to explain how a hybrid system should be designed to utilize the advantages of HRR, while minimizing the negative effects of dispersion and absorption. This system is fundamentally designed around precursors.

Precursors were first explained in 1914 by Sommerfeld and Brillouin.[1,2] Their primary focus was on analyzing these pulses with respect to causality. The conclusion of these papers was that the leading edge of the Sommerfeld precursor travels at the vacuum speed of light, but is absolutely causal. Similarly, the Brillouin precursor tends to have a majority of its energy at the leading, and corresponding trailing edges of the pulse and is causal. Unfortunately Brillouin concluded, due to incorrect asymptotics, that these pulses would not be useful. Recent work has shown that Brillouin's analysis was flawed and that the Brillouin precursor is the dominant term in the far field of any dispersive and absorbing media.[3]

The fundamental property which makes precursors so attractive is that they are not exponentially attenuated by the media through which they pass. The energy in a precursor is only attentuated at a rate of $1/\sqrt{z}$, as opposed to $exp(-\alpha(f_k)z)$ for a given frequency f_k and absorption coefficient $\alpha(f_k)$. We will show that the utilization of this property is fundamentally important if one is to acquire significant signal strength, through an absorbing media layer.

This work was supported by the Air Force Office of Scientific Research's Electromagnetics Program.

2. Standard HRR Processing

When trying to design new radar systems, it is very important to understand the positive aspects of the gold standards which are utilized in similar applications. This is especially true when the goal of the new system is far more difficult than that of the standard systems. Synthetic High Range Resolution Radar (HRR) has not been successful in a foliage penetration situation, but it is the standard among one-dimensional processing algorithms. In addition, the gold standard in two-dimensional processs, Synthetic Aperture Radar (SAR), utilizes many of the same techniques. We will briefly outline the positive characteristics of HRR, and the shortcomings of HRR so that we can focus the direction of this program.

HRR radar systems are commonly used for both attack and surveillance by the military. Radar systems engineering is often times a tradeoff between achieving proper resolution and maintaining acceptable signal to noise ratios. Synthetic HRR is a technique to overcome these difficulties.

The basic idea is to transmit N different signals, which are N times longer than the desired resolution, and use the N different responses to recover the desired resolution. There are several advantages to this approach, from a signal to noise point of view.

To begin with, we will assume that the HRR system is transmitting at N different, equally spaced frequencies, f_k. Thus the polarized signal can be represented as $y_k(t) = (\cos(2\pi f_k t) + i\sin(2\pi f_k t))\,\mathcal{X}^l(t) = \exp(2\pi i f_k t)\mathcal{X}^l(t)$, where $\mathcal{X}^l(t)$ is a characteristic function representing the time length of the signal. The received signal will arrive with a time lag $\tau = 2R/c$, where R is the distance to the target, and c is the speed of light. Thus neglecting target velocity, the returned signal can be represented as $r_k(t) = A\exp(2\pi i f_k(t-\tau))\mathcal{X}^l(t-\tau)$, where A is a constant proportional to the RCS of the target.

Upon reception this signal is mixed with the matched filter, $z_k(t) = \exp(-2\pi i f_k t)$, and the resulting output has constant phase and amplitude, and thus the output of the mixer is a constant phase signal $o_k(t) = \exp(-2\pi i f_k \tau)\mathcal{X}^l(t-\tau)$. At this point in time, it would be possible to solve for τ, by standard arithmetic means, such as an inverse tangent. It could also obviously be measured by the $\mathcal{X}^l(t-\tau)$ term. There are two signal to noise improvements which make HRR more signal to noise robust than these basic techniques would impart.

The first is that by making the signal N times longer than the desired bandwidth, one can easily increase the signal to noise ratio by integrating or averaging the constant phase signal $o_k(t)$, which will increase the signal power by a factor of N, while only increasing the noise power by a factor of $\sqrt{N}$. Thus the signal to noise ratio had been increased by a factor of $\sqrt{N}$. Once again, at this point, you could directly estimate τ, as long as the possible range of τ's respects the periodic nature of phase.

HRR takes this process one step further, however. The system transmits N of these signals y_k, and measures the averaged phase values of each. Thus N values $o_k(t) = \exp(-2\pi i f_k \tau)$ are measured and stored in a vector $\vec{o}$. Now, assuming that the frequencies of the f_k are evenly spaced, and neglecting discretization effects of the continuous variable τ, this vector $\vec{o}$ can easily be seen as a frequency shifted column of a standard FFT matrix. Thus, an inverse FFT will result in an approximate δ function response, at the time lagged position τ.

The second signal to noise effect is achieved above. The orthogonal matrix takes a constant amplitude vector, and transforms all of the power of that vector into one fine range bin, increasing the localized signal power by a factor of N. Assuming that the noise is white, however, the noise power will be evenly spread across the range bins, so the signal to noise ratio has been increased by a factor of N in this step. The total increase in signal to noise, in this idealistic model, is therefore $N\sqrt{N}$. This process is illustrated in Figure 1.

2.1. Absorption Problems and Solutions:

The performance of HRR in freespace is well documented. We are interested in penetrating an absorbing and dispersive media, however. A number of the assumptions in the above outlined HRR discussion break down in this case. First, the returned signals will not have constant phase when they exit the mixer. More importantly, they will not have equal amplitude, but rather will be absorbed at different rates. Finally, much less power will return to the receiver, due to the absorbtion. Much of the noise in the system is signal independent (ambient noise), so the SNR will be greatly degraded.

We will now outline the basis of our precursor based HRR system. This system is explained most easily with the help of Figure 2. In order to induce the precursor phenomena we swap the phase of the real and imaginary

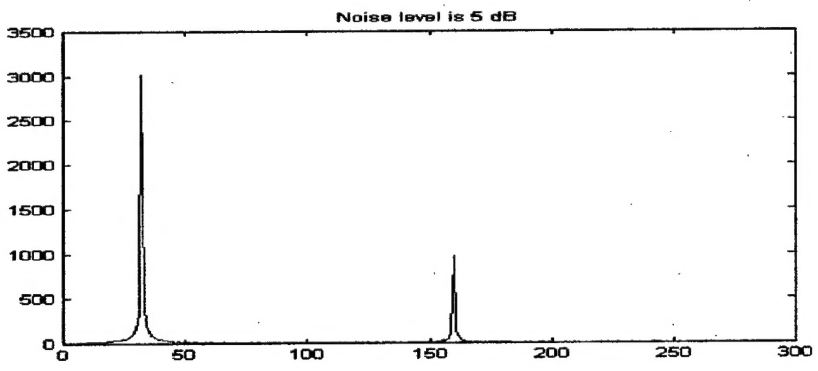

Figure 1: The robustness of a standard free-space HRR system is illustrated above. A point target was theoretically placed at the point of the first peak. The system transmitted 128 pulses that were 128 feet long. The processing outlined above produced a final resolution of 1 foot. The noise level at the receiver was 5 dB, and the noise is almost completely suppressed. The secondary peak is a result of "range walk", to the second gross range bin. For foliage penetration this effect is neglegible, because the ground will act as a barrier, and objects outside of the 128 foot initial gross range bin will be ignored. Without dispersion or absorption, this system will perform well even at noise levels of -10 dB.

components of the transmitted signals, at every other zero crossing. An additional detail, however, is that the real and imaginary components are phase lagged, from a standard exponential. Note that the real and imaginary components, shown in the top of Figure 2, are π out of phase with each other. This is necessary to make sure that the received signals, shown at the bottom of Figure 2, are $\pi/2$ out of phase, as would be the case with a standard exponential.

Precursor HRR: The basic steps in the precursor HRR system are outlined below. Note that with the exception of the transmitter, everything else is nearly identical to traditional HRR.

- Transmit signals that are phase swapped every cycle, and phase delayed as illustrated in the top illustratiion of Figure 2.
- The signals travel through the material, and are received as in the bottom illustration of Figure 2.
- Mix the received signals with appropriate exponentials producing nearly constant phase outputs as in HRR.
- Integrate the output of the mixer over appropriate large range bins.
- Collect 128 of these signals, and use the matched filter to produce the final output.

To give a baseline for our material model, we illustrate its effect on one of the standard HRR signals. In Figure 3, we have transmitted a standard HRR signal, and its corresponding precursor HRR signal. Both signals originally were at the same frequency, with phase swapping used on the precursor HRR signal. Note that the precursor signal was received with 5.8 times more power than the standard HRR signal. This effect gets larger for higher frequency signals, and correspondingly lower at lower frequencies, with the maximum ratio being 8, and the minimum being 1.09. This example was at appoximately 350 Mhz.

We would like to study the behavior of HRR and our precursor based hybrid HRR through an absorbing and dispersive media. We outline the assumptions and rules that will be used throughout this comparison below:

- The noise figure stated is the signal to noise ratio of a freespace system without absorption and dispersion. This recognizes that there is inherent ambient noise in the radar system, and that the medium will then create a much lower signal to noise ratio.

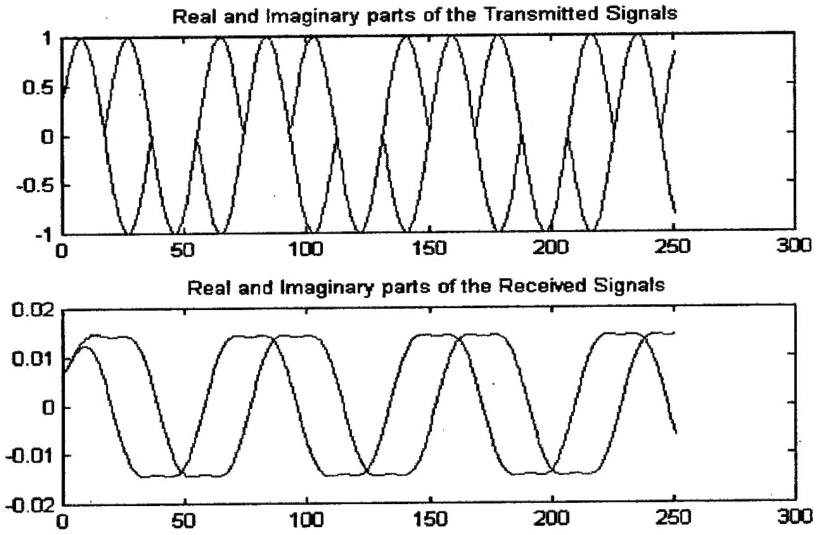

Figure 2: We present the signals that are transmitted for the precursor HRR above. The real and imaginary components of the transmit signal are presented at the top. We swap the phase of the signals at every other zero crossing. Note also that the real and imaginary components of the transmit signal are π out of phase with each other, as compared to $\pi/2$ for a standard exponential. This is necessary so that the received signals, shown at the bottom, will be $\pi/2$ out of phase, enabling standard HRR processing of the received signals. Note that the precursor behavior has resulted in a frequency halving of the signal, but the signals will be nearly constant phase after mixing with a proper exponential (they are nearly exponentials themselves).

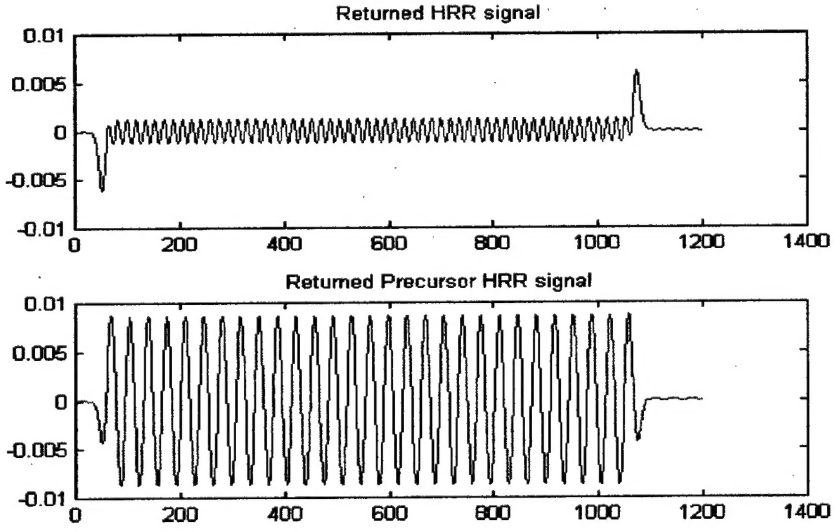

Figure 3: We illustrate the effect of our material model above. A standard HRR signal was transmitted, at approximatly 350 Mhz, and the resulting received signal is displayed at the top. Note the strong precursor effect at the leading and trailing edge. We believe that the foliage model utilized here is consistent with measured precursor effects through realistic foliage. Note that the basis of the precursor HRR is to induce the increased power shown above at the leading and trailing edges, throughout the pulses. This is shown in the bottom figure, where the corresponding received signal from the precursor HRR system is displayed. There is 5.8 times more power in the precursor signal, giving hope for increased system performance.

- We will study standard HRR and our precursor HRR with various base-band (lowest), frequency settings. We have chosen 200, 300, and 600 Mhz as our initial basebands, with approximately 500 Mhz of frequency utilized above each of these basebands. We believe that this is a realistic comprimise range between antennae size and power considerations.
- In each study, there will be 128 pulses which are 128 feet long, appropriately spaced in frequency via HRR rules to yield 1 foot of resolution in a freespace HRR system.
- There are two gross-range bins included in our study (128 feet long), which are then resolved into 128 fine range bins (at least in the freespace example). Since the ground presents a definite base for range gating, we feel this is more than sufficient.
- We utilize one point target, placed approximatly 31 feet into the first gross range bin.
- We will report the emperical resolution of each trial. This is defined for our purposes as being the number of fine range bins which exceed 1/3 of the peak value of the transfer function. Thus if the peak value is 150, and there are 11 fine range bin values around the peak of the transfer function over 50, the resolution would be reported as being 11 feet.

We begin this comparison by studying the lowest frequency problem. The baseband frequency is 200 Mhz, and approximately 200-700 Mhz of frequency range is utilized. In Figure 4, we consider the precursor-HRR and the standard HRR. Note that detection for this point target is possible with either system, but that the precursor HRR had a much higher emperical resolution of 3 feet, as opposed to 11 feet for the standard HRR.

To try and close this resolution gap, we utilized the standard assumption of HRR, that equal power will return from each frequency, to invert the spreading of the transfer function and try to reachieve high range resolution. The result is shown in Figure 5. As one might expect, noise from the higher frequency systems has essentially eliminated the ability to locate the target. Thus we were not able to get the standard HRR system to perform at the same noise levels, with the same resolution as the precursor system.

Figure 6, is the analogue of Figure 4, with the baseband being 300 Mhz. Once again the targets are identifiable, but the precursor HRR has much higher emperical resolution (3 feet), than the standard HRR (11 feet). Figure 7 is the analogue of Figure 5, at 300 Mhz. We attempted to recover the resolution from the standard HRR but the noise levels were prohibitive.

Figure 8 shows a comparisons of the systems with a base frequency of 600 Mhz, and is analogous to Figures 4 and 6. Note, however, that noise has absolutely overcome the HRR system, making target identification nearly impossible. In addition, we removed the noise to test the resolution of the two systems. The precursor HRR had a 3 foot resolution, just as at 200 and 300 MHz, while the resolution of the standard HRR system had dropped to 22 feet, making target identification nearly impossible.

We illustrate the singular values of the systems at 600 Mhz baseband in Figure 9. The singular values of the HRR system are much smaller than those of the precursor HRR system, explaining the large differences which were noted in Figure 8. Recall that larger singular values imply transmission of more power and information.

REFERENCES

1. L. Brillouin, "Über die fortpflanzung des licht in disperdierenden medien," Ann. Phys. 44, 203 (1914).
2. A Sommerfeld, "Über die fortpflanzung des lichtes in disperdierenden medien," Ann. Phys. 44, 177 (1914).
3. K. E. Oughstun and G. C. Sherman, "Propagation of electromagnetic pulses in a linear dispersive medium with absorption (the Lorentz medium)", J. Opt. Soc. Am. B 5, 817 (1988).
4. K.E. Oughstun and G.E. Sherman, Electromagnetic Pulse Propagation in Causal Dielectrics, Springer-Verlag, Heidelberg, 1994.
5. D. Slepian and H. O. Pollack, "Prolate spheroidal wave functions, Fourier analysis and uncertainty, I", Bell System Tech. J. 40, pp. 43-64, 1961.

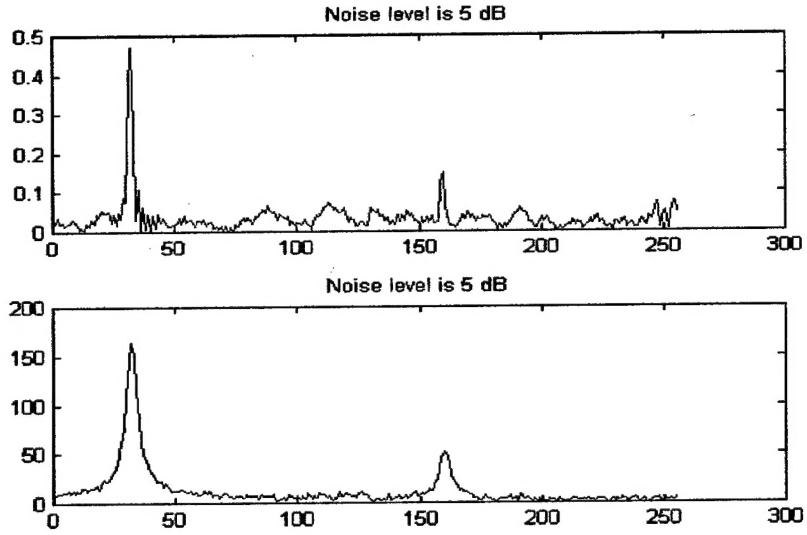

Figure 4: Above we present a comparison of the precursor HRR, on top, vs. standard HRR with at 200 Mhz below. While both systems identify the targets, the precursor HRR has an emperical resolution of 3 feet, while the standard HRR has an emperical resolution of 11 feet.

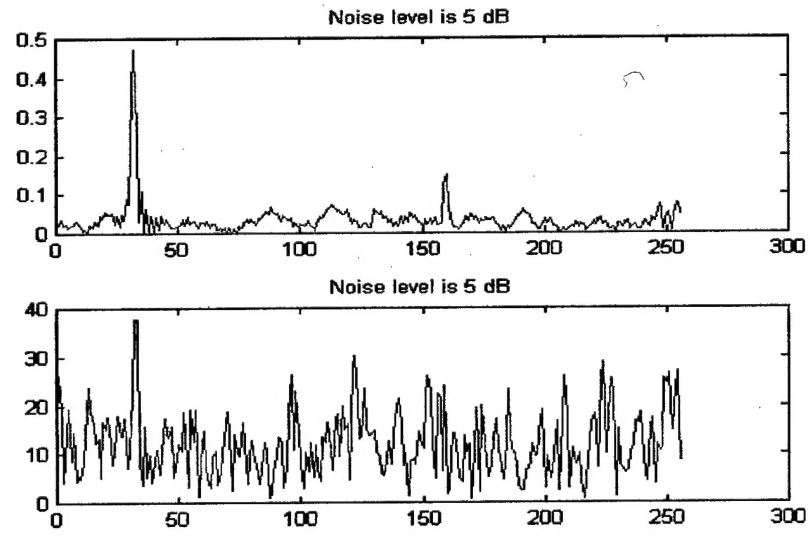

Figure 5: Comparison of the precursor HRR, vs. standard HRR with inversion attempted on the HRR, at 200 Mhz. Note that the standard HRR, with frequency equalization, is too noisy for realistic use.

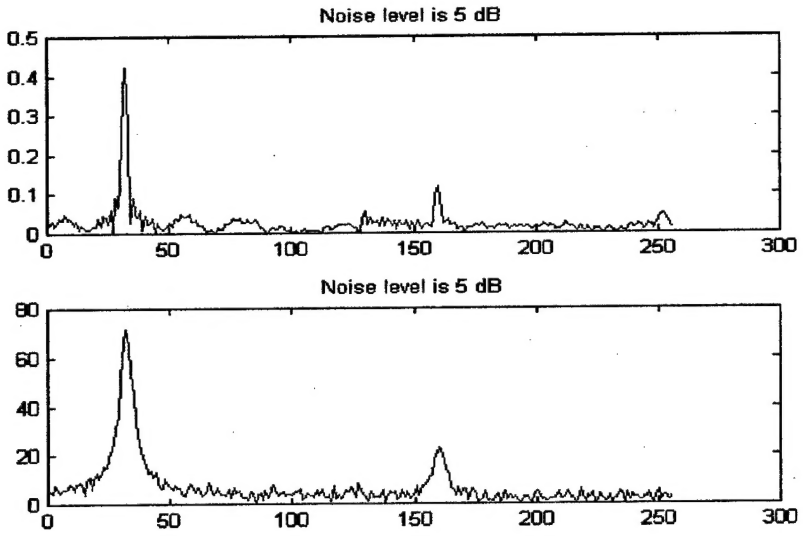

Figure 6: Above we present a comparison of the precursor HRR at top, vs. standard HRR at 300 Mhz. As in Figure 4, both identify the target, but the precursor HRR has a resolution of 3 feet, versus a resolution of 11 feet for the standard HRR.

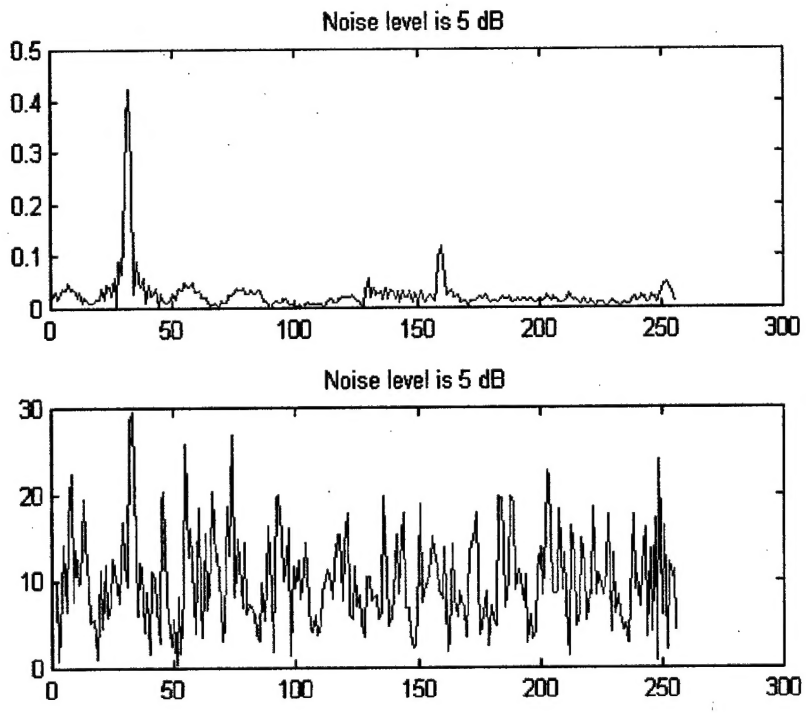

Figure 7: Above we present a comparison of the precursor HRR at top, vs. standard HRR at 300 Mhz. As in Figure 5 we attempted to recover the resolution from the HRR system, and noise effects made this non-viable.

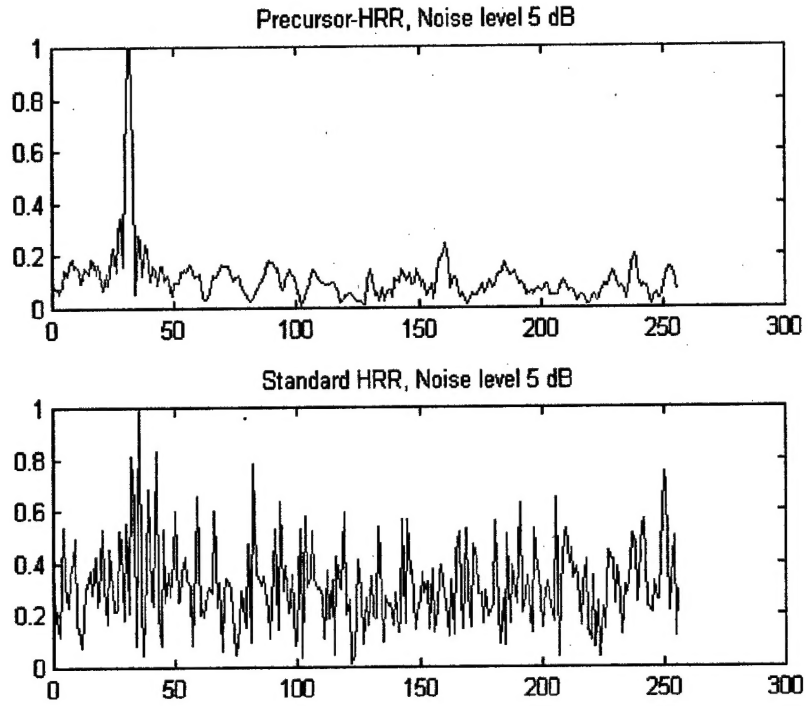

Figure 8: Above we present a comparison of the precursor HRR at top, vs. standard HRR with at 600 Mhz. As opposed Figures 4 and 6, the standard HRR cannot identify the target. The precursor HRR, however, demonstrates robustness and still has an emperical resolution of 3 feet. Testing the resolution of the HRR system, with essentially no noise, revealed that it was 22 feet. Since the noise is already prohibitive in the HRR system, we did not attempt to recover the resolution of the system as in Figures 5 and 7.

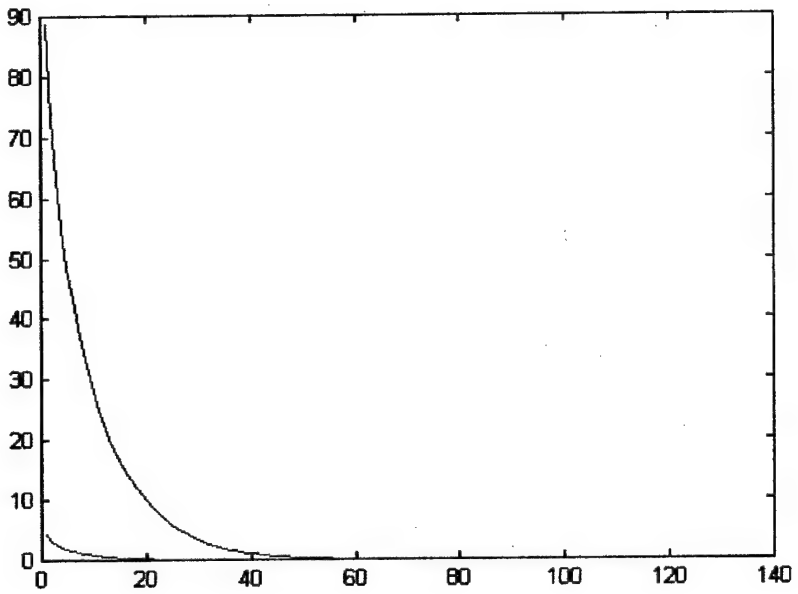

Figure 9: Comparison of the singular values of precursor HRR, in blue, and traditional HRR, in green, with the lowest frequency being 600 Mhz. The norm of the singular values of the precursor HRR are 25 times, i.e. the Hilbert-Schmidt norm of the system, is 25 times larger than that of the standard HRR system.

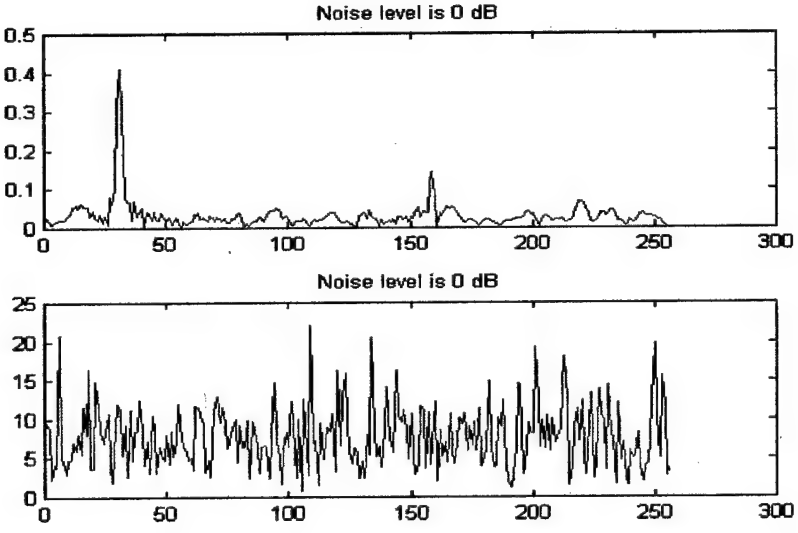

Figure 10: Above we present a comparison of the precursor HRR, on top, vs. standard HRR with at 200 Mhz below. This is analogous to Figure 4, but with a noise level of 0 dB instead of 5 dB in Figure 4. Note that the HRR system did not identify the target at all, while hte precursor HRR system accurately performed with this high noise level.

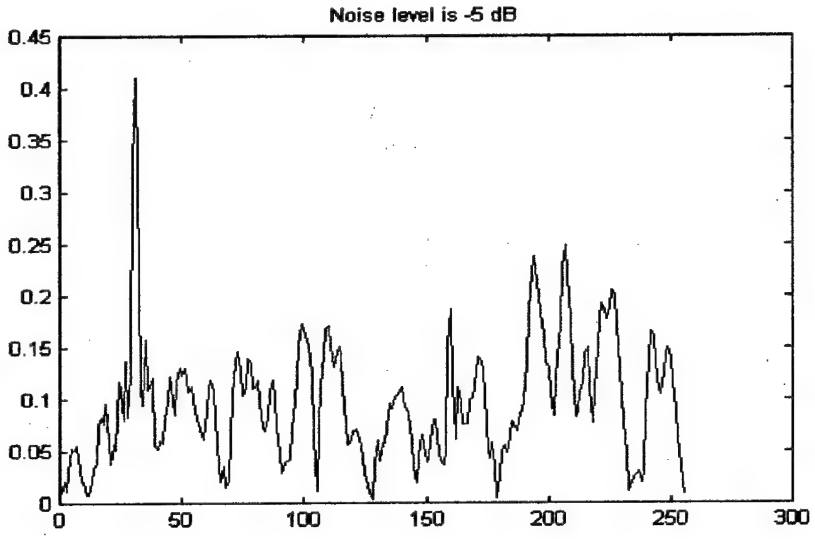

Figure 11: Above we present the output of the precursor HRR at 200 Mhz, with a very low signal to noise ratio of -5 dB. Note that the standard HRR system could not accurately obtain the resolution obtained here, namely 3 feet, at +5 dB. The precursor HRR system accurately detects the system at -5 dB, indicating a 10 dB win.

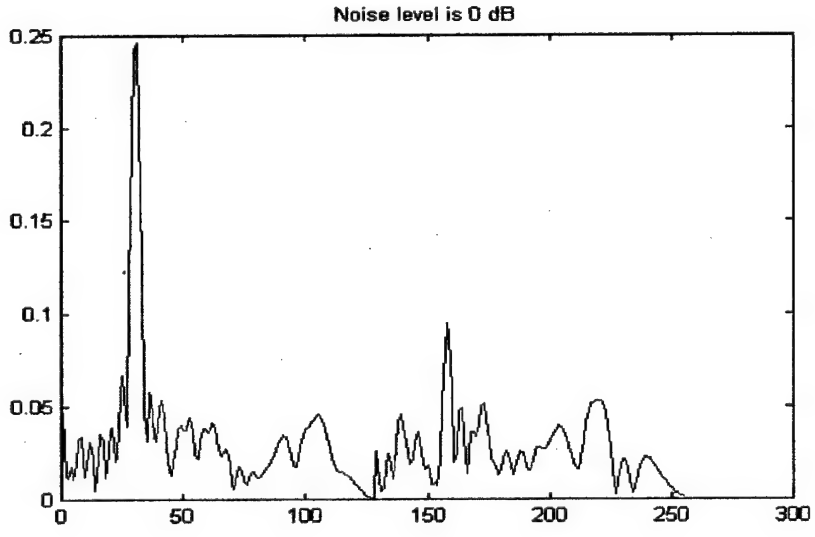

Figure 12: Above we present the output of the precursor HRR at 600 Mhz, with a low signal to noise ratio of 0 dB. Note that the standard HRR system could not accurately obtain the resolution obtained here, namely, at +5 dB. In addition its transfer function had a resolution of only 20 feet.

Derivation of Precursors via Finite Toeplitz Forms

Tim Olson
Department of Mathematics
The University of Florida
364 Little Hall
Gainesville, FL 32611-8105

ABSTRACT

In this paper we derive "precursors" from basic principles of linear algebra and operator theory. Evidence is given that these are indeed the Brillouin precursors.[1] We give numerous numerical examples and illustrate that by imposing a finite time limit the signals, the precursor phenomena will be generated from the infinite Toeplitz form.

1. Introduction

Precursors were first explained in 1914 by Sommerfeld and Brillouin.[1,2] Their primary focus was on analyzing these pulses with respect to causality. The conclusion of these papers was that the leading edge of the Sommerfeld precursor travels at the vacuum speed of light, but is absolutely causal. Similarly, the Brillouin precursor tends to have a majority of its energy at the leading, and corresponding trailing edges of the pulse and is causal. Unfortunately Brillouin concluded, due to incorrect asymptotics, that these pulses would not be useful. Recent work has shown that Brillouin's analysis was flawed and that the Brillouin precursor is the dominant term in the far field of any dispersive and absorbing media.[3]

The methods of Brillouin, Sommerfeld and Oughstun were asymptotic in nature. In that work, the dominant nature of precursors was found using advanced techniques to approximately solve a complex integral. Often in applied mathematics, we strive to understand the structure of transmission operators via operator theory. If the transmission operator can be examined as a compact operator, the generated structure is very informative. The inputs and outputs to the operator are separated into orthogonal subspaces, with the power passing through each subspace clearly described by the singular values, which are analagous to eigenvalues. We will show that Brillouin precursors, or pulses remarkably similar to Brillouin precursors, are the dominant singular vectors associated with transmission through media such as foliage or water using basic techniques of operator theory or linear algebra.

2. Background material and notation

We begin in the spirit of Slepian and Pollack.[5] In that work, the singular functions of the joint time-frequency cut off operators were derived, resulting in the prolate spheroidal wave functions. We will consider operators which are similar, but more general than the joint time-frequency operator. These operators are physically motivated by a wide variety of electromagnetic propagation problems. The convolution operators which describe the evolution of a pulse $r(t,z)$ through a homogeneous linear medium have a very simple form. Given an initial plane wave signal which is incident on a homogeneous medium, $s(t,0) = s(t)$, the pulse at time t, and distance z is appropriately modeled by

$$r(t,z) = \int s(\tau) A_z(\tau - t) d\tau = L_z(s(t)). \tag{1}$$

Unless otherwise noted, all integrals are over the real line. Convolution operators L of the type (1) have been heavily studied and are well understood. The Fourier transform diagonalizes the operator and the spectrum of the operator is the continuous Fourier transform of A_z, for any fixed distance z. A monochromatic signal $s(t)$ transmitted at a frequency w_0, will be absorbed according the real part of the Fourier transform $\hat{A}_z(w_0)$. Dispersion is described by the complex portion of $\hat{A}_z(w_0)$. When the signal is not monochromatic, then the resulting signal $r(t,z) \equiv r_z(t)$ has a Fourier transform which is the product of $\hat{A}$, and $\hat{s}$, i.e. $\hat{r}_z(w) = \hat{A}_z(w)\hat{s}(w)$.

This work was supported by the Air Force Office of Scientific Research.

Slepian and Pollack utilized the finite length of signals to alter an operator of the type (1). This alteration creates a compact operator, with a corresponding discrete set of singular values and singular vectors as opposed to the continuous spectrum of L_z. Following this development we will consider pulses of finite length l, and corresponding new operators L_z^l, which describe a pulse evolving through a distance z of a medium. Formally we have

$$r(t,z) = \int_{-\infty}^{\infty} s(\tau)A_z(\tau - t)d\tau = \int_{\infty}^{\infty} s(\tau)\mathcal{X}_l(\tau)A_z(\tau - t)d\tau = L_z^l(s(t)), \tag{2}$$

where $\mathcal{X}_l(\tau) = 1$ for $\tau \in [0, l]$, and is 0 otherwise. Thus our old kernel was $A_z(t)$ and our new kernel is $K_z^l(t,\tau) = \mathcal{X}_l(\tau)A_z(\tau - t)$. A basic result of functional analysis states that when a kernel of the type $K_z^l(t,\tau)$ is square integrable, the corresponding operator L_z^l is a compact operator. This is stated clearly in

THEOREM 1 (THE HILBERT-SCHMIDT THEOREM:). *Let an operator L be defined by*

$$L(f)(t) = \int f(\tau)G(t,\tau)d\tau \tag{3}$$

and let $\|G(t,\tau)\|_2 < \infty$. Then L is a compact operator, and it follows that there exist singular vectors and singular values $\{u_k\}$, $\{v_k\}$, and $\{\sigma_k\}$ such that

$$L(f)(t) = \int f(\tau)G(t,\tau)d\tau = \sum_{k=0}^{\infty} \sigma_k \langle f, v_k \rangle u_k. \tag{4}$$

The values σ_k are called the singular values and the vectors $\{u_k\}$ and $\{v_k\}$ are correspodingly called the left and right singular vectors. Moreover, the energy of the singular values is exactly that of the kernel, or

$$\int\int |G(t,\tau)|^2 dt d\tau = \sum_{k=0}^{\infty} \sigma_k^2. \tag{5}$$

At this time, let us adopt some notation. We are dealing with a class of compact operators which is indexed by the initial finite signal length l, and the propagation distance z, so we refer to the kernels of these operators as K_z^l. Similarly we will refer to the corresponding singular values $\sigma_k(z,l)$, where k is the index, and likewise the left singular vectors $u_k(z,l)$, and right singular vectors $v_k(z,l)$. Thus k runs from 0 to ∞, and the necessarily positive singular values decrease by convention. Thus the dominant left and right singular vectors are always $u_0(k,l)$, and $v_0(k,l)$. We will also refer to the transmission operator, without regard to the finite pulse length as L_z.

3. Basic Results:

With basic development of theory, we will now calculate a specific example from third party electromagnetic data. The data we have utilized was provided by the computational electromagnetics group at Brooks Air Force base, and this specific data set is attributed to Grant. The transfer function generated by the absorption coefficient, i.e. $exp(-\alpha(w))$ is shown in Figure 3.

We will now analyze the singular value decompositions of the generated operators at various distances, and with various initial pulse widths. To begin with we start out with a pulse which is only 7.5 cm long. Thus we will be considering the optimal pulse to transmit one meter through water, assuming that the initial pulse is less than 7.5 cm long. The spectrum and time plot of this dominant singular vector, $u_0(7.5, 1)$, is shown in Figure 3.

We have arbitrarily picked 1 meter as our propagation distance, and 7.5 centemeters as our initial allowed pulse length. Natural questions at this time revolve around these arbitrary choices, namely:

- What effect does the initial finite pulse length have on the singular vectors in the far field?
- Does the dominant singular vector at 1 meter propagate well over 20 meters?

We will suggest answers to these questions now. The answers seems to be as following

- Over short distances, the dominant pulse depends on length and propagation distances.
- Over longer distances, the dominant pulse becomes independent of initial pulse length and propagation distance.

Let us look at a couple of examples to support these claims.

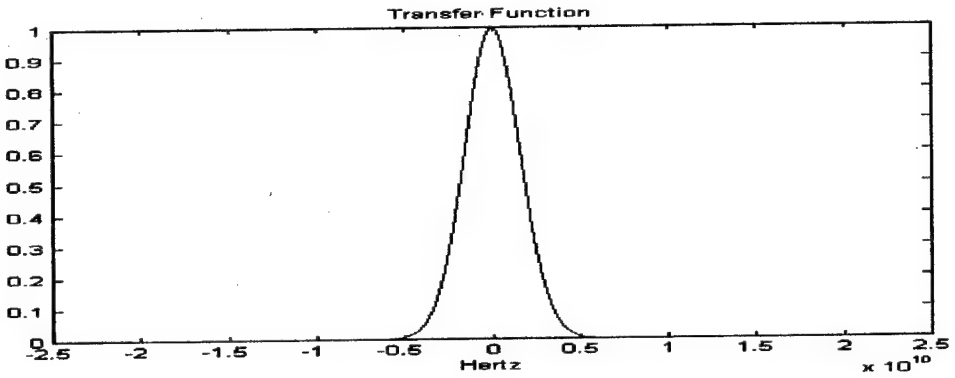

Figure 1: Testing the water

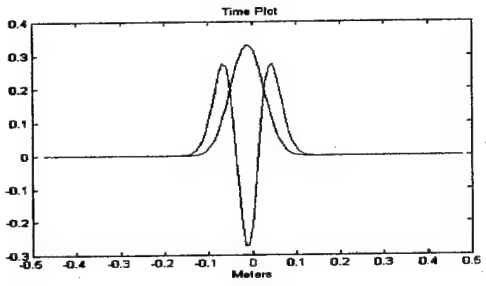

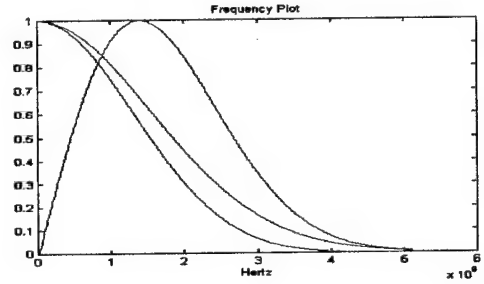

Figure 2: On the left we have displayed a time plot of the dominant singular function, and the second singular function. Note that the dominant singular (in blue) function looks very similar to the leading edge of a Brillouin precursor. On the right we have displayed the transfer function for the operator (in blue), and the absolute value of the spectrum of the dominant singular function and the second singular function (in green and red respectively). Note that the spectrum of the dominant singular function is very nearly that of the transfer function or kernel.

3.1. How does propagation distance affect the singular vectors?

To begin with, we want to compare the propagation of two different singular vectors; 1) The dominant singular vector for propagating through 1 meter of water, and 2) the dominant singular vector for propagating through 20 meters of water. We will fix the pulse length at 7.5 centimeters.

The test is set up in the following way. We calculate the singular vectors in the above to situations. Then we propagate them through a) 1 meter of water, and b) 50 meters of water. The first singular vector was calculated to be optimal for experiment a) or 1 meter of water, and the second singular vector for propagation through b) 50 meters of water. The question is: "Do they both perform well?".

The answer was very conclusive. The results were nearly identical after propagating through the various distanceds. This can be seen in Figures 3 and 4 where we tested the results through 1 and 20 meters of water respectively. Note that the time plots of these singular vectors are nearly indistinguishable. The frequency plots show the transfer function, the first singular vector, and the second singular vector for each case. Note that the dominant "precursor" pulse in each case is indistinguishable whether it was originally calculated at 1 meter, or 50 meters, but the second singular vectors are orthogonal and therefore very different.

We then asked the question: "How close are the singular vectors to being identical when they are calculated at different distances, originally, and then propagated toward the far field?" The answer to this is given in Figure 5. The singular vectors calculated at a short distance, and a very long distance, are extremely similar, with all correlations $> .99$.

The conclusion of this experiment is that the dominant singular vectors, calculated for propagation distances, propagate to become nearly the dominant singular vectors at the next distance. Thus they appear to be precursors.

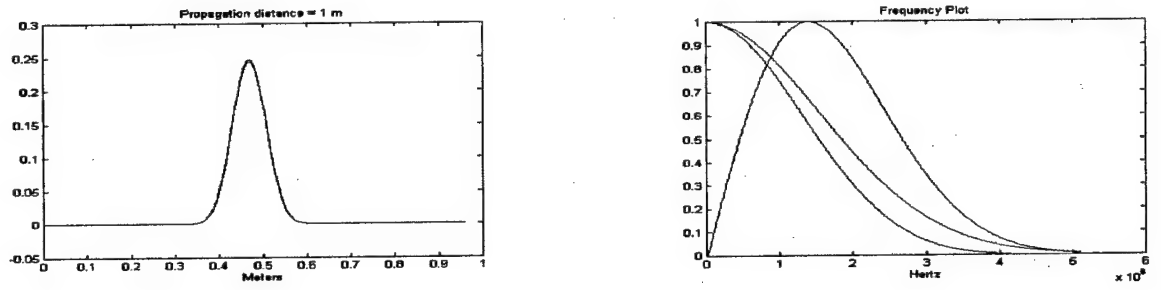

Figure 3: On the left we have displayed a time plot of the dominant singular function after traveling 1 m through water (in blue), and the dominant singular function for propagating through 20 m, after it has propagated through 1 m of water. Symbolically this is $u_0(7.5, 1) = L^1(v_0(7.5, 1))$, compared against a second vector $L^1(v_0(7.5, 20))$. Note that the dominant singular calculated for 20 m of water, is also nearly equal to the dominant singular vector for propagation through 1 m of water. Thus the arbitrary choice of propagation distance does not seem to matter. The dominant singular vector for propagating through 20 m, had a correlation with the other singular vector of .997. The red curve on the right is that of the second singular function. Since it is orthogonal to the first singular function calculated at 1 m, it will be nearly orthogonal to the singular function calculated at 20 m, because of the noted correlation above.

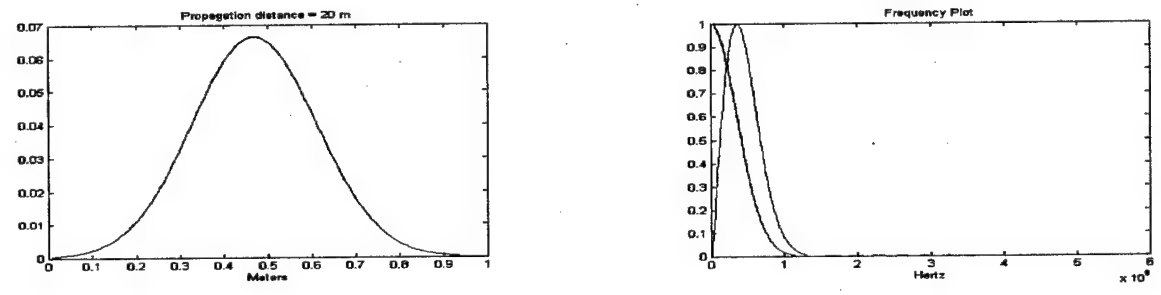

Figure 4: On the left we have displayed a time plot of the dominant singular function after traveling 20 m through water (in blue), and the dominant singular function for propagating through 1 m, after it has propagated through 20 m of water. Symbolically this is $u_0(7.5, 20) = L^{20}(v_0(7.5, 20))$, compared against a second vector $L^{20}(v_0(7.5, 1))$. Note that the dominant singular vector calculated for 1 m of water, is also nearly equal to the dominant singular vector for propagation through 20 m of water. Thus the arbitrary choice of propagation distance does not seem to matter. The dominant singular vector for propagating through 20 m, had a correlation with the other singular vector of .997. Once again the red curve at the right is the second singular function calculated at 20 m, which will be orthogonal to the dominant singular functions.

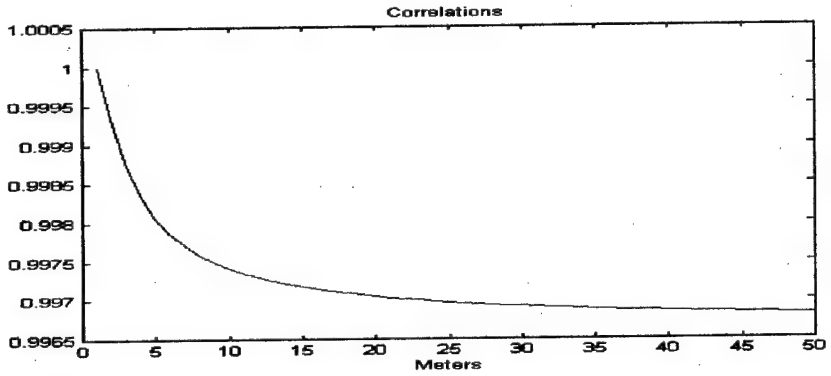

Figure 5: Above we illustrate the projection of the dominant left singular vector calculated at 1 m, onto the dominant left singular vectors for distances 1-50. Symbolically we are calculating the projection of $L^k(v_0(7.5,1))$ onto $u_0(7.5,k) = L^k(v_0(7.5,k))$. Note that there is almost no difference in the singular vectors.

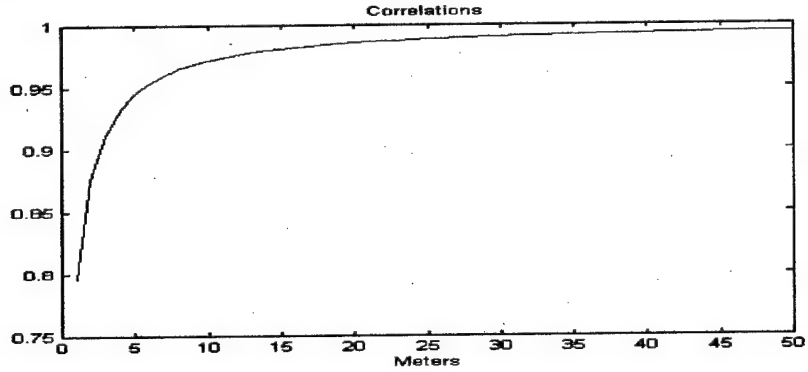

Figure 6: Above we illustrate the projection of the dominant left singular vector calculated at distances 1-50 m, with initial time contraints of either 7.5 cm, or 15 cm. Symbolically we are calculating the projection of $u_0(7.5,k) = L^k(u_0(7.5,k))$ onto $u_0(15,k) = L^k(u_0(15,k))$. The initial pulse length seems to become irrelevant in the far field, as the distance increases, as is illustrated by the correlation going to one, i.e. the left singular vectors are converging to one another.

Our study of the dependence of the dominant singular vectors on distance, has indicated that the dominant subspace which is generated by the first singular vector seems to propagate. In other words if we launch a right singular vector into the material, the output at 1 meter is dominant left singular vector. Very importantly, however, the results of the last section suggest that if we let this vector propagate an additional 19 meters, it will still be nearly the dominant singular vector for the medium at 20 meters. Thus we do not have to know the nature of the medium, or perhaps the depth of the foliage, exactly in order to lauch a pulse which is close to optimal from a penetration viewpoint.

3.2. Dependence on the initial time length

We now study the dependence of the singular vectors on the initial pulse length. Since we arbitrarily chose the initial pulse length of 7.5 cm, we need to understand how this initial choice affects the calculated singular vectors.

To do this, we calculated the optimal singular vectors first at a distance z, with initial pulse length 7.5 cm, and then at distance z, with initial pulse length 15 cm. These results are shown in Figure 5. Note that since the correlation converges towards 1, it is safe to assume that the singular vectors are converging to a single precursor in the far field.

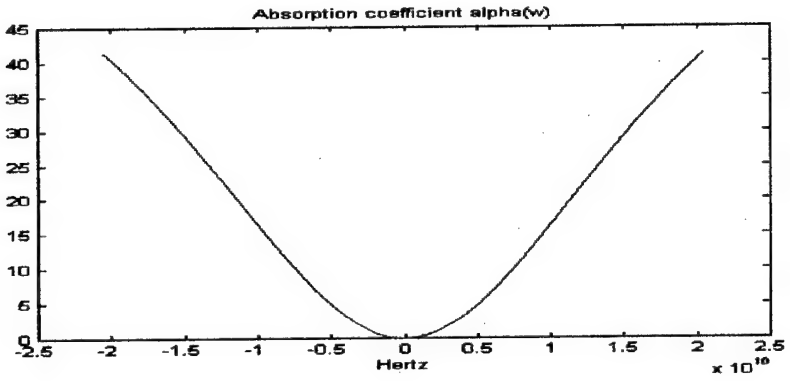

Figure 7: Above we illustrate the absorption coefficient which was utilized for the computations, as a function of frequency. Notice that it is nearly linearly dependent upon frequency.

4. Asymptotic Results

We will now prove one of the major theorems of this paper. Much of the fascination with precursors is due to the fact that they propagate with an absorption which is $z^{-1/2}$ rather than e^{-kz}. We will now give a simple proof of this fact, under a basic hypothesis which seems valid in the case of the water data which we have just presented.

Our primary assumption, for the purpose of this result is that the absorption coefficient $\alpha(w)$ is linearly dependent upon the frequency for low frequencies, or $\alpha(w) \approx kw$ for w small where k is a positive constant. We now present the following

THEOREM 2 (ASYMPTOTIC DECAY). *Assume that propagation within a dielectric material is modeled correctly by (2). Assume further that the absorption coefficient $\alpha(w) \approx kw$, where k is a positive constant. Then the energy of the kernels associated with propagation of a distance z, $K_z^l(t,\tau)$, decays at the rate $O(z^{-1/2})$. Moreover, by the Hilbert-Schnidt Theorem, it follows therefore that the sum of the squares of the singular values also decays at a rate of $O(z^{-1/2})$.*

Proof. The proof is very straight forward manipulation of the integrals, since

$$\begin{aligned}
\int_{-\infty}^{\infty}\int_{-\infty}^{\infty}|K_z^l(t,\tau)|^2 dt d\tau &= \int_{-\infty}^{\infty}\int_{-\infty}^{\infty}|\mathcal{X}_l(t)A_z(\tau-t)|^2 dt d\tau \\
&= \int_{-\infty}^{\infty}\int_{-l}^{l}|\mathcal{X}_l(t)A_z(\tau-t)|^2 dt d\tau \\
&= \int_{-l}^{l}\int_{-\infty}^{\infty}|A_z(\tau-t)|^2 d\tau dt \\
&= \int_{-l}^{l}\int_{-\infty}^{\infty}|A_z(\tau)|^2 d\tau dt \\
&= 2l\int_{-\infty}^{\infty}|A_z(\tau)|^2 d\tau. \qquad (6)
\end{aligned}$$

Now the Fourier Isometry and (6) gives us that

$$\begin{aligned}
\|K_z^l\|^2 &= 2l\int_{-\infty}^{\infty}|A_z(\tau)|^2 d\tau \\
&= 2l\int_{-\infty}^{\infty}|\hat{A}_z(w)|^2 dw \\
&= 4l\int_{0}^{\infty}e^{-2\alpha(w)z} dw
\end{aligned}$$

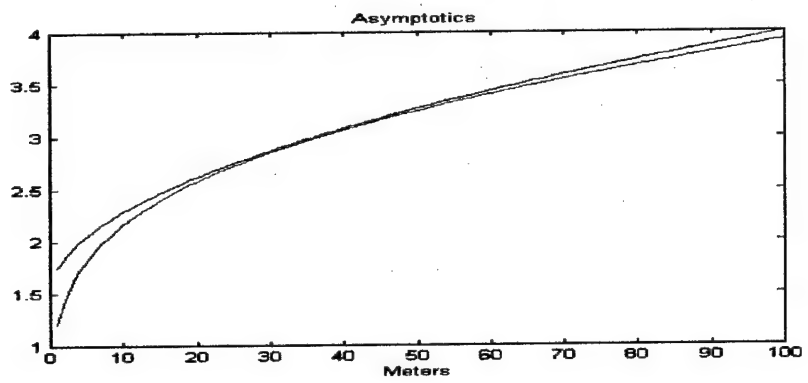

Figure 8: We illustrate the asymptotics of the singular vector which we believe to be the precursor field above. We have plotted $\sqrt{(}z) * .25 + 1.5$ in blue, and $1/\sigma(7.5, z)$ in green. Note that the fit is very good, emphasizing that the singular vector, which we believe to be the precursor, does indeed display $O(z^{-1/2})$ behavior.

$$= \quad 4l \int_0^\infty e^{-2kwz} dw. \tag{7}$$

From the substitution $u = kwz$, it follows that $dw = 1/(kz)du$, and

$$\|K_z^l\|^2 = 4l \frac{1}{kz} \int_0^\infty e^{-2u} du = O(z^{-1}). \tag{8}$$

By taking a square root, we end up with the result that $\|K_z^l\| = O(z^{-1/2})$ which corresponds with the result of Brillouin. □

While we have shown that the rate of decay of the operator is $O(z^{-1/2})$, we have not yet proven that the dominant singular values decay at this rate. It is the case that each frequency in the kernel decays exponentially, except for the origin, but the energy of the kernel decays much more slowly, i.e. $O(z^{-1/2})$. From the Hilbert-Schmidt Theorem we know that the sum of the squares of the singular values decays as $O(z^{-1/2})$, but perhaps each of them decay exponentially just as the frequencies in the operator.

To study this, we present a final numerical computation. We begin by showing that the singular vector associated with the precursor does indeed display aymptotics which seem to be $O(z^{-1/2})$. This is seen in Figure 8. Secondly, we will compare the amount of energy in the precursor field, to the total energy in the operator, which is seen in Figure 9.

5. Relationship to Standard Brillouin Precursors

We have shown that basic operator theory generates the dominant singular vector for transmission through a medium, and that this dominant singular vector looks qualitatively similar to a Brillouin precursor. We have also shown that this dominant singular vector seems to be relatively robust to changes in the finite time restriction, and distance through the material.

We have not directly compared this dominant singular vector, which we believe to be the Brillouin precursor, to a Brillouin precursor computed in a traditional manner. We present this experiment below. In Figure 10 we illustrate the result of propagating a square windowed sinusoid through an absorbing and dispersive media. Note the two Brillouin precursors at the leading and trailing edges. In Figure 11 we compare the Brillouin precursor, generated as in Figure 10, to the dominant singular vector for the transmission operator, which we claim is the Brillouin precursor or nearly the Brillouin precursor. Note that they are very similar.

We will now examine whether the dominant singular vector becomes more or less similar to the Brillouin precursor, as distance increases. The question being "Are they asymptotically the same". The literature provides great motivation for this question. It has been proven that the Brillouin precursor is the dominant effect in the far field.[3,4] The dominant singular vector is by definition the dominant effect. Science leaves little room for these two dominant effects to be dissimilar. The experiment illustrated in Figure 12 suggests that yes, they are the same in the far field.

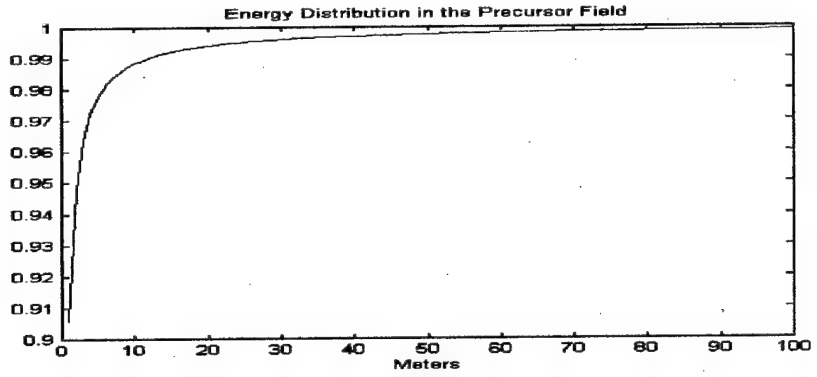

Figure 9: We have tested the dominance of the precursor field in the above diagram. We have plotted the ratio, $\|L_z^l\|_2/\sigma_z(7.5,0)$, or the ratio of the operator norm to the value of the dominant singular value. Note that this ratio is strictly bounded above by 1, and that the ratio rapidly approaches 1, starting out at over .9. Thus nearly all of the energy of the operator is quickly in the precursor field.

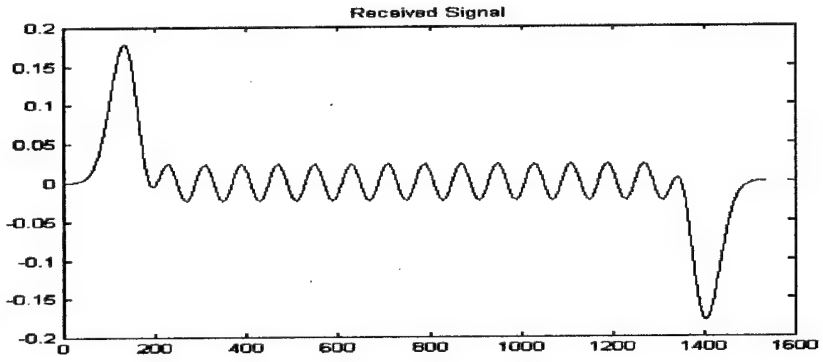

Figure 10: In this figure we illustrate two classical Brillouin precursors, the first at the beginning of the pulse, and the second, with a negative orientation at the end of the pulse. This is typical of the effect realized when one transmits a square windowed sinusoid through and absorbing and dispersive media.

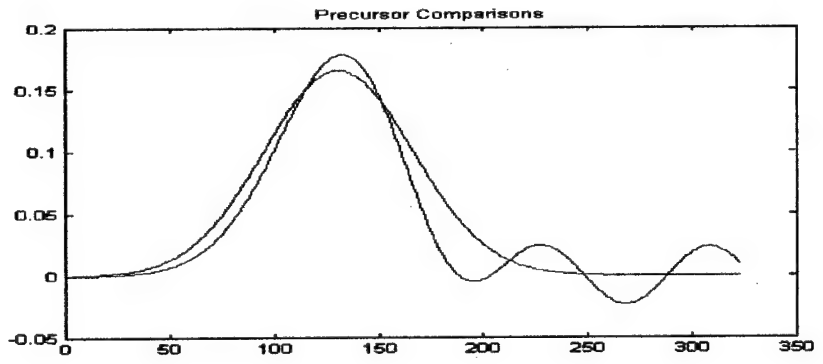

Figure 11: In this figure we illustrate the singular vectors of the transmission operator, which we believe to be essentially Brillouin precursors, against a Brilluin precursor which was generated by sending a square wave through the same finite distance of an absorbing media, such as in Figure 10. Note that they are extremely close in size and shape.

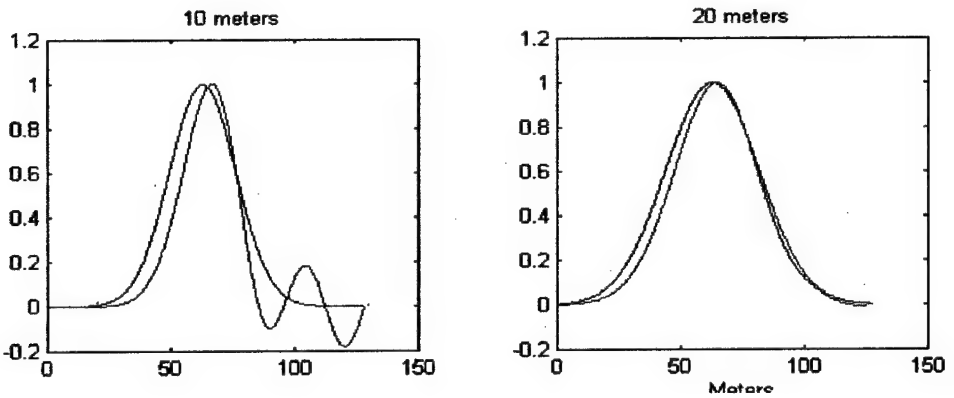

Figure 12: Above left we illustrate the singular vectors of the transmission operator at 10 meters, and Brillouin precursor which was generated by sending a square wave through 10 meters of an absorbing media. Above right we illustrate the same thing, but after 20 meters of material. Note that they are originally close, but are becoming closer with distance suggesting asymptotic convergence.

6. Conclusion:

REFERENCES

1. L. Brillouin, "Über die fortpflanzung des licht in disperdierenden medien," Ann. Phys. 44, 203 (1914).
2. A Sommerfeld, "Über die fortpflanzung des lichtes in disperdierenden medien," Ann. Phys. 44, 177 (1914).
3. K. E. Oughstun and G. C. Sherman, "Propagation of electromagnetic pulses in a linear dispersive medium with absorption (the Lorentz medium)", J. Opt. Soc. Am. B 5, 817 (1988).
4. K.E. Oughstun and G.E. Sherman, Electromagnetic Pulse Propagation in Causal Dielectrics, Springer-Verlag, Heidelberg, 1994.
5. D. Slepian and H. O. Pollack, "Prolate spheroidal wave functions, Fourier analysis and uncertainty, I", Bell System Tech. J. 40, pp. 43-64, 1961.
6. U. Grenader and G. Szegö, *Toeplitz Forms and Their Applications*, Univ. of Cal. Press, 1958.

Electromagnetic pulse propagation in passive media by path integral methods

Sergei V. Shabanov[1]

Department of Mathematics, University of Florida, Gainesville, FL 32611, USA

Abstract

A novel time domain solver of Maxwell's equations in passive (dispersive and absorbing) media is proposed. The method is based on the path integral formalism of quantum theory and entails the use of (*i*) the Hamiltonian formalism and (*ii*) pseudospectral methods (the fast Fourier transform, in particular) of solving differential equations. In contrast to finite differencing schemes, the path integral based algorithm has no artificial numerical dispersion (dispersive errors), operates at the Nyquist limit (two grid points per shortest wavelength in the wavepacket) and exhibits an exponential convergence as the grid size increases, which, in turn, should lead to a higher accuracy. The Gauss law holds exactly with no extra computational cost. Each time step requires $O(N \log_2 N)$ elementary operations where N is the grid size. It can also be applied to simulations of electromagnetic waves in passive media whose properties are time dependent when conventional stationary (scattering matrix) methods are inapplicable. The stability and accuracy of the algorithm are investigated in detail.

[1]electronic mail: shabanov@phys.ufl.edu

1 Introduction

In this study a time domain solver of Maxwell's equation in passive (dispersive and absorbing) media is developed. The main motivation of this work is to bring methods of computational quantum physics into classical electromagnetic theory. One of the great advantages of time domain methods over stationary (scattering matrix) methods is that a single simulation of the scattering of a wide band wave packet can determine basic physical properties of the target (e.g., transmission and reflection coefficients) in the entire frequency band covered by the initial wave packet. Time domain methods also allow for a unique possibility to observe all immediate effects on fields caused by the target or by a surrounding passive medium, which greatly facilitates qualitative understanding of the interaction of an electromagnetic pulse with media and targets. Another important advantage is that the target geometry (or medium physical properties) may vary with time and this time dependence cannot be removed by going over to a moving reference frame. Stationary methods are simply inapplicable to these kind of problems.

From the computational point of view, the proposed approach is based on pseudospectral methods. The essential advantages of pseudospectral algorithms over conventional finite element or finite difference schemes in solving differential equations are [1]: (*i*) the exponential versus polynomial rate of convergence as the grid size (or the basis dimension) increases; (*ii*) the absence of dispersive errors and (*iii*) efficiency in numerical calculations. Time domain algorithms in combination with pseudospectral methods have become the state-of-the-art technique in numerical studies of quantum dynamics by solving the corresponding initial value problem for the Schrödinger equation (see, e.g., [2]). A typical algorithm entails an approximate computation of an object called the path integral (or functional integral) introduced by Feynman [4]. Here Maxwell's theory in general dispersive media is reformulated in the Schrödinger (Hamiltonian) formalism. Then the path integral formalism is applied to the initial value problem in Maxwell's theory in passive media to develop a numerical algorithm. The main objective of this work is to give a theoretical assessment of the path integral based solver of the initial value problem for Maxwell's equations. Numerical tests and applications will be discussed elsewhere [3].

It is shown here that basic principles of the path integral formalism lead to a true time domain algorithm which indeed enjoys the advantages of pseudospectral methods. In particular, among the aforementioned features, (*i*) is provided by the use of the fast Fourier method [5] as a part of the algorithm, (*ii*) is a consequence of Nelson's construction [6] of the path integral which is embedded in our algorithm, (*iii*) is due to the fast Fourier method and some analytical results that speed up numerical computations. The algorithm has another great advantage over finite difference schemes: The Gauss law is implemented exactly with no extra computational cost (Theorem 8.2). For widely used multi-resonant Lorentz models of passive media, the algorithm is unitary, meaning that, the energy of a wave packet is preserved exactly in dispersive media with no attenuation (Theorem 6.1). It is also unconditionally stable (Theorems 7.1 and 7.3) versus conditionally stable finite element

or finite difference algorithms [1] (see also [7]). A possible drawback of the algorithm (to be tested numerically) is that the use of the fast Fourier method in combination with Nelson's construction of the path integral might require additional computational costs for boundary value problems with complicated boundary geometry. In our approach, conventional boundary conditions are not imposed on electromagnetic fields. Targets and medium interfaces are modeled by discontinuous medium parameters. The problem arises from well known features of the Fourier method [5]: Aliasing and low convergence rates for non-smooth functions. In this study we offer one possible way to deal with this problem while keeping the Fourier basis in the algorithm. Alternative pseudospectral approaches to circumvent the problem exist and are mentioned here, but not discussed in detail.

The basic idea of the path integral approach to solving linear, homogeneous, evolutionary differential equations (numerically or analytically) is based on the Hamiltonian formalism. In the framework of the Hamiltonian formalism, an original system of differential equations is transformed to an equivalent system of first-order (in time) differential equations by expanding the original configuration space, that is, by going over to a generalized phase space where all time derivatives, save for the one of highest order, become independent variables [8]. A generic linear homogeneous first-order system can be written in the form

$$\partial_t \Psi_t = \mathcal{H}\Psi_t \ , \qquad \Psi_{t=0} = \Psi_0 \ , \tag{1.1}$$

where ∂_t stands for the partial derivative with respect to time t, a linear operator $\mathcal{H}$ is called Hamiltonian, while Ψ_t is called a state vector (or wave function). It is an element of the generalized phase space of the system and viewed as a collection (column) of the original variables and their time derivatives. The generalized phase space is equipped with an inner product and becomes a Hilbert space. State vectors are typically vector-valued functions in $\mathbb{R}^3$, and the Hamiltonian is a differential operator. The choice of the inner product depends on the problem at hand. One usually requires that componets of Ψ_t are elements of $\mathbb{L}_2(\mathbb{R}^3)$.

In general, upon going over to the Hamiltonian formalism, there might occur constraints [9, 10]

$$\mathcal{C}_a \Psi_t = 0 \ , \tag{1.2}$$

with $\mathcal{C}_a$ being a set of linear operators which do not contain time derivatives; a enumerates the constraint operators. The constraints must be preserved in the time evolution which is described by (1.1). In other words, the solution is sought in the subspace of the Hilbert space defined by (1.2). Depending on the type of constraints, there are different ways of developing the corresponding path integral formalism. In Maxwell's theory, the constraint is the Gauss law, and it is of the "first class" in the Dirac terminology [10]. The characteristic feature of a first class constrained system is that

$$[\mathcal{H}, \mathcal{C}_a] \sim \mathcal{C}_a \ , \qquad [\mathcal{C}_a, \mathcal{C}_b] \sim \mathcal{C}_c \ . \tag{1.3}$$

A consequence of (1.3) is that if the initial configuration Ψ_0 satisfies the constraints, then so does the solution of (1.1). However, after the projection of the Hilbert space spanned by Ψ_t

onto a finite-dimensional subspace (e.g., a projection on a subspace associated with a finite spatial grid as is done in Section 3), which is required for numerical simulations, the involution condition (1.3) can be violated causing problems in simulations. For instance, the Gauss law is typically violated in any finite differencing approach to simulations of electromagnetic wave packet propagation. Special efforts have to be made to ensure the transversality of the radiation field in Maxwell's theory, which, in turn, complicates simulation algorithms and increases computational costs (e.g., when enforcing the Gauss law in finite difference schemes on the grid via the Lagrange multiplier method). It is one of the advantages of the proposed path integral based algorithm that the Gauss law can be strictly enforced with no additional computational costs for generic passive media (Theorem 8.2).

The solution to Eq. (1.1) is

$$\Psi_t = \exp(t\mathcal{H})\,\Psi_0 \equiv \mathcal{U}_t\Psi_0\,, \quad t \geq 0\,, \tag{1.4}$$

assuming that the exponential of $\mathcal{H}$ exists. If the Hamiltonian is time dependent then the following replacement has to be made in (1.4)

$$\exp(t\mathcal{H}) \to T\exp\left(\int_0^t d\tau\mathcal{H}_\tau\right) = \mathcal{U}_t\,, \tag{1.5}$$

where $T\exp$ stands for the time-ordered exponential. The operator $\mathcal{U}_t$ is defined as the fundamental solution of (1.1), $\partial_t\mathcal{U}_t = \mathcal{H}_t\mathcal{U}_t$ with $\mathcal{U}_{t=0}$ being the identity operator. The fundamental solution has the semigroup property, $\mathcal{U}_{t_1+t_2} = \mathcal{U}_{t_1}\mathcal{U}_{t_2}$. The action of the evolution operator $\mathcal{U}_t$ on the initial configuration can be written via its integral kernel,

$$\Psi_t(\mathbf{r}) = \int_{\mathbb{R}^3} d\mathbf{r}'\mathcal{U}_t(\mathbf{r},\mathbf{r}')\Psi_0(\mathbf{r}')\,. \tag{1.6}$$

Using the semigroup property of the evolution operator, the entire time evolution can be viewed as consecutive actions of the infinitesimal evolution operator $\mathcal{U}_{\Delta t}$, where Δt is a time step. If the kernel of the infinitesimal evolution operator is known, then the kernel of the evolution operator can be computed as the convolution

$$\mathcal{U}_t(\mathbf{r},\mathbf{r}') = \int_{\mathbb{R}^3} d\mathbf{r}_1\cdots d\mathbf{r}_n\mathcal{U}_{\Delta t}(\mathbf{r},\mathbf{r}_n)\mathcal{U}_{\Delta t}(\mathbf{r}_n,\mathbf{r}_{n-1})\cdots\mathcal{U}_{\Delta t}(\mathbf{r}_1,\mathbf{r}') \tag{1.7}$$

with $\Delta t(n+1) = t$. The integration variables can be regarded as points $\mathbf{r}_k = \mathbf{r}(t_k)$, where $t_k = k\Delta t$, $k = 0, 1, ..., n+1$, on a path $\mathbf{r}(\tau)$ connecting points $\mathbf{r}(\tau = t) = \mathbf{r}$ and $\mathbf{r}(\tau = 0) = \mathbf{r}'$. In the limit $\Delta t \to 0$ the convolution (1.7) can be viewed as a sum over all paths connecting the initial and final points. This is the gist of the Feynman path integral representation of the fundamental solution of (1.1). A nontrivial problem is to find the measure on the space of paths. For example, if $\mathcal{H} = \Delta$ (the Laplace operator), it can be shown that the limit exists, and that the measure coincides with the Wiener measure which has support in the space of all continuous, but nowhere differentiable paths (trajectories of the Brownian motion) pinned at the end points. In quantum mechanics, the problem is more subtle, but

can still be solved [11]. The existence of the proper measure on the space of paths opens up an attractive possibility to use Monte-Carlo methods of computing the sum over paths which is the gold standard algorithm in quantum and statistical physics.

However, the present study does not intend to tackle the measure problem for the path integral representation of Maxwell's theory, but rather offers a solution of a more modest problem. Namely, how the conventional way, outlined above, of deriving the path integral from the original differential equation can be used to obtain an algorithm for numerical simulations of the convolution (1.7) for a small, but finite Δt. Similar ideas have been applied to non-dispersive and/or random media as well as to scattering problems and waveguides [12]. Our approach applies to general passive media and goes beyond the eikonal approximation of geometric optics and/or the diffraction theory used in earlier works on path integrals in electromagnetic theory. The results obtained here are believed to be useful for further development of path integral methods in theoretical and numerical studies of propagation of electromagnetic wave packets in passive media.

The idea of numerical simulations follows from (1.7) rather straightforwardly, namely,

$$\Psi_{t+\Delta t} = \mathcal{U}_{\Delta t}\Psi_t \ . \tag{1.8}$$

Thus, finding a state of the system in a sequential moment of time amounts to computing the action of the exponential of a differential operator $\mathcal{H}$ on the state at the preceding moment of time. Theoretically, it is sufficient to know $\mathcal{U}_{\Delta t}$ up to $(\Delta t)^2$. The limit $\Delta t \to 0$ in (1.7) would not change if we replace the exact infinitesimal evolution operator kernel by such an approximation. In numerical simulations, the limit is never achieved. Therefore a higher accuracy is required to make errors small. Note that the errors are accumulated as more iterations (1.8) are taken. An expansion of $\exp(\Delta t\mathcal{H})$ into the power series up to some desired order is known to produce unstable algorithms. Yet another obvious drawback is the lack of unitarity of the time evolution, that is, if the Hamiltonian is skew-symmetric (anti-Hermitian, if a complex phase space is used), $\mathcal{H}^* = -\mathcal{H}$, then $\mathcal{U}_t^*\mathcal{U}_t = 1$. In the Maxwell theory, as we shall see, the squared norm of Ψ_t with respect to the $\mathbb{L}_2(\mathbb{R}^3)$ scalar product $(\Psi_1, \Psi_2) = \int d\mathbf{r}\Psi_1^*\Psi_2$ is proportional to the electromagnetic energy of the system. Consequently, for non-absorbing media the unitarity of the time evolution is required in simulations to provide the energy conservation.

We shall apply Nelson's method of obtaining the path integral representation of the fundamental solution of Maxwell's equations for passive media. It is based on the Kato-Trotter product formula for the exponential of a sum of two noncommuting operators and the use of the Fourier basis to compute exponentials of differential operators. Actually, in practical applications, a simpler version, known as the Lie-Trotter product formula, is used (see the textbooks [13] for details and references therein). In computational quantum mechanics this is also known as the split operator method. It allows one to keep the differential operators in the exponential, and thereby, ensures the correct dispersion relation of simulated electromagnetic waves. It will be shown that there exists a particular realization of this idea in which the Gauss law holds exactly in simulations. In general, the Gauss law can be enforced by the

projection operator formalism developed for the path integral representation of constrained dynamical systems (for a review see [14] and references therein, a numerical application to constrained wave packet propagation can be found in [15]). The idea is to replace the Hamiltonian by its projection on the subspace (1.3). If $\mathcal{P}$ is the projection operator, that is, $\mathcal{C}_a\mathcal{P}\Psi = 0$ for any Ψ, $\mathcal{P}^2 = \mathcal{P}$ and $\mathcal{P}^* = \mathcal{P}$, then $\mathcal{H}$ is replaced by $\mathcal{PHP}$. In Maxwell's theory the projection can be implemented in our algorithm with no extra computational costs. A significant difference from the quantum mechanical case is that the Hamiltonian $\mathcal{H}$ (or its projection) is not normal, that is, it does not commute with its adjoint. This feature complicates the stability analysis because the von Neumann criteria is no longer sufficient for stability, while still being necessary [16]. Nevertheless, the stability, accuracy and convergence analysis of the algorithm can be carried out in rather general settings.

Since time domain simulations are performed on finite lattices, there is always a moment of time when the simulated signal first reaches the lattice boundary. One typically uses lattices with periodic boundary conditions. So, the pulse would appear on the other side of the lattice interfering with itself, thus leading to totally disastrous results for simulations. The problem is usually solved by introducing absorbing boundary conditions (see, e.g., [17] (for quantum mechanics) and [18] (for electrodynamics)). It is convenient to set a conducting layer at the grid boundary whose conductivity is chosen so that it neither transmits nor reflects within the designated accuracy in the frequency domain of the initial pulse. In Appendix we briefly describe how such a conducting layer can be obtained.

2 Maxwell theory in the Hamiltonian formalism

Dynamics of electromagnetic waves in continuous media is governed by Maxwell's equations

$$\partial_t \mathbf{D}_t = c\boldsymbol{\nabla} \times \mathbf{H}_t \tag{2.1}$$

$$\partial_t \mathbf{B}_t = -c\boldsymbol{\nabla} \times \mathbf{E}_t \,, \tag{2.2}$$

where c is the speed of light, boldface letters denote three-vector fields in $\mathbb{R}^3$ whose spatial arguments are suppressed and the time dependence is indicated by a subscript. No external currents and charges (antennas) are included in this study. However, the formalism being developed is readily generalized to the case when external time dependent sources are present. The electric and magnetic induction vectors, $\mathbf{D}_t$ and $\mathbf{B}_t$, respectively, are subject to the constraints (the Gauss law)

$$\boldsymbol{\nabla} \cdot \mathbf{D}_t = \boldsymbol{\nabla} \cdot \mathbf{B}_t = 0 \,. \tag{2.3}$$

In linear response theory, assumed through out the paper, the electric induction is related to the electric field as [19]

$$\mathbf{D}_t = \mathbf{E}_t + \int_{-\infty}^{t} d\tau \, \chi^e_{t-\tau} \mathbf{E}_\tau \equiv \mathbf{E}_t + \mathbf{P}_t \,, \tag{2.4}$$

where χ_t^e is an electric response function of the medium and $\mathbf{P}_t$ is the medium polarization vector. A similar relation can be written for the magnetic field and induction, $\mathbf{B}_t = \mathbf{H}_t + \mathbf{M}_t$, where magnetization $\mathbf{M}_t$ is determined by the applied magnetic field and the magnetic response function of the medium.

The relation between inductions and fields must be causal, meaning that the response of the medium, $\mathbf{P}_t$ and $\mathbf{M}_t$, can only depend on fields applied to the medium prior to the current time t, (e.g., $\chi_t^e = 0$ for $t < 0$) [19]. A natural way to ensure the causality is to require that the response function satisfies a differential equation. In other words, the response function is assumed to be the fundamental solution of some time evolution differential equation. This differential equation can be obtained from a particular physical model of the medium in question. A popular model is the multi-resonant Lorentz model. Let $\tilde{\mathbf{D}}_\omega$ and $\tilde{\mathbf{E}}_\omega$ be the Fourier transforms of the electric induction and field. Then from (2.4) it follows that $\tilde{\mathbf{D}}_\omega = \varepsilon_\omega \tilde{\mathbf{E}}_\omega$. The dielectric constant in the Lorentz model has the form

$$\varepsilon_\omega = 1 + \sum_{a=1}^{N} \frac{\omega_{pa}^2}{\omega_a^2 - \omega^2 - 2i\gamma_a\omega} , \tag{2.5}$$

and $\mathbf{M}_t = \mathbf{0}$. The physical meaning of the model is transparent. The medium is assumed to be made of N sorts of damped harmonic oscillators with resonant frequencies ω_a and damping coefficients γ_a. Parameters ω_{pa}, called the plasma frequencies, are proportional to coupling constants of the oscillators to the external electric field (the electric dipole coupling) and also depend on the density of oscillators of the sort a. The density may vary in space. So ω_{pa} are assumed to be functions of spatial coordinates. In an empty space, $\omega_{pa} = 0$. If the resonant frequency is zero, the one-resonant Lorentz model is equivalent to the Drude model of metals [19]. In the Lorentz medium the magnetic response function is zero, while the electric response function can easily be found by taking the Fourier transform of (2.5). Its explicit form is omitted here because it will not be used. The medium polarization is determined by a set of second-order differential equations

$$\partial_t^2 \mathbf{P}_t^a + 2\gamma_a \partial_t \mathbf{P}_t^a + \omega_a^2 \mathbf{P}_t^a = \omega_{pa}^2 \mathbf{E}_t , \qquad \mathbf{P}_t = \sum_{a=1}^{N} \mathbf{P}_t^a . \tag{2.6}$$

Together with Maxwell's equations, Eq. (2.6) form a system of sought-for causal evolution equations which are to be transformed into a system of first order equations by means of the Hamiltonian formalism. In finite difference time domain numerical schemes, the Hamiltonian formalism for the Lorentz model has been used in [20] to study propagation of an electromagnetic pulse in homogeneous Lorentz media.

In our approach no boundary conditions are imposed on electromagnetic fields at medium and/or target interfaces. The latter are modeled by spatially dependent couplings of media to electromagnetic fields which are included into the system Hamiltonian. At any interface, the couplings are allowed to have discontinuities, or, from a physical point of view, they remain smooth but change rapidly, $\lambda_w |\nabla \omega_p| / \omega_p \gg 1$, at the interface, where λ_w is a typical wave

length of the incoming wave packet. The conventional boundary conditions are automatically generated by the dynamics [19]. Thus, the initial value problem is solved in $\mathbb{L}_2(\mathbb{R}^3)$ for every matter and electromagnetic field component. This implies that the energy of the propagating wave packet remains finite (in contrast to the scattering matrix approach based on plane wave solutions).

Let us now formulate the initial value problem for a generic passive medium and then apply the formalism to multi-resonant Lorentz models. Combine the fields, inductions and medium responses into columns:

$$\psi_t^F = \begin{pmatrix} \mathbf{E}_t \\ \mathbf{H}_t \end{pmatrix} , \quad \psi_t^I = \begin{pmatrix} \mathbf{D}_t \\ \mathbf{B}_t \end{pmatrix} , \quad \psi_t^R = \begin{pmatrix} \mathbf{P}_t \\ \mathbf{M}_t \end{pmatrix} .$$

Assuming linear response theory, one can write for the Fourier transforms

$$\tilde{\psi}_\omega^R = \tilde{\chi}_\omega \tilde{\psi}_\omega^F , \tag{2.7}$$

where the Fourier transform of a general response function, $\tilde{\chi}_\omega$, has to satisfy a dispersion relation that ensures causality (like the Kramer-Kronig relations for the dielectric constant) [19]. For anisotropic media, $\tilde{\chi}_\omega$ is a symmetric matrix acting on components of electromagnetic fields. With this type of generality all possible media are covered as long as linear response theory is valid. The response function $\tilde{\chi}_\omega$ can either be modeled or measured and tabulated in some frequency range of interest (determined by the frequency bandwidth of the initial wavepacket), say, $\omega \in [\omega_1, \omega_2]$. Next, the components of $\tilde{\chi}_\omega^{-1}$ are expanded in a basis of suitable orthogonal polynomials. An optimal expansion is often achieved in the Chebyshev polynomial basis. Chebyshev polynomials are defined in the interval $[-1, 1]$ so a corresponding rescaling and translation of $[\omega_1, \omega_2]$ must be done. By taking the Fourier transform of $\tilde{\chi}_\omega^{-1} \tilde{\psi}_\omega^R = \tilde{\psi}_\omega^F$ we obtain the desired differential equation

$$\sum_{n=0}^{N} \chi_n \partial_t^n \psi_t^R = \omega_p \psi_t^F , \tag{2.8}$$

where $\omega_p = \omega_p(\mathbf{r})$ plays the role of the coupling constant between matter and electromagnetic fields. The order N is determined by the highest order of polynomials used to approximate $\tilde{\chi}_\omega^{-1}$. The expansion coefficients χ_n and the coupling ω_p are matrices for anisotropic media.

The basic idea of the Hamiltonian formalism is to convert the system (2.6) or (2.8) into a system of first-order differential equations by introducing auxiliary (matter) fields. The number of such fields is determined by the order of the original evolution equation for matter. For instance, in the case of the multi-resonant Lorentz model, there are N fields $\mathbf{P}_t^a$ each of which satisfies a second order differential equation. In the Hamiltonian formalism one would have $2N$ real vector fields, $\boldsymbol{\xi}_t^j$, $j = 1, 2, ..., 2N$. A simple possibility is to set

$$\mathbf{P}_t^a = (\omega_{pa}/\omega_a)\, \boldsymbol{\xi}_t^{2a-1} , \tag{2.9}$$

$$\partial_t \boldsymbol{\xi}_t^{2a-1} = \omega_a \boldsymbol{\xi}_t^{2a} , \tag{2.10}$$

$$\partial_t \boldsymbol{\xi}_t^{2a} = -2\gamma_a \boldsymbol{\xi}_t^{2a} - \omega_a \boldsymbol{\xi}_t^{2a-1} + \omega_{pa} \mathbf{E}_t . \tag{2.11}$$

The reasor of inserting the factor ω_{pa}/ω_a in the definition (2.9) of the auxiliary fields will be evident from what follows. Note that the medium polarization $\mathbf{P}_t$ must be zero in empty space where $\omega_{pa} = 0$. The factor ω_a^{-1} in (2.9) simplifies the energy conservation and stability analysis.

For the Lorentz model there is another convenient way to introduce the Hamiltonian formalism by using N complex vector fields $\boldsymbol{\zeta}_t^a$ which satisfy the first order differential equation

$$\partial_t \boldsymbol{\zeta}_t^a = \lambda_a \boldsymbol{\zeta}_t^a - i\omega_{pa}\mathbf{E}_t \,, \tag{2.12}$$

$$\mathbf{P}_t^a = \frac{\omega_{pa}}{2\nu_a}\left(\boldsymbol{\zeta}_t^a + \bar{\boldsymbol{\zeta}}_t^a\right) \,, \tag{2.13}$$

where $\lambda_a = -\gamma_a + i\nu_a$ and $\nu_a = \sqrt{\omega_a^2 - \gamma_a^2}$. This representation is defined only if $\gamma_a < \omega_a$ (i.e., the attenuation is not high). From the numerical point of view, solving a *decoupled* system of N first order differential equation and taking complex conjugation (denoted here by an over bar) is less expensive than solving an original system of differential equations to compute the medium polarization.

Returning to the general case, we introduce a set of auxiliary fields ξ_t to convert (2.8) into a first-order system,

$$\partial_t \xi_t = \mathcal{H}_M^F \xi_t + \mathcal{V}_{MF}\psi_t^F \,. \tag{2.14}$$

The operators $\mathcal{H}_M^F$ and $\mathcal{V}_{MF}$ are determined by the details of going over to the Hamiltonian formalism. We shall call $\mathcal{H}_M^F$ the matter Hamiltonian; it governs time evolution of the medium when no external fields are applied. The index F indicates that the electromagnetic degrees of freedom are described by fields, not inductions. We shall see shortly that the matter Hamiltonian depends on whether ψ_t^I or ψ_t^F is used as independent electromagnetic variables. The matrix $\mathcal{V}_{MF}$ describes the coupling of matter to the electromagnetic fields, which is emphasized by the index MF (matter-to-field coupling). We introduce a linear time independent operator $\mathcal{R}$ that acts in the space of auxiliary (matter) fields so that

$$\psi_t^R = \mathcal{R}\xi_t \,, \tag{2.15}$$

that is, the (response) operator $\mathcal{R}$ maps a given configuration of auxiliary fields onto the corresponding physical response field. It depends on the definition of the matter fields (cf. (2.9) and (2.13)). A passive medium is not excited, $\xi_t = 0$, if no external electromagnetic field is applied; that is, the initial condition for Eq. (2.14) is such that it has only the trivial solution whenever $\psi_t^F = 0$. Under this condition, the solution of (2.14) reads

$$\xi_t = \int_{-\infty}^{t} d\tau e^{(t-\tau)\mathcal{H}_M^F}\mathcal{V}_{MF}\psi_\tau^F \,.$$

Hence, the linear response operator $\tilde{\chi}_\omega$ in (2.7) is the Fourier transform of the operator $\chi_t = \theta_t \mathcal{R}\exp(t\mathcal{H}_M^F)\mathcal{V}_{MF}$, where θ_t is the Heaviside function. Or, vice versa, $\mathcal{R}$, $\mathcal{H}_M^F$ and $\mathcal{V}_{MF}$ must be chosen so that the Fourier transform of χ_t coincides with the known response function $\tilde{\chi}_\omega$ of the medium in a designated frequency range.

Maxwell's equations without external currents can be rewritten in the Hamiltonian form

$$\partial_t \psi_t^F = \mathcal{H}_F \psi_t^F - \partial_t \psi_t^R = \mathcal{H}_F \psi_t^F + \mathcal{V}_{FM} \xi_t \,. \tag{2.16}$$

The field-to-matter coupling $\mathcal{V}_{FM}$ and the field Hamiltonian $\mathcal{H}_F$ are deduced from (2.14) by acting on the latter by the operator $\mathcal{R}$, which yields

$$\mathcal{V}_{FM} = -\mathcal{R}\mathcal{H}_M^F \,, \tag{2.17}$$

$$\mathcal{H}_F = \begin{pmatrix} 0 & c\boldsymbol{\nabla}\times \\ -c\boldsymbol{\nabla}\times & 0 \end{pmatrix} - \mathcal{R}\mathcal{V}_{MF} \equiv \mathcal{H}_0 - \mathcal{R}\mathcal{V}_{MF} \,. \tag{2.18}$$

It is always possible to set up the Hamiltonian formalism so that $\mathcal{R}\mathcal{V}_{MF} \equiv 0$ and, hence, $\mathcal{H}_F = \mathcal{H}_0$. It is not difficult to verify that this holds for the Lorentz model discussed above. In the general case, the standard procedure of going over to the Hamiltonian formalism [8], where components of ξ_t are identified with time derivatives of the response field, $\xi_t^k \sim \partial_t^k \psi_t^R$, leads to the same result that $\mathcal{R}\mathcal{V}_{MF} = 0$. Thus, without loss of generality, the last term in the field Hamiltonian (2.18) can be omitted.

The auxiliary matter and electromagnetic fields (or inductions) are unified into a larger column

$$\Psi_t^F = \begin{pmatrix} \psi_t^F \\ \xi_t \end{pmatrix} \,, \quad \Psi_t^I = \begin{pmatrix} \psi_t^I \\ \xi_t \end{pmatrix} \,. \tag{2.19}$$

The wave function Ψ_t^F satisfies the Schrödinger equation

$$\partial_t \Psi_t^F = \mathcal{H}^F \Psi_t^F \,, \quad \mathcal{H}^F = \begin{pmatrix} \mathcal{H}_0 & \mathcal{V}_{FM} \\ \mathcal{V}_{MF} & \mathcal{H}_M^F \end{pmatrix} \,. \tag{2.20}$$

which has to be solved with the initial field configuration $\psi_{t=0}^F = \psi_0$, while the matter fields are assumed to be zero at the initial moment of time, $\xi_{t=0} = 0$, e.g., the initial wave packet is localized in an empty space region. Equations (2.14) and (2.16) are equivalent to (2.20). In a similar fashion, one can derive the Schrödinger equation for Ψ_t^I. Note that

$$\Psi_t^I = \mathcal{S}\Psi_t^F \,, \quad \mathcal{S} = \begin{pmatrix} 1 & \mathcal{R} \\ 0 & 1 \end{pmatrix} \,, \quad \mathcal{S}^{-1} = \begin{pmatrix} 1 & -\mathcal{R} \\ 0 & 1 \end{pmatrix} \,, \tag{2.21}$$

Hence,

$$\partial_t \Psi_t^I = \mathcal{H}^I \Psi_t^I \,, \quad \mathcal{H}^I = \mathcal{S}\mathcal{H}^F \mathcal{S}^{-1} \,. \tag{2.22}$$

The corresponding blocks of $\mathcal{H}^I$ have the form

$$\mathcal{H}_I = \mathcal{H}_0 \,, \quad \mathcal{V}_{MI} = \mathcal{V}_{MF} \,, \tag{2.23}$$

$$\mathcal{V}_{IM} = \mathcal{V}_{FM} + \mathcal{R}\mathcal{H}_M - \mathcal{H}_0\mathcal{R} = -\mathcal{H}_0\mathcal{R} \,, \tag{2.24}$$

$$\mathcal{H}_M^I = \mathcal{H}_M^F - \mathcal{V}_{MF}\mathcal{R} \,. \tag{2.25}$$

To simplify $\mathcal{V}_{IM}$, Eq. (2.17) has been applied. Observe in (2.25) the aforementioned dependence of the matter Hamiltonian on the representation of electromagnetic degrees of

freedom. The use of either (2.20) or (2.22) in numerical simulations has its own advantages and disadvantages which are discussed below.

As an example, we give an explicit form of the Hamiltonian for the Lorentz model when the auxiliary field are defined by (2.9)

$$\mathcal{V}_{FM} = (\mathcal{V}_{FM1}, \mathcal{V}_{FM2}, \cdots, \mathcal{V}_{FMN}) , \quad \mathcal{V}_{FMa} = \begin{pmatrix} 0 & -\omega_{pa} \\ 0 & 0 \end{pmatrix} , \tag{2.26}$$

$$\mathcal{V}_{MF} = -\mathcal{V}_{FM}^{*} , \tag{2.27}$$

$$\mathcal{H}_{M}^{F} = \mathsf{diag}\ (\mathcal{H}_{M1}^{F}, \mathcal{H}_{M2}^{F}, \cdots, \mathcal{H}_{MN}^{F}) , \quad \mathcal{H}_{Ma}^{F} = \begin{pmatrix} 0 & \omega_a \\ -\omega_a & -2\gamma_a \end{pmatrix} , \tag{2.28}$$

where **diag** indicates that the corresponding matrix is block-diagonal with blocks listed in the order from the upper left to lower right corners. Note that the matrices $\mathcal{V}_{FMa}$ and $\mathcal{H}_{FMa}$ act on a six-dimensional column $(\xi_t^{2a-1}, \xi_t^{2a})^*$. Therefore they should be understood as composed of 3×3 blocks. Each block is obtained by multiplying the unit matrix by the number indicated in place of the block in (2.26) and (2.28).

Our final remark in this section concerns "canonical" transformations in the Hamiltonian formalism. As has been pointed out, the auxiliary fields are not uniquely defined. There is a freedom of making general complex nonsingular linear transformations such as

$$\xi_t \to \mathcal{S}_M \xi_t , \quad \det \mathcal{S}_M \neq 0 . \tag{2.29}$$

If the infinitesimal evolution operator $\mathcal{U}_{\Delta t}^{(F,I)} = \exp(\Delta t \mathcal{H}^{(F,I)})$ is computed with one choice of the auxiliary fields, a simple similarity transformation, like the one in (2.22), would allow us to compute it in any other basis of auxiliary fields. This is an important observation because the auxiliary field basis can be chosen in a way that facilitates computation of the evolution operator (e.g., to improve the convergence rate or speed up simulations). For instance, in the complex representation (2.13) of the auxiliary fields in the Lorentz model, the matter Hamiltonian is diagonal. The corresponding transformation of the auxiliary fields is given by

$$\begin{pmatrix} \xi_t^{2a-1} \\ \xi_t^{2a} \end{pmatrix} = \frac{1}{2\nu_a} \begin{pmatrix} \omega_a & \omega_a \\ \lambda_a & \bar{\lambda}_a \end{pmatrix} \begin{pmatrix} \zeta_t^a \\ \bar{\zeta}_t^a \end{pmatrix} \equiv \mathcal{S}_M \begin{pmatrix} \zeta_t^a \\ \bar{\zeta}_t^a \end{pmatrix} . \tag{2.30}$$

To transform the whole system into this representation, the Hamiltonian $\mathcal{H}^F$ is replaced by $\mathcal{S}^{-1}\mathcal{H}^F\mathcal{S}$ and the wave function Ψ_t^F by $\mathcal{S}\Psi_t^F$ where $\mathcal{S}$ is block-diagonal with the unit matrix in the upper left (field) corner and with $\mathcal{S}_M$ in the lower right (matter) corner.

3 The grid representation of Maxwell's theory

Consider an equidistantly spaced finite grid with periodic boundary conditions. Let Δr be the grid step and $\mathbf{n}$ be a vector with integer valued components. Then the dynamical

variables are projected onto the grid by taking their values at grid points $\mathbf{r} = \mathbf{n}\Delta r$,

$$\Psi_t^Q(\mathbf{r}) \to \Psi_t^Q(\mathbf{n}\Delta r) \,, \tag{3.1}$$

where Q denotes the representation, I or F. For simplicity, a cubic grid is assumed here. It is straightforward to generalize the discussion to a generic rectangular grid. Consider a discrete Fourier transformation associated with the grid [5, 21]

$$\tilde{\Psi}_t^Q(\mathbf{n}k_0) = \sum_{\mathbf{n}'} \mathcal{F}_{\mathbf{n}\mathbf{n}'} \Psi_t^Q(\mathbf{n}'\Delta r) \,, \quad \mathcal{F}^*\mathcal{F} = \mathcal{F}\mathcal{F}^* = 1 \,, \tag{3.2}$$

where the dual lattice step is $k_0 = 2\pi/\Delta r$. The grid spatial size L and step must be chosen so that the Fourier transform of the initial wavepacket has support within the region $k \in [k_{min}, k_{max}]$ where $k = |\mathbf{k}|$, $k_{max} = k_0$ and $k_{min} = 2\pi/L$. The Hamiltonian $\mathcal{H}^Q$ is split into a sum

$$\mathcal{H}^Q = \mathcal{H}_0^Q + \mathcal{V}^Q \,, \tag{3.3}$$

where all the spatial derivatives are included into $\mathcal{H}_0^Q$ and $\mathcal{V}^Q$ contains multiplications by position dependent functions. This is always possible for the Hamiltonian described in the preceding section. The operator $\mathcal{V}^Q$ is projected naturally

$$\mathcal{V}^Q(\mathbf{r})\Psi_t^Q(\mathbf{r}) \to \mathcal{V}^Q(\mathbf{n}\Delta r)\Psi_t^Q(\mathbf{n}\Delta r) \,. \tag{3.4}$$

Consider $\mathcal{H}_0^Q$ in the Fourier basis, $\mathcal{H}_0^Q(\boldsymbol{\nabla}) \to \mathcal{H}_0^Q(i\mathbf{k})$. The projection is then done via the discrete Fourier transform

$$\mathcal{H}_0^Q(\boldsymbol{\nabla})\Psi_t^Q(\mathbf{r})\Big|_{\mathbf{r}=\mathbf{n}\Delta r} \to \sum_{\mathbf{n}'} (\mathcal{F}^*)_{\mathbf{n}\mathbf{n}'} \mathcal{H}_0^Q(i\mathbf{n}'k_0)\tilde{\Psi}_t^Q(\mathbf{n}'k_0) \,. \tag{3.5}$$

The projection (3.5) as well as any action of $\mathcal{H}_0^Q$ on state vectors is performed by the fast Fourier method [5]. It requires $N \log_2 N$ elementary operations (flops) with N being the grid size.

In what follows, the rules (3.4) and (3.5) *define* the action of the operators $\mathcal{V}^Q$ and $\mathcal{H}_0^Q$ and their functions on any state vector. The action of a product of $\mathcal{V}^Q$ and $\mathcal{H}_0^Q$ on any state vector is understood as consecutive actions of these operators according to the rules (3.4) and (3.5), in the order specified in the product.

In finite differencing schemes, the action of $\mathcal{H}_0^Q$ on a state vector would require mN_d operations where the integer m depends on a particular difference scheme used to approximate derivatives, and N_d is the grid size used in the differencing scheme. It should be noted that, as shown below, the use of the fast Fourier transform eliminates the phase error (because the correct electromagnetic dispersion relation is preserved) and operates at the Nyquist limit. These two features allows one to reduce substantially the grid size as compared with that in a finite differencing scheme, while providing the same accuracy in simulations. Recall that, in scattering problems, the phase of the return signal contains the most significant information

about the target. So, in practice, grids in finite differencing schemes are significantly larger (more dense) than grids used in the fast Fourier method in order to reduce the phase errors in the former. Needless to say, the advantage of the fast Fourier method in reducing the phase error becomes even more significant in higher dimensions because $N_d/N = (n_d/n)^D$ where n_d and n are the corresponding numbers of grid points per shortest wave length in the wave packet, and D is the grid dimension. The Nyquist limit is $n = 2$, while n_d is of order 10 or higher.

4 The split operator method

Let $|\Psi|$ denote the $\mathbb{L}_2(\mathbb{R}^3)$ norm of the wave function, or the Euclidean norm of the corresponding vector (3.1) in the grid representation. One possible way to compute numerically the path integral (1.7) is based on the Kato-Trotter product formula [13]

$$\lim_{n\to\infty} \left| e^{t(\mathcal{A}+\mathcal{B})}\Psi - \left(e^{t\mathcal{A}/2n} e^{t\mathcal{B}/n} e^{t\mathcal{A}/2n}\right)^n \Psi \right| = 0 \,, \tag{4.1}$$

for a general Ψ and under certain assumptions about the linear operators $\mathcal{A}$ and $\mathcal{B}$ in the Hilbert space spanned by Ψ. For our purposes it is sufficient to note that for bounded operators, (4.1) always holds and is known as the Lie-Trotter product formula. In the grid representation, which would always be assumed, unless stated otherwise, operators $\mathcal{A}$ and $\mathcal{B}$ are finite matrices and, hence, bounded.

Let us apply (4.1) to the split (3.3), meaning that the operator $\mathcal{H}_0^Q$ is used in place of $\mathcal{A}$ (or $\mathcal{B}$) and, respectively, the operator $\mathcal{V}^Q$ is used in place of $\mathcal{B}$ (or $\mathcal{A}$). The infinitesimal evolution operator in (1.8) can be approximated by the first term in the following expansion

$$\mathcal{U}_{\Delta t}^Q = e^{\Delta t(\mathcal{A}+\mathcal{B})} = \mathcal{G}_{\Delta t}^Q + \Delta t^3 \mathcal{W}_{\Delta t} \tag{4.2}$$

$$\mathcal{G}_{\Delta t}^Q = e^{\Delta t\mathcal{A}/2} e^{\Delta t\mathcal{B}} e^{\Delta t\mathcal{A}/2} \tag{4.3}$$

$$\mathcal{W}_{\Delta t} = -\frac{1}{24}\left([\mathcal{A},[\mathcal{A},\mathcal{B}]] - 2[\mathcal{B},[\mathcal{B},\mathcal{A}]]\right) + O(\Delta t) \,. \tag{4.4}$$

By making n larger while keeping $n\Delta t = t$ fixed, the strong convergence in (4.1) guarantees that the error can be made arbitrary small for any initial state,

$$|(\mathcal{U}_{\Delta t}^Q)^n \Psi_0 - (\mathcal{G}_{\Delta t}^Q)^n \Psi_0| \to 0 \tag{4.5}$$

as $n \to \infty$ for any Ψ_0. The numerical iteration algorithm is then based on the replacement of the exact evolution (1.8) by the approximate one

$$\Psi_{t+\Delta t}^Q = \mathcal{G}_{\Delta t}^Q \Psi_t^Q \,. \tag{4.6}$$

The quantity $t\Delta t^2 |\mathcal{W}_0^Q \Psi_0|/|\Psi_0|$ can be used to roughly estimate the accuracy of the algorithm. A more detailed accuracy analysis is given in Section 8. By making use of the

Campbell-Hausdorf formula for the exponential of the sum of operators it is possible to obtain the symmetric product formula in (4.2) to approximate $\mathcal{U}_{\Delta t}$ up to any desired order in Δt, presumably achieving a higher accuracy [22]. This would come at the price of having more exponentials in the symmetric product $\mathcal{G}^Q_{\Delta t}$. In numerical simulations, one should keep in mind that computational costs of decreasing Δt in the third order split (4.2) (i.e., increasing the number of steps in the time evolution) might be less than those of computing a lesser number of actions of $\mathcal{G}^Q_{\Delta t}$ in higher order splits. So, the higher order splits are not always optimal to achieve a better accuracy [2].

On the grid, the action of the amplification operator $\mathcal{G}^Q_{\Delta t}$ is computed according to the rules (3.4) and (3.5) applied to, respectively, $\exp(\Delta t \mathcal{V}^Q)$ and $\exp(\Delta t \mathcal{H}^Q_0)$. Explicit formulas for the exponentials of the corresponding operators can be worked out in the field and induction representations. If the fields are used as independent variables, then a natural choice is

$$\mathcal{H}^F = \mathcal{H}^F_0 + \mathcal{V}^F = \begin{pmatrix} \mathcal{H}_0 & 0 \\ 0 & \mathcal{H}^F_M \end{pmatrix} + \begin{pmatrix} 0 & \mathcal{V}_{FM} \\ \mathcal{V}_{MF} & 0 \end{pmatrix} . \tag{4.7}$$

The matter Hamiltonian $\mathcal{H}^F_M$ can also be transferred into $\mathcal{V}^F$ if so desired. This rearrangement affects the accuracy of the method, meaning that the operator (4.4) would change. In turn, a rearrangement of operators in the split can be used to improve the accuracy. We shall discussed this issue later. Using the Taylor series we infer that

$$\exp(t\mathcal{H}^F_0) = \begin{pmatrix} \exp(t\mathcal{H}_0) & 0 \\ 0 & \exp(t\mathcal{H}^F_M) \end{pmatrix} , \tag{4.8}$$

$$\exp(t\mathcal{H}_0) = 1 + \left[\cos(ct\sqrt{-\Delta}) - 1\right] \mathcal{P}_\perp + \frac{\sin\left(ct\sqrt{-\Delta}\right)}{c\sqrt{-\Delta}} \mathcal{H}_F , \tag{4.9}$$

where $\Delta = \boldsymbol{\nabla} \cdot \boldsymbol{\nabla}$ is the Laplace operator and $\mathcal{P}_\perp = 1 - \boldsymbol{\nabla}(\Delta^{-1}\boldsymbol{\nabla}\cdot\ )$ is the projector on transverse fields, that is, $\mathcal{P}_\perp \mathbf{E} = \mathbf{E}$ if $\boldsymbol{\nabla} \cdot \mathbf{E} = 0$ and $P_\perp \mathbf{E} = 0$ if the vector field $\mathbf{E}$ is conservative, $\mathbf{E} = \boldsymbol{\nabla}\phi$. The projector $\mathcal{P}_\perp$ can be omitted in (4.9) if it is known (e.g. from a theoretical analysis of the system) that the fields remain transversal in due course. In this case, the two first terms in (4.9) are equal to $\cos(ct\sqrt{-\Delta})$. The action of $\exp(t\mathcal{H}_0)$ is computed by the fast Fourier transform according to (3.5). In the Fourier basis, $-\Delta = \mathbf{k}^2 = \mathbf{n}^2 k_0^2$. Note also that the Fourier transform of the fields ψ^F_t is required, while the auxiliary fields remain in the grid basis all the time. The exponentials of $\mathcal{H}^F_M$ and $\mathcal{V}^F$ can either be computed analytically for simple models like the Lorentz model, as is shown Section 5, or, in general case, by direct diagonalization at each grid site.

Alternatively, the following approximation of the exponential of an operator can be used

$$e^{\Delta t \mathcal{B}} = \frac{1 + \Delta t\mathcal{B}/2 + \Delta t^2 \mathcal{B}^2/12}{1 - \Delta t\mathcal{B}/2 + \Delta t^2 \mathcal{B}^2/12} + O(\Delta t^5) = \frac{1 + \Delta t\mathcal{B}/2}{1 - \Delta t\mathcal{B}/2} + O(\Delta t^3) . \tag{4.10}$$

If the matrix $\mathcal{B}$ is anti-hermitian, then the approximations (4.10) of the exponential of $\mathcal{B}$ retain unitarity, which is important for stability of the split algorithm (see Theorems 7.1

and 7.3). On the other hand, costs of computing the inverse matrices in the right hand side of (4.10) can be less than those of computing the exponential.

If the inductions are used as independent variables, then a natural choice of the split would be

$$\mathcal{H}^I = \mathcal{H}_0^I + \mathcal{V}^I = \begin{pmatrix} \mathcal{H}_0 & -\mathcal{H}_0\mathcal{R} \\ 0 & 0 \end{pmatrix} + \begin{pmatrix} 0 & 0 \\ \mathcal{V}_{MI} & \mathcal{H}_M^I \end{pmatrix} . \tag{4.11}$$

Making use of the Taylor expansion again we deduce that

$$\exp(t\mathcal{H}_0^I) = \begin{pmatrix} \exp(t\mathcal{H}_0) & [1 - \exp(t\mathcal{H}_F)]\,\mathcal{R} \\ 0 & 1 \end{pmatrix} . \tag{4.12}$$

and, similarly,

$$\exp(t\mathcal{V}^I) = \begin{pmatrix} 1 & 0 \\ (\mathcal{H}_M^I)^{-1}[\exp(t\mathcal{H}_M^I) - 1]\mathcal{V}_{MI} & \exp(t\mathcal{H}_M^I) \end{pmatrix} . \tag{4.13}$$

Now we can compare the two splits. The split (4.7) has an advantage over (4.11) because it requires less calls of the fast Fourier transform. Indeed, in the former the fast Fourier transform is called only for the fields ψ_t^F. As it follows from (4.12), the operator $\exp(t\mathcal{H}_0)$ acts on both the inductions ψ_t^I and the auxiliary fields. Hence the fast Fourier transform must be called for the entire column Ψ_t^I. If the number of auxiliary fields is large, there might be a substantial difference in the computational speed of two algorithms. The latter, however, depends on the choice of the matter fields which, in turn, determines $\mathcal{R}$ and therefore the number of calls of the fast Fourier transform. Note that the matter fields can always be chosen in such a way that only one of the components of ξ_t specifies the response field ψ_t^R. Thus, the canonical transformation (2.29) can be used to reduce the number of calls of the fast Fourier transform. If $\mathcal{R}$ is chosen so that it depends on position, multiplication of the matter fields by $\mathcal{R}$ must be done before calling the fast Fourier transform. A significant advantage of the split in the induction representation is that the Gauss law can be exactly fulfilled without altering the algorithm (see Theorem 8.2).

In empty space either of the splits reproduces an *exact* solution of Maxwell's equations for any period of time t, provided the initial pulse is bandwidth limited. Indeed, on the grid, the initial wave packet is a superposition of a finite number of plane waves. Thanks to the linearity of the theory, each Fourier mode is evolved exactly, that is, *without* any phase error, by $\exp(t\mathcal{H}_0)$ for any $t > 0$. As final remarks in this section, we note that the algorithm can operate at the Nyquist limit: Two grid points per shortest wavelength in the initial wave packet [5]. Yet, for the multiresonant Lorentz model, it is *unconditionally* stable (see Theorems 7.1 and 7.3). These features cannot be achieved in any finite difference scheme.

5 A multi-resonant Lorentz model

An analytical expression for the exponents of $\mathcal{H}^Q_M$ and $\mathcal{V}^Q$ helps to reduce computational costs. Here such analytical expressions are derived for multi-resonant Lorentz models. Let us take first the field representation. Due to the block diagonal structure of $\mathcal{H}^F_M$ we get

$$\exp(t\mathcal{H}^F_M) = \mathsf{diag}\left(\exp(t\mathcal{H}^F_{M1}),\, \exp(t\mathcal{H}^F_{M2}),\, \cdots,\, \exp(t\mathcal{H}^F_{MN})\right) , \tag{5.14}$$

$$\exp(t\mathcal{H}^F_{Ma}) = e^{-\gamma_a t}\left[\cosh\tilde{\nu}_a t + \frac{\sinh\tilde{\nu}_a t}{\tilde{\nu}_a}\left(\mathcal{H}^F_{Ma} + \gamma_a\right)\right] , \tag{5.15}$$

where $\tilde{\nu}_a = (\gamma_a^2 - \omega_a^2)^{1/2}$. The exponential (5.15) is easy to compute by expanding $\mathcal{H}^F_{Ma}$ in the Pauli matrix basis, which is also a basis for the Lie algebra $su(2)$, and then by using the well known formula for the exponential of a linear combination of Pauli matrices. For small attenuation, $\gamma_a < \omega_a$, we get $\tilde{\nu}_a = i\nu_a$. The hyperbolic functions in (5.15) become trigonometric ones and $\tilde{\nu}_a$ is replaced by ν_a. The eigenvalues of the matter Hamiltonian are $\lambda_a = -\gamma_a \pm \tilde{\nu}_a$. Hence, $\mathrm{Re}\,\lambda_a < 0$ and amplitudes of the matter fields are always exponentially attenuated as $t \to \infty$, unless $\gamma_a = 0$ leading to $\mathrm{Re}\,\lambda_a = 0$.

Computation of $\exp(t\mathcal{V}^F)$ is a bit more subtle. We start with the observation that the characteristic polynomial of $\mathcal{V}^F$ has a simple form

$$\det\left(\mathcal{V}^F - \lambda\right) = \lambda^{2N}(\lambda^2 + \omega_p^2) , \qquad \omega_p^2 = \sum_{a=1}^{N} \omega_{pa}^2 . \tag{5.16}$$

This can be proved either by a direct computation or by mathematical induction. So, $\mathcal{V}^F$ has $2N$ zero eigenvalues and two non-zero ones, $\lambda = \pm i\omega_p$. Let X be the eigenvector of $\mathcal{V}^F$ corresponding to the eigenvalue $i\omega_p$. Its components have the form

$$X_j = \omega_p^{-1}\left[\mathcal{V}^F_{j1} + i\omega_p\delta_{j1}\right] , \quad j = 1, 2, ..., 2(N+1) ,$$

so that $\bar{X}\cdot X = 1$ and $\bar{X}\cdot\bar{X} = X\cdot X = 0$ where the dot denotes the Euclidean scalar product. The skew-symmetric matrix $\mathcal{V}^F$ has the following spectral decomposition

$$\mathcal{V}^F = i\omega_p\left(X\otimes\bar{X} - \bar{X}\otimes X\right) . \tag{5.17}$$

Taking the square of (5.17) we also infer that

$$X\otimes\bar{X} = -\omega_p^{-2}\left(\mathcal{V}^F\right)^2 - i\omega_p^{-1}\mathcal{V}^F . \tag{5.18}$$

The exponential of (5.17) is obtained via the Taylor series and making use of (5.18). The final result reads

$$\exp(t\mathcal{V}^F) = 1 + \frac{\sin\omega_p t}{\omega_p}\,\mathcal{V}^F + 2\left(\frac{\sin(\omega_p t/2)}{\omega_p}\right)^2\left(\mathcal{V}^F\right)^2 . \tag{5.19}$$

In the induction representation, an explicit formula for $\exp(t\mathcal{H}^I_M)$ is not that simple. To avoid unnecessary technicalities, we limit the discussion to the simplest case of the one-resonant Lorentz model. We choose the matter fields so that $\boldsymbol{\xi}^1_t = \mathbf{P}_t$ and $\boldsymbol{\xi}^2_t = \partial_t \boldsymbol{\xi}^1_t$. In this case, non-zero elements of the matter Hamiltonian are $\mathcal{H}^I_{M12} = 1$, $\mathcal{H}^I_{M21} = -\omega_0^2 - \omega_p^2$, and $\mathcal{H}^I_{M22} = -2\gamma$. The coupling matrix $\mathcal{V}_{MI}$ has only one non-zero element, $\mathcal{V}_{MI21} = \omega_p^2$. Here ω_0 is the resonant frequency, γ is the attenuation constant and ω_p is the plasma frequency. Using the Pauli matrix basis again, we find that the expression (5.15) holds for $\exp(t\mathcal{H}^I_M)$ if we replace in it ν_a by $\nu_p = \sqrt{\omega_0^2 + \omega_p^2 - \gamma^2}$, γ_a by γ and $\mathcal{H}^F_M$ by $\mathcal{H}^I_M$. The lower left corner of (4.13) has the form

$$\left(\mathcal{H}^I_M\right)^{-1} \left(\exp(t\mathcal{H}^I_M) - 1\right) \mathcal{V}_{MI} = -\frac{\omega_p}{\omega_0^2 + \omega_p^2} \left(\exp(t\mathcal{H}^I_M) - 1\right) \begin{pmatrix} 1 & 0 \\ 0 & 0 \end{pmatrix} . \tag{5.20}$$

A further simplification can be achieved by going over to the complex representation (2.12) of the auxiliary fields in which the matter Hamiltonian is diagonal. The transformation rule is explained in the paragraph after Eq. (2.30).

6 Energy and norm conservation

Consider the $\mathbb{L}_2(\mathbb{R}^3)$ norm of Ψ^Q_t, $|\Psi^Q_t|^2 = \int d\mathbf{r} \Psi^{Q*}_t \Psi^Q_t \equiv (\Psi^Q_t, \Psi^Q_t)$. In the grid representation, the norm coincides with the corresponding (complex) Euclidean norm, $(\Psi^Q_t, \Psi^Q_t) = \Delta r \sum_{\mathbf{n}} \Psi^{Q*}_t(\mathbf{n}\Delta r)\Psi^Q_t(\mathbf{n}\Delta r)$ where the sum is taken over all grid sites. By taking the time derivative of $|\Psi^Q_t|^2$ and using the evolution equation (1.1), it is not hard to deduce that the norm is conserved, provided the Hamiltonian is anti-Hermitian

$$\mathcal{H}^{Q*} = -\mathcal{H}^Q . \tag{6.1}$$

For a generic passive media this is not the case. So the norm is generally not conserved in contrast to the quantum mechanical case. However, we shall see that in the case when the matter evolution is described by second order differential equations in time and no attenuation is present, the norm coincides with the system energy and is conserved. In numerical simulations, this important property can be used to help to control the accuracy.

Consider multi-resonant Lorentz models with no attenuation, $\gamma_a = 0$. We start with the observation that the field and matter evolution equations can be obtained from the variational principle for the action

$$S = \int dt L = \int dt \int d\mathbf{r} \left[\frac{1}{2} \left(\mathbf{E}_t^2 - \mathbf{B}_t^2 \right) + \frac{1}{2} \sum_a \left((\partial_t \boldsymbol{\vartheta}^a_t)^2 - \omega_a^2 \boldsymbol{\vartheta}^{a2}_t \right) + \sum_a \omega_{pa} \boldsymbol{\vartheta}^a_t \cdot \mathbf{E}_t \right] , \tag{6.2}$$

where the electromagnetic degrees of freedom are described by vector and scalar potentials, respectively, $\mathbf{A}_t$ and φ_t, so that $\mathbf{E}_t = \boldsymbol{\nabla}\varphi_t - \partial_t \mathbf{A}_t$ and $\mathbf{B}_t = \boldsymbol{\nabla} \times \mathbf{A}_t$. The units are chosen in

this Section so that $c = 1$. The polarization of the medium is expressed via the matter fields as $\mathbf{P}_t = \sum_a \omega_{pa} \boldsymbol{\vartheta}_t^a$. The least action principle for the scalar potential φ_t leads to the Gauss law, $\boldsymbol{\nabla} \cdot \mathbf{D}_t = 0$, for the vector potential $\mathbf{A}_t$ to the Maxwell's equation, $\partial_t \mathbf{D}_t = \boldsymbol{\nabla} \times \mathbf{B}_t$, and for the matter field $\boldsymbol{\vartheta}_t^a$ to the medium polarization evolution equation of the Lorentz model with no attenuation, $\gamma_a = 0$. The second Maxwell's equation and the Gauss law for the magnetic field follow from the relation $\mathbf{B}_t = \boldsymbol{\nabla} \times \mathbf{A}_t$ by taking its time derivative and divergence, respectively. The energy of the system coincides with the canonical Hamiltonian which is obtained by a Legendre transformation [8] of the Lagrangian L for the velocities $\partial_t \mathbf{A}_t$ and $\partial_t \boldsymbol{\vartheta}_t^a$. Doing the Legendre transformation, we find the canonical Hamiltonian (energy) of the system

$$E_t = \frac{1}{2} \int d\mathbf{r} \left[\mathbf{E}_t^2 + \mathbf{B}_t^2 + \sum_a \left(\boldsymbol{\pi}_t^{a2} + \omega_a^2 \boldsymbol{\vartheta}_t^{a2} \right) \right] = \frac{1}{2} \left| \Psi_t^F \right|^2 , \tag{6.3}$$

where $\boldsymbol{\pi}_t^a = \delta L / \delta (\partial_t \boldsymbol{\vartheta}^a)$ are canonical momenta of the matter fields. To get the last equality in (6.3), we have used the relations $\boldsymbol{\xi}_t^{2a} = \boldsymbol{\pi}_t^a$ and $\boldsymbol{\xi}_t^{2a-1} = \omega_a \boldsymbol{\vartheta}_t^a$ which follow from comparison of the canonical Hamiltonian equations of motion for the canonically conjugate variables $\boldsymbol{\vartheta}_t^a$ and $\boldsymbol{\pi}_t^a$ and Eqs. (2.10) and (2.11) with $\gamma_a = 0$. Note that the canonical momentum conjugate to the vector potential $\mathbf{A}_t$ coincides with $-\mathbf{D}_t = -\mathbf{E}_t - \mathbf{P}_t$, not $-\mathbf{E}_t$ in this system. Therefore, the coupling between the electromagnetic and matter degrees of freedom is included into the term $\mathbf{E}_t^2 = (\mathbf{D}_t - \mathbf{P}_t)^2$ of the canonical Hamiltonian. Equation (6.3) becomes the conventional expression for the electromagnetic energy in a passive medium [19] when $\boldsymbol{\pi}_t^a$ and $\boldsymbol{\vartheta}_t^a$ are replaced by the corresponding solutions of the equations of motion with initial conditions $\boldsymbol{\pi}_0^a = \boldsymbol{\vartheta}_0^a = 0$. The energy conservation can be deduced either from the Noether theorem (because E_t is the Noether integral of motion corresponding to the time translational symmetry of the action) or directly from the norm conservation of Ψ_t^F (because the evolution operator $\exp(t\mathcal{H}^F)$ is unitary when $\gamma_a = 0$).

In numerical simulations, an exact unitary evolution operator $\mathcal{U}_{\Delta t}^Q$ is replaced by its approximation $\mathcal{G}_{\Delta t}^Q$. However, the energy remains conservative:

Theorem 6.1. The split algorithm is unitary for multiresonant Lorentz models with no attenuation, that is, the split algorithm preserves the energy $E_{t+\Delta t} = E_t$.

Proof. In the field representation, $\mathcal{H}_0^{F*} = -\mathcal{H}_0^F$ and $\mathcal{V}^{F*} = -\mathcal{V}^F$ and, therefore, $\mathcal{G}_{\Delta t}^F$ is unitary. As a result, the algorithm preserves the initial wave packet energy and the norm,

$$\left| \mathcal{G}_{\Delta t}^F \Psi_t^F \right| = \left| \Psi_{t+\Delta t}^F \right| = \left| \Psi_t^F \right| . \tag{6.4}$$

In the induction representation, the energy coincides with the norm of Ψ_t^I in the measure space. The measure is determined by the transformation law $\Psi_t^I = \mathcal{S} \Psi_t^F$,

$$E_t = \frac{1}{2} (\Psi_t^F, \Psi_t^F) = \frac{1}{2} (\Psi_t^I, \mu \Psi_t^I) \equiv \frac{1}{2} \left| \Psi_t^I \right|_\mu^2 , \qquad \mu = \mathcal{S}^{-1*} \mathcal{S}^{-1} . \tag{6.5}$$

Since $\mathcal{H}^I$ is similar to $\mathcal{H}^F$, the Hamiltonian $\mathcal{H}^I$ is anti-Hermitian relative to the μ scalar product,

$$\mathcal{H}^{I*} \mu = -\mu \mathcal{H}^I . \tag{6.6}$$

The norm conservation (unitarity) in the split algorithm requires in addition that the amplification matrix $\mathcal{G}^I_{\Delta t}$ satisfies the unitarity condition

$$\mathcal{G}^{I*}_{\Delta t}\mu\mathcal{G}^I_{\Delta t} = \mu \ . \tag{6.7}$$

This is indeed the case. To prove (6.7), we show that $\mathcal{H}^I_0$ and $\mathcal{V}^I$ satisfy the condition (6.6) and, hence, the product of their exponentials is a unitary operator relative to the μ scalar product. Consider $\mathcal{H}^I = \mathcal{S}\mathcal{H}^F\mathcal{S}^{-1} = \mathcal{H}^I_0 + \mathcal{V}^I$ so that $\mathcal{H}^F = \mathcal{S}^{-1}\mathcal{H}^I_0\mathcal{S} + \mathcal{S}^{-1}\mathcal{V}^I\mathcal{S}$. For the Lorentz model,

$$\mathcal{S}^{-1}\mathcal{H}^I_0\mathcal{S} = \begin{pmatrix} \mathcal{H}_0 & 0 \\ 0 & 0 \end{pmatrix} = -\left(\mathcal{S}^{-1}\mathcal{H}^I_0\mathcal{S}\right)^* \ . \tag{6.8}$$

Therefore $\mathcal{H}^I_0$ satisfies (6.6). From the anti-Hermiticity of $\mathcal{H}^F$ and (6.8) it follows that

$$\left(\mathcal{S}^{-1}\mathcal{V}^I\mathcal{S}\right)^* = -\mathcal{S}^{-1}\mathcal{V}^I\mathcal{S} \ . \tag{6.9}$$

Hence, $\mathcal{V}^I$ also satisfies (6.6). Thus,

$$\left|\mathcal{G}^I_{\Delta t}\Psi^I_t\right|_\mu = \left|\Psi^I_{t+\Delta t}\right|_\mu = \left|\Psi^I_t\right|_\mu \ , \tag{6.10}$$

which completes the proof.

The norm (energy) conservation can be used to control numerical convergence, especially when the aliasing problem in the fast Fourier transform is present, i.e., when parameters of the medium are discontinuous functions in space. In a properly designed algorithm the loss of energy (norm) due to attenuation should be controlled by the symmetric part of the Hamiltonian operator

$$\partial_t E_t = -\sum_a \gamma_a |\xi^{2a}_t|^2 \equiv \frac{1}{2}\left(\Psi^Q_t, \mathcal{V}^Q_\gamma \Psi^Q_t\right) \le 0 \ , \tag{6.11}$$

where $\mathcal{V}^{Q*}_\gamma = \mathcal{V}^Q_\gamma = (\mathcal{H}^{Q*} + \mathcal{H}^Q)/2 \le 0$ (a negative semidefinite operator) which is, in this case, a diagonal matrix with nonpositive elements.

7 Stability of the algorithm

The norm of an operator $\mathcal{H}$ is defined as

$$\|\mathcal{H}\| = \sup_{|\Psi|=1} |\mathcal{H}\Psi| \ . \tag{7.1}$$

If the operator is normal, that is, it commutes with its adjoint, then its norm coincides with its spectral radius $\rho(\mathcal{H})$, the supremum absolute value of its eigenvalues. In general,

$\rho(\mathcal{H}) \leq \|\mathcal{H}\|$. A family of amplification operators (matrices) $\mathcal{G}_{\Delta t}(\alpha)$ is called conditionally stable if there exists a constant $C(\tau, T)$ such that [16]

$$\|\mathcal{G}^n_{\Delta t}(\alpha)\| \leq C(\tau, T) \,, \tag{7.2}$$

for all $\Delta t \in (0, \tau)$, all $0 \leq n\Delta t \leq T$ for some positive τ and T, and all parameters α. The unconditional stability of $\mathcal{G}_{\Delta t}(\alpha)$ means that (7.2) holds uniformly in $n \geq 0$ for any $\Delta t > 0$ and for all α, that is, C is independent of T and τ. Parameters α can be all wave vectors $\mathbf{k}$ supported by the grid or simply grid values of the position vector $\mathbf{x}$. They can also include parameters of the medium. Note that if $\mathcal{G}_{\Delta t}$ is not normal, then $\rho(\mathcal{G}_{\Delta t}) \leq \|\mathcal{G}_{\Delta t}\|$ and, therefore, the von Neumann condition $\rho(\mathcal{G}_{\Delta t}) \leq 1$ is no longer sufficient for stability, while still being necessary.

Theorem 7.1. For multiresonant Lorentz models, the split algorithm in the field representation is unconditionally stable.

Proof. We shall prove that

$$\|\mathcal{G}^F_{\Delta t}\| \leq 1 \,, \tag{7.3}$$

which leads to the theorem statement

$$\|(\mathcal{G}^F_{\Delta t})^n\| \leq \|\mathcal{G}^F_{\Delta t}\|^n \leq 1 \,. \tag{7.4}$$

By definition and making use of the inequality, $\|\mathcal{A}\mathcal{B}\| \leq \|\mathcal{A}\|\,\|\mathcal{B}\|$, we get

$$\begin{aligned} \|\mathcal{G}^F_{\Delta t}\| &= \|e^{\Delta t \mathcal{H}^F_0/2} e^{\Delta t \mathcal{V}^F} e^{\Delta t \mathcal{H}^F_0/2}\| \\ &\leq \|e^{\Delta t \mathcal{H}^F_0/2}\|^2 \end{aligned} \tag{7.5}$$

because $e^{\Delta t \mathcal{V}^F}$ is a unitary operator, so its norm equals 1. The operator $e^{t\mathcal{H}^F_0}$ is block-diagonal (see (4.8) and (5.14)). The norm of a block-diagonal operator is the maximal norm of its blocks. The upper left corner block is given by the unitary operator $e^{t\mathcal{H}_0}$ whose norm equals 1. We have then

$$\|e^{t\mathcal{H}^F_0}\| = \max_a \left\{1,\ \|e^{t\mathcal{H}^F_{Ma}}\|\right\}. \tag{7.6}$$

The norm of the exponential of $\mathcal{H}^F_{Ma}$ can be found by direct calculation using the fact that $\|\mathcal{A}\|^2 = \|\mathcal{A}^*\mathcal{A}\| = \rho(\mathcal{A}^*\mathcal{A})$ and the explicit form of $e^{t\mathcal{H}^F_{Ma}}$ given in (5.15). For small attenuation, $\omega_a^2 - \gamma_a^2 = \nu_a^2 \geq 0$, we define $z_a = (\gamma_a/\nu_a)\sin(\nu_a t)$ so that the largest eigenvalue has the form

$$\begin{aligned} \|e^{t\mathcal{H}^F_{Ma}}\|^2 &= \|(e^{t\mathcal{H}^F_{Ma}})^* e^{t\mathcal{H}^F_{Ma}}\| \\ &= e^{-2\gamma_a t}\left(1 + 2z_a^2 + 2z_a\sqrt{1+z_a^2}\right) \,. \end{aligned} \tag{7.7}$$

Since $z_a \leq \gamma_a t \equiv y$ for $t \geq 0$, the function (7.7) is bounded from above by $f(y) = e^{-2y}(1 + 2y^2 + 2y\sqrt{1+y^2})$. It is not hard to verify that the derivative $f'(y)$ is negative for all $y > 0$, and that $f(0) = 1$. Hence, replacing t by $\Delta t/2$, we conclude that

$$\|e^{\Delta t \mathcal{H}^F_{Ma}/2}\| \leq 1 \,, \tag{7.8}$$

from which (7.3) follows. For large attenuation (like in Drude metals), $\omega_a^2 - \gamma_a^2 = -\nu_a^a \le 0$, in (7.7) we get $z_a = (\gamma_a/\nu_a)\sinh(\nu_a t) \equiv z_a(t)$. For $t \ge 0$ the latter relation defines the inverse function $t = t(z_a)$. Once again, the derivative of (7.7) with respect to z_a can be shown to be negative for all positive z_a while at $z_a = 0$ the function equals 1. So inequalities (7.8) and (7.3) hold in this case too. This completes the proof.

The proof of Theorem 7.1 given above is not the most economical. However, the idea of estimating the norm of the exponential of the matter Hamiltonian in order to investigate stability of the algorithm can be applied numerically to systems more general than the Lorentz model because $\mathcal{H}_M^F$ is local on the grid, that is, it does not contain derivatives. So the exponentials of $\mathcal{H}_M^F$ and its adjoint are not expensive to calculate numerically for some trial values of Δt to see if (7.8) holds.

We give an alternative proof of the unconditional stability in the case of the induction representation of the multi-resonant Lorentz model where an analytical expression of the exponent of the matter Hamiltonian is too hard to find, not to mention its norm. We shall make use of the following obvious lemma.

Lemma 7.2. Let a vector ψ_t, $t \ge 0$, be a solution of the linear equation $\partial_t \psi_t = (\mathcal{H}+\mathcal{V})\psi_t$ where the linear operators $\mathcal{H}$ and $\mathcal{V}$ satisfy the conditions $\mathcal{H}^* = -\mathcal{H}$ and $\mathcal{V}^* = \mathcal{V} \le 0$ (negative semidefinite). Then $|\psi_t| \le |\psi_0|$ for all $t \ge 0$.

The proof follows from an obvious relation

$$\partial_t |\psi_t|^2 = 2(\psi_t, \mathcal{V}\psi_t) \le 0 \,. \tag{7.9}$$

As a consequence we also get

$$\|e^{t(\mathcal{H}+\mathcal{V})}\| \le 1 \,, \tag{7.10}$$

for all $t \ge 0$.

Theorem 7.3. For multiresonant Lorentz models, the split algorithm in the induction representation is unconditionally stable.

Proof. If the attenuation is absent, the amplification matrix $\mathcal{G}_{\Delta t}^I$ is unitary with respect to the energy scalar product (μ-scalar product) as is shown in (6.10). Hence, $\|(\mathcal{G}_{\Delta t}^I)^n\|_\mu = 1$. When the attenuation is switched on, the unitarity of the amplification matrix can get violated only through $\exp(\Delta t \mathcal{V}^I)$ because the operator $\exp(\Delta t \mathcal{H}_0^I)$ remains unitary with respect to the μ-scalar product. The idea is to prove the unconditional stability with respect to the μ-norm. The theorem statement would follow from the equivalence of the Euclidean and μ- norms. Recall that two norms $|\Psi|$ and $|\Psi|'$ are equivalent if there exist two positive constants $C_{1,2}$ such that

$$C_1|\Psi| \le |\Psi|' \le C_2|\Psi| \,, \tag{7.11}$$

for all Ψ. All topological properties of the space spanned by Ψ are the same in one norm as in the other; in particular convergence of a sequence, boundedness of a set, boundedness of a

linear operator, and uniform boundedness of a family of operators are all invariant concepts under a change of one norm to the other. If $|\Psi|' = |\Psi|_\mu$, then $\|\mathcal{A}\|_\mu = \|\mathcal{S}^{-1}\mathcal{A}\mathcal{S}\|$ and

$$\begin{aligned} |\Psi|_\mu &= |\mathcal{S}^{-1}\Psi| \le \|\mathcal{S}^{-1}\| \, |\Psi| \, , \\ |\Psi| &= |\mathcal{S}\Psi|_\mu \le \|\mathcal{S}\|_\mu |\Psi|_\mu = \|\mathcal{S}\| \, |\Psi|_\mu \, , \end{aligned}$$

so that the two norms are indeed equivalent

$$\|\mathcal{S}\|^{-1}|\Psi| \le |\Psi|_\mu \le \|\mathcal{S}^{-1}\| \, |\Psi| \, . \tag{7.12}$$

Since $\|\mathcal{A}\mathcal{U}\| = \|\mathcal{A}\|$ for any bounded operator $\mathcal{A}$ and a unitary operator $\mathcal{U}$, we infer that

$$\|(\mathcal{G}^I_{\Delta t})^n\|_\mu \le \|\mathcal{G}^I_{\Delta t}\|^n_\mu = \|e^{\Delta t \mathcal{V}^I}\|^n_\mu = \|e^{\Delta t \mathcal{S}^{-1}\mathcal{V}^I\mathcal{S}}\|^n \, . \tag{7.13}$$

When $\gamma_a = 0$ (no attenuation), the operator $\mathcal{S}^{-1}\mathcal{V}^I\mathcal{S}$ is skew-symmetric (cf. (6.9)). When $\gamma_a \neq 0$, the operator $\mathcal{S}^{-1}\mathcal{V}^I\mathcal{S}$ acquires an addition which is a diagonal operator with nonpositive elements as follows from (2.25) and (2.28). Therefore the inequality (7.10) must hold for it as a consequence of Lemma 7.2,

$$\|e^{\Delta t \mathcal{S}^{-1}\mathcal{V}^I\mathcal{S}}\| \le 1 \, ,$$

from which the uniform boundedness of the family $(\mathcal{G}^I_{\Delta t})^n$ with respect to the μ-norm immediately follows. By the equivalence of the two norms (7.12), the family $(\mathcal{G}^I_{\Delta t})^n$ is also uniformly bounded in the Euclidean norm,

$$\|(\mathcal{G}^I_{\Delta t})^n\| \le \|\mathcal{S}\| \, \|\mathcal{S}^{-1}\| \, , \tag{7.14}$$

which completes the proof.

Comment. The same idea of making use of the norm equivalence, which actually goes in line with the Kreiss matrix theorem (its last part) [23, 16], can be applied to analyze the stability of the split algorithm for generic passive media. It is not hard to find a quadratic Lagrangian local in time such that the corresponding Euler equations describe propagation of an electromagnetic pulse in generic non-absorbing media. Due to time translation symmetry, the system should have a conserved quantity according to the Noether theorem [8]. This integral of motion coincides with the canonical Hamiltonian which is a quadratic form of Ψ^Q_t if the linear response approximation is valid. By analogy with the μ-norm, one could try to identify the canonical Hamiltonian with the new norm of Ψ^Q_t which is conserved by construction and, hence, in an attenuation-free medium the corresponding evolution operator is unitary. Thus, it would always be possible to arrange the split so that the amplification operator is unitary too. From the physical point of view, it is then naturally expected that, when absorption is added to the system, the attenuation operator $\mathcal{V}^Q_\gamma$ would generally satisfy the condition (6.11) because Fourier amplitudes of fields are exponentially attenuated in passive media. The latter would make it possible to apply Lemma 7.2 to prove the unconditional stability of the amplification operator with respect to the norm defined by

the canonical Hamiltonian along the lines similar to the proof of Theorem 7.3. An obstacle for this rather natural idea to generalize Theorem 7.3 to generic passive media is that the canonical Hamiltonian is not, in general, positive definite. It becomes positive only on solutions of the equations of motion for matter fields, which is a rather common feature of Lagrangian systems with higher order time derivatives. Thus, the canonical Hamiltonian does not always define a positive definite quadratic form in the Hilbert space for a generic passive media, and, hence, cannot serve as a new (conservative) norm. The study of conditions on attenuation-free media under which a positive definite and conserved quadratic form does exist goes beyond the scope of this paper since it would require the canonical formalism and the Noether theorem for theories with higher-order time derivatives, which is rather involved for generic passive media. The question can be addressed more easily for each particular medium model of interest. However, the unconditional stability might be excessive as far as practical needs are concerned. It is more important to make the split algorithm convergent for a generic passive medium. Then one should use the equivalence of (conditional) stability and convergence according to the fundamental convergence theorem due to Kantorovich [24, 16].

Our findings in this latter approach are summarized in the following theorem.

Theorem 7.4. Suppose that the medium response function satisfies the causality conditions (that is, its Fourier transform has poles only in the lower half of the frequency plane, $\mathrm{Im}\,\omega \le 0$). Let $\mathcal{U}_t$ be an exact evolution matrix in the grid representation (as defined in Section 3), and $\mathcal{G}_{\Delta t}$ be an amplification matrix in some third order split algorithm. Then for band-width limited wave packets the split algorithm is (conditionally) stable and for all $0 \le n \le N$, $T = N\Delta t$, and $0 < \Delta t < \tau$, there exist a constant C_m, which depends only on the medium parameters, and a constant W_m, which depends also on τ, such that

$$\|\mathcal{G}^n_{\Delta t}\| \le C_m + \delta(\Delta t, T)\,, \tag{7.15}$$

$$\delta(\Delta t, T) = C_m\left(e^{W_m T \Delta t^2} - 1\right) = O(\Delta t^2)\,, \tag{7.16}$$

$$\|\mathcal{U}_{n\Delta t} - \mathcal{G}^n_{\Delta t}\| \le \delta(\Delta t, T)\,. \tag{7.17}$$

Remark. Before proving the theorem, let us discuss its significance for practical applications. Inequality (7.15) implies conditional stability, while (7.17) establishes a relation between the accuracy (and convergence) of the split approximation and the uniform bound in the stability condition (7.15). By making the time step Δt smaller, any desired accuracy can be achieved during the total (fixed) simulation time T. The latter implies, of course, that the grid is assumed to be chosen fine enough (in accord with the Shannon sampling theorem) to accurately reproduce the initial pulse configuration via the fast Fourier method. Indeed, let $\Psi^{app}_{n\Delta t} = \mathcal{G}^n_{\Delta t}\Psi_0$ be a simulated solution, and $\Psi_t = \mathcal{U}_t\Psi_0$ be an exact solution, then from (7.17) it follows that

$$|\Psi_t - \Psi^{app}_t| \le \delta(\Delta t, T)|\Psi_0| = O(\Delta t^2)\,, \tag{7.18}$$

for all $0 \le t \le T$ and any *fixed* total simulation time T which is roughly $2L/c$ where L is the simulation box size and c the speed of light. Now we turn to the proof.

Proof. In the grid Fourier basis, $\mathcal{U}_t\Psi_0^Q = \sum_{\mathbf{k}} \Psi_t^Q(\mathbf{k})e^{i\mathbf{k}\cdot\mathbf{x}}$, where $\mathbf{k}$ spans the dual lattice. By construction of the Hamiltonian, each Fourier mode $\Psi_t^Q(\mathbf{k})$ evolves exactly as in the continuum case. Since the medium response function satisfies the causality conditions, Fourier amplitudes of the electromagnetic and response fields as well as their time derivatives are bounded functions of time. The amplitudes cannot grow infinitely large because of dissipation [19]. The number of Fourier modes is finite on the grid (only bandwidth limited initial wave packets are considered) and, hence, $|\Psi_t^Q| \leq C_Q$ for all $t \geq 0$ because components of the auxiliary field ξ_t are linear combinations of the response field and its time derivatives. The latter inequality is equivalent to the evolution matrix being uniformly bounded for all $t \geq 0$,

$$\|\mathcal{U}_t\| \leq C_m \ . \tag{7.19}$$

Let $\mathcal{U}_{\Delta t} - \mathcal{G}_{\Delta t} = \Delta t^3 \mathcal{W}_{\Delta t}$ and $\mathcal{W}_{\Delta t} = \mathcal{W}_0 + O(\Delta t)$ for small Δt according to a third order split (cf. (4.2) - (4.4)). Let $W_m = C_m \sup_{\Delta t} \|\mathcal{W}_{\Delta t}\|$ for $0 < \Delta t < \tau$ and some positive finite τ. Using the semigroup property $\mathcal{U}_{\Delta t}^k = \mathcal{U}_{k\Delta t}$ and (7.19) we infer that

$$\begin{aligned}
\|\mathcal{G}_{\Delta t}^n\| &= \|\mathcal{U}_{\Delta t}^n - (\mathcal{U}_{\Delta t}^n - \mathcal{G}_{\Delta t}^n)\| \\
&\leq \|\mathcal{U}_{\Delta t}^n\| + \|\mathcal{U}_{\Delta t}^n - \mathcal{G}_{\Delta t}^n\| && (7.20) \\
&\leq C_m + \|\mathcal{U}_{\Delta t}^n - (\mathcal{U}_{\Delta t} - \Delta t^3 \mathcal{W}_{\Delta t})^n\| && (7.21) \\
&= C_m + \| - \Delta t^3 \left(\sum_{k=0}^{n-1} \mathcal{U}_{\Delta t(n-k-1)} \mathcal{W}_{\Delta t} \mathcal{U}_{k\Delta t} \right) + \cdots \| && (7.22) \\
&\leq C_m + C_m \left[(1 + \Delta t^3 W_m)^n - 1 \right] && (7.23) \\
&\leq C_m + \delta(\Delta t, T) \ . && (7.24)
\end{aligned}$$

Inequality (7.17) readily follows from comparing the right hand side of (7.20) with those of (7.21)-(7.24). This completes the proof.

8 Convergence and accuracy analysis

To estimate the accuracy of the algorithm at a fixed finite grid size N, consider the following quantity

$$\beta_n(N, \Delta t) = \left| \left((\mathcal{U}_{\Delta t}^Q)^n - (\mathcal{G}_{\Delta t}^Q)^n \right) \Psi_0^Q \right| / |\Psi_0| \leq \left\| (\mathcal{U}_{\Delta t}^Q)^n - (\mathcal{G}_{\Delta}^Q)^n \right\| \tag{8.1}$$

which specifies a deviation of the approximate solution from the exact one relative to a given norm. Here $\mathcal{U}_{\Delta t}^Q$ is an exact evolution operator. The accuracy estimate $\beta_n(N, \Delta t)$ is a norm dependent quantity. The choice of norm is usually determined by practical needs. We use the norm related to the electromagnetic energy of the system and investigate, first, the behavior of $\beta_n(N, \Delta t)$ as Δt goes to zero, while $\Delta t n = t$ remains fixed and does not exceed some positive constant, $t \leq T$.

Theorem 8.1. For multi-resonant Lorentz models, there exists a positive constant W^Q such that

$$\left\|(\mathcal{U}^Q_{\Delta t})^n - (\mathcal{G}^Q_{\Delta})^n\right\| \le \Delta t^2 T W^Q c_Q^2 \,, \tag{8.2}$$

where $c_F = 1$ and $c_I = \|\mathcal{S}\|\,\|\mathcal{S}^{-1}\|$, for all $\Delta t \in (0,\tau)$ and $n\Delta t \le T$.

Proof. In the field representation $Q = F$, $\|(\mathcal{U}^F_{\Delta t})^n\| \le 1$ and $\|\mathcal{G}^F_{\Delta t})^n\| \le 1$ for any integer n, as a consequence of Lemma 7.2 for the multi-resonant Lorentz model. The same inequalities hold in the induction representation if the norm is replaced by the μ-norm. According to the split algorithm (4.2)-(4.4), $\mathcal{U}^Q_{\Delta t} - \mathcal{G}^Q_{\Delta t} = \Delta t^3 \mathcal{W}^Q_{\Delta t}$. Let $W^Q = \sup_{\Delta t} \|\mathcal{W}^Q_{\Delta t}\|$ for $\Delta t \in (0,\tau)$ for some positive τ (a maximal time step used in simulations). We then have the following chain of inequalities that lead to the theorem statement

$$\begin{aligned}
\|(\mathcal{U}^F_{\Delta t})^n - (\mathcal{G}^F_{\Delta})^n\| &= \left\|\sum_{k=1}^{n-1} (\mathcal{U}^F_{\Delta t})^k \,(\mathcal{U}^F_{\Delta t} - \mathcal{G}^F_{\Delta t})\,(\mathcal{G}^F_{\Delta t})^{n-k}\right\| && (8.3)\\
&\le (n-1)\Delta t^3 \|\mathcal{W}^F_{\Delta t}\| && (8.4)\\
&\le \Delta t^2 T W^F \,, && (8.5)
\end{aligned}$$

In the case of the induction representation, inequality (8.4) holds relative to the μ-norm. The theorem statement (8.2) follows from the norm equivalence (7.12), $c_I^{-1}\|\mathcal{A}\| \le \|\mathcal{A}\|_\mu \le c_I \|\mathcal{A}\|$ for any operator $\mathcal{A}$. The proof is complete.

Remark. In simulations, the continuum limit $N \to \infty$ is never achieved. Hence the operators in the split algorithm (4.1) remain bounded versus the unbounded case of (4.1). It is known that the convergence rate of $\beta_n(\infty, \Delta t)$ as $\Delta t \to 0$ estimated by the operator norm as in the right hand side of (8.1) is no longer of order $O(\Delta t^2)$ but rather of $O(\sqrt{\Delta t})$ (see, e.g., [25] and references therein). For unbounded operators, the estimate (8.5) is not valid. This suggests that the convergence rate $\beta_n(N, \Delta t)$ may depend, even significantly, on the initial vector Ψ_0 as N increases.

In a general case, the quantity $\delta(\Delta t, T)$ in Theorem 7.4 determines the accuracy of the split algorithm with respect to the norm (7.1) on a finite grid. To make simulation errors small, it is sufficient to require that

$$\|\mathcal{U}_{\Delta t} - \mathcal{G}^Q_{\Delta t}\| = \Delta t^3 \|\mathcal{W}^Q_{\Delta t}\| \ll 1 \,. \tag{8.6}$$

Making use of (4.4) and the fact that the norm of a matrix does not exceed the maximal norm of its blocks, we infer for a multi-resonant Lorentz model that, in order for (8.6) to hold, the following inequalities are sufficient:

$$\omega_{pa}\Delta t \ll 1 \,, \quad \omega_{max}\Delta t \ll 1 \,, \quad \omega_a \Delta t \ll 1 \,, \quad \gamma_a \Delta t \ll 1 \,, \tag{8.7}$$

and, yet another one,

$$\frac{|\boldsymbol{\nabla}\omega_{pa}|}{\omega_{pa}}\, c\Delta t \ll 1 \,. \tag{8.8}$$

Here ω_{max} is the maximal frequency of the initial wave packet. The right hand side of (8.6) is a sum of two types of terms. There are terms of the cubic order in numbers (8.7) as well as a term linear in (8.8) with the coefficient being quadratic in (8.7). The ratio in (8.8) can roughly be estimated from $|\nabla\omega_{pa}| \leq \omega_{pa}/\Delta r$ with Δr being the grid step. The condition (8.8) implies then that the distance traveled by the wave packet during one time step should be much smaller than the grid step.

To complete the discussion, one should also analyze the accuracy of the Gauss law (2.3). Note that the constraints are automatically fulfilled in the continuum theory due to the Dirac involution relations (1.3). By projecting the continuum theory onto a finite grid and replacing the exact evolution operator by its approximation in the split algorithm, the involution relations might be violated, thus leading to errors and potential instabilities of the algorithm. A good example of this kind is numerical general relativity (although the nonlinearity of the equations of motion plays the central role in generating instabilities due to the violation of the Dirac involution relations).

It is not hard to be convinced that the Gauss law (2.3) is equivalent to the following constraint on state vectors

$$\mathcal{C}^I\Psi^I_t = 0\,, \quad \mathcal{C}^I = \begin{pmatrix} \mathcal{C} & 0 \\ 0 & 0 \end{pmatrix}\,, \quad \mathcal{C} = \begin{pmatrix} 1 & 0 \\ 0 & 1 \end{pmatrix}\mathcal{P}_\parallel\,, \quad \mathcal{P}_\parallel = 1 - \mathcal{P}_\perp\,. \tag{8.9}$$

The operator $\mathcal{P}_\parallel$ projects a vector field onto its longitudinal component. In other words, it acts as the identity operator if the vector field is conservative, and it annihilates any rotational vector field (which is the curl of another vector field). In the field representation we get $\mathcal{C}^F = \mathcal{S}^{-1}\mathcal{C}^I\mathcal{S}$ with $\mathcal{S}$ defined in (2.21). On the grid, the action of the operator $\mathcal{C}^Q$ is defined by the rule (3.5), that is, by (8.9) we understand $(\mathcal{F}\mathcal{C}^Q\mathcal{F}^*)\mathcal{F}\Psi^Q_t = 0$. Thus, the Gauss law requires that the Fourier transform of the inductions should not acquire components parallel to wave vectors of the dual grid. This is obviously guaranteed if the exact evolution operator, $\mathcal{U}^Q_t = \exp(t\mathcal{H}^Q)$, is used to generate the time evolution because

$$\mathcal{C}^Q\mathcal{H}^Q = 0\,, \tag{8.10}$$

and, hence, $\mathcal{C}^Q\mathcal{U}^Q_t\Psi^Q_0 = \mathcal{C}^Q\Psi^Q_0 = 0$. A problem may arise when the approximate evolution operator, $(\mathcal{G}^Q_{\Delta t})^n$, is used to evolve the initial wave packet Ψ^Q_0. From linearity of the system, it is natural to expect that the Gauss law violation should be of the same order as the accuracy of a numerical solution of dynamical Maxwell's equations. However, we shall take a closer look at the problem and find a pleasant result important in practice, which is stated in the following theorem.

Theorem 8.2. Assuming linear response theory for any passive medium, the Gauss law holds exactly in the split algorithm in the induction representation.

Proof. In the induction representation, identity (8.10) is equivalent to two identities for the blocks of $\mathcal{C}^Q\mathcal{H}^Q$, namely, $\mathcal{C}\mathcal{H}_0 = 0$ and $\mathcal{C}\mathcal{V}_{IM} = 0$. The first one is obvious. The second

one follows from (2.24) established for any passive medium. The key observation is that the identity

$$\mathcal{C}^I \mathcal{H}_0^I = 0 \tag{8.11}$$

holds thanks to the two above identities and (4.11). Indeed, in the Fourier basis (8.11) is equivalent to the vanishing of the triple vector product $\mathbf{k} \cdot (\mathbf{k} \times \mathbf{A})$ for some $\mathbf{A}$ regular at $\mathbf{k} = 0$. Then from (8.9) and (8.11) it follows that

$$\mathcal{C}^I \mathcal{V}^I = \mathcal{C}^I (\mathcal{H}^I - \mathcal{H}_0^I) = 0 \,. \tag{8.12}$$

As a consequence of (8.11) and (8.12), we infer that

$$\mathcal{C}^I \left(\mathcal{G}_{\Delta t}^I\right)^n \Psi_0^I = \mathcal{C}^I e^{\Delta t \mathcal{H}_0^I/2} e^{\Delta t \mathcal{V}^I} e^{\Delta t \mathcal{H}_0^I/2} \left(\mathcal{G}_{\Delta t}^I\right)^{n-1} \Psi_0^I = \mathcal{C}^I \left(\mathcal{G}_{\Delta t}^I\right)^{n-1} \Psi_0^I = \mathcal{C}^I \Psi_0 = 0 \,, \tag{8.13}$$

which is the statement of the theorem.

In the field representation the Gauss law can be enforced by means of the projection formalism discussed in Section 1. The projection operator is, obviously, $\mathcal{P} = 1 - \mathcal{C}^F$. Its action is computed in the grid representation by the fast Fourier method according to the rule (3.5). Without the use of the projection formalism, the accuracy of the Gauss law is stated in the following technical proposition.

Proposition 8.3. Let $W = \|\mathcal{W}_{\Delta t}^F\|$ and $W_C = \|[\mathcal{C}^F, \mathcal{W}_{\Delta t}^F]\| C_m (1 + \delta(\Delta t, T))$ where C_m and $\delta(\Delta t, T)$ are defined in Theorem 7.4, then

$$\left|\mathcal{C}^F \left(\mathcal{G}_{\Delta t}^F\right)^n \Psi_0^F\right| / |\Psi_0^F| \leq T W_C \Delta t^2 + \Delta t^4 W W_C e^{TW\Delta t^2} (\Delta t^2 + T^2/2) = O(\Delta t^2) \,, \tag{8.14}$$

for all $0 \leq n \leq N$, $T = N\Delta t$ and any positive Δt.

Proof. Since $\mathcal{C}^F \mathcal{U}_t^F = \mathcal{C}^F$, assuming that the initial state Ψ_0^F satisfies the Gauss law we get

$$\begin{aligned}
\mathcal{C}^F (\mathcal{G}_{\Delta t}^F)^n \Psi_0^F &= -\mathcal{C}^F \left\{(\mathcal{U}_{\Delta t}^F)^n - (\mathcal{G}_{\Delta t}^F)^n\right\} \Psi_0^F \\
&= -\mathcal{C}^F \sum_{k=1}^{n-1} (\mathcal{U}_{\Delta t}^F)^k \left(\mathcal{U}_{\Delta t}^F - \mathcal{G}_{\Delta t}^F\right) (\mathcal{G}_{\Delta t}^F)^{n-k} \Psi_0^F \\
&= -\Delta t^3 [\mathcal{C}^F, \mathcal{W}_{\Delta t}^F] \sum_{k=1}^{n-1} (\mathcal{G}_{\Delta t}^F)^{n-k} \Psi_0^F + \Delta t^3 \mathcal{W}_{\Delta t}^F \sum_{k=1}^{n-1} \mathcal{C}^F (\mathcal{G}_{\Delta t}^F)^{n-k} \Psi_0^F \,.
\end{aligned} \tag{8.15}$$

Denoting the left hand side of (8.14) by α_n, we infer from (8.15), by taking the norm of both sides, that

$$\alpha_n \leq \Delta t^3 \left\|[\mathcal{C}^F, \mathcal{W}_{\Delta t}]\right\| \sum_{k=1}^{n-1} \|(\mathcal{G}_{\Delta t}^F)^{n-k}\| + \Delta t^3 \|\mathcal{W}_{\Delta t}^F\| \sum_{k=1}^{n-1} \alpha_{n-k} \,,$$

for $n > 1$ and $\alpha_1 \leq W_C \Delta t^3$. By Theorem 7.4, powers of the amplification matrix $\mathcal{G}_{\Delta t}^F$ are bounded. Hence the following recursion inequality holds

$$\alpha_n \leq (n-1)\Delta t^3 W_C + \Delta t^3 W (\alpha_{n-1} + \alpha_{n-2} + \cdots + \alpha_1) \,. \tag{8.16}$$

Iterating (8.16) $n-1$ times, we deduce that

$$\begin{aligned}\alpha_n &\leq (n-1)\Delta t^3 W_C + \Delta t^3 W \left\{(n-2)\Delta t^3 W_C + (1+\Delta t^3 W)(\alpha_{n-2}+\alpha_{n-3}+\cdots\alpha_1)\right\} \\ &\leq (n-1)\Delta t^3 W_C + \Delta t^6 W W_C \left\{\sum_{k=0}^{n-2}(n-2-k)(1+\Delta t^3 W)^k + (1+\Delta t^3 W)^{n-2}\right\}.\end{aligned}$$

One can find an explicit form for the sum in the latter equation. However, it is a cumbersome expression. For practical purposes, we give a simpler estimate which is stated in (8.14). First, factor out $(1+\Delta t^3 W)^{n-2}$ in the brackets, and then use obvious inequalities $(1+\Delta t^3 W)^{-k} \leq 1$ and $(1+\Delta t^3 W)^{n-2} \leq \exp(TW\Delta t^2)$, which leads to (8.14).

In the case of the Lorentz model, $W_C = \|[\mathcal{C}^F, \mathcal{W}^F_{\Delta t}]\|$ because all powers the amplification matrix are uniformly bounded by 1. For small Δt, a good estimate can be obtained by computing W_C for $\Delta t = 0$ using (4.4).

The convergence rate as the number of grid points N increases is determined by the convergence rate of the fast Fourier transform which is exponential versus polynomial in finite difference schemes, provided parameters of the medium are smooth functions of position [1, 5]. As is well known from Fourier analysis, the convergence rate can be affected for functions which have discontinuities [5]. The latter is, unfortunately, the case in electromagnetic scattering problems. Suppose there is an interface between two media. It can be deduced from the Maxwell's equations that the components of the electric and magnetic fields, $\mathbf{E}_t$ and $\mathbf{H}_t$, tangential to the interface must be continuous, provided there is no surface electric current on the interface. From the Gauss law it follows that the components of the inductions, $\mathbf{D}_t$ and $\mathbf{B}_t$, normal to the interface must be continuous, provided there is no surface charge on the interface. In contrast, the normal components of the fields and the tangential components of the inductions can be discontinuous. Their discontinuities are proportional to discontinuities of medium parameters (e.g., discontinuities in plasma frequencies in Lorentz models). Therefore, in either the induction or field representation, there are components which suffer discontinuities at the interface. Consequently, the convergence rate of the split algorithm for Maxwell's theory might be slower than that in quantum mechanics with a discontinuous potential because in the latter case the wave function remains continuous.

Another source of errors that affects the convergence rate as N increases is the aliasing problem in the fast Fourier transform on the grid. Note that, even though the initial wave packet is band-width limited and the grid is chosen fine enough to eliminate errors in doing its fast Fourier transform back and forth, the wave packet looses this property after the operator $\exp(\Delta t \mathcal{V}^Q)$ is applied to it. As a result, the aliasing problem arises in spatial domains where $\mathcal{V}^Q$ varies (typically at interfaces between different types of media).

The above two problems that also reduce the accuracy of the algorithm are well known and studied in the theory of the fast Fourier transform [5]. The only way to cope with them is to make the grid finer in the areas where medium parameters have discontinuities. However, the fast Fourier algorithm requires a uniform equispaced lattice, which might lead

to wasting computer resources if the increased resolution is necessary only in relatively small areas of the computational volume of the problem (e.g., only near an interface between two media). There are several ways to modify the algorithm when the above problems are too expensive to overcome by making a uniform grid finer.

First, the grid can be made fine enough so that the action of powers of the Hamiltonian $\mathcal{H}^Q$ on the state vector Ψ_0^Q is sufficiently accurate in the Fourier basis as specified by the rules (3.4) and (3.5). The operator $\mathcal{H}^Q$ is projected onto the Krylov space spanned by vectors $(\mathcal{H}^Q)^k\Psi_0^Q$, $k = 0, 1, ..., n$. Its exponent (the evolution operator) is then computed by diagonalizing $\mathcal{H}^Q$ instead of using the Lie-Trotter formula. Usually, it is sufficient to take a low dimensional Krylov space. This method is known as the Lanczos method [26]. A detailed study of the Krylov-Lanczos method as well as other similar pseudospectral methods in Maxwell theory will be given elsewhere.

Second, one can give up a uniform grid, while preserving basic advantages of pseudospectral methods such as, e.g., exponential convergence. A possible way to emulate a non-uniform grid in a multiscale problem is to use wavelet bases. The problem here is to compute the action of $\exp(\Delta t\mathcal{H}_0^Q)$ in the split algorithm because the derivative operator ∇ is not diagonal in this basis (in contrast to the Fourier basis). However, $\mathcal{H}_0^Q$ is expected to be sparse in a wavelet basis so that its direct diagonalization might not be expensive, and a significant reduction of computational costs can be achieved in the split algorithm, by using the fast wavelet transform, as compared to that in the Fourier basis. Otherwise, the use of (4.10) might be helpful in place of the direct diagonalization method. This approach has proved to be successful in solving multiscale initial value problems for the Schrödinger equation [27]. In the framework of Maxwell's theory for passive media, additional studies of several issues in time domain wavelet based algorithms, like, e.g., stability, would still be needed.

Third, the fast Fourier transform algorithm remains in place but is applied to an auxiliary uniform grid that is related to a non-uniform grid in physical coordinates by a change of variables. Consider a change of variables $\mathbf{y} = \mathbf{y}(\mathbf{x})$. A uniform grid in the new variables $\mathbf{y}$ would generate a non-uniform grid in the original Euclidean (physical) coordinates $\mathbf{x}$. A desired local density of grid points in the physical space, to enhance the sampling efficiency in designated regions, can be achieved by an appropriate choice of the functions $\mathbf{y}(\mathbf{x})$ [28]. By necessity, the auxiliary grid spans a rectangular box (with periodic boundary conditions). Its pre-image in the physical space would not be a box in general, save for the case when the map $\mathbf{y}(\mathbf{x})$ splits into three individual one-dimensional maps $y_j = y_j(x_j)$, $j = 1, 2, 3$. Since, the derivatives are transformed as $\nabla_{\mathbf{x}} = \mathcal{A}(\mathbf{y})\nabla_{\mathbf{y}}$ where the 3×3 matrix $\mathcal{A}$ is position dependent, the operator $\mathcal{H}_0^Q$ cannot be kept in the exponential. The action of its exponential on the state vector can be approximated by the leapfrog method in which only the action of $\mathcal{H}_0^Q$ on Ψ^Q is required. The latter can be done by the fast Fourier method according to the rules (3.5) and (3.4) applied to an operator being a product of position and derivative dependent operators. In contrast to the well studied quantum mechanical case, the algorithm appears to be unstable for media with absorption. In Section 9 a modification of the leapfrog scheme is proposed to achieve conditional stability.

9 The temporal leapfrog scheme

Here we discuss a temporal finite difference scheme applied to the Maxwell theory for passive media in the Hamiltonian formalism. As has been pointed out, such a scheme might be helpful for reducing computational costs by using non-uniform grids in combination with some pseudospectral methods (e.g., wavelet bases or the fast Fourier method with a change of variables). A temporal finite difference scheme can be obtained by the following procedure. Let us integrate (1.1) over the interval $(t, t+n\Delta t)$. We have

$$\Psi_{t+n\Delta t} = \Psi_t + \mathcal{H}\int\limits_t^{t+n\Delta t} d\tau\Psi_\tau \ = \Psi_t + \Delta t\mathcal{H}\left(\sum_{k=0}^{n-1} C_k^{(n)}\Psi_{t+k\Delta t}\right) + O(\Delta t^{n+1}) \ , \tag{9.1}$$

where the coefficients $C_k^{(n)}$ used to approximate the integral are well known for any n as well as the accuracy of the approximation. For example, one can use the 3/8 Simpson rule for $n = 3$ or Bode's rule for $n = 4$. The iterating scheme allows one to compute the wave function at the sequential moment of time if it is known for n preceding moments of time. Only the simplest case $n = 2$, for which the mid-point approximation for the integral is taken, leading to $C_0^{(2)} = 0$ and $C_1^{(2)} = 2$, will be considered in detail. It is also known as the leapfrog scheme:

$$\Psi_{t+\Delta t} = \Psi_{t-\Delta t} + 2\Delta t\mathcal{H}\Psi_t \ . \tag{9.2}$$

The action of the Hamiltonian is computed in a suitable basis (as has been noted above). Apart from violation of the dispersion relation of electromagnetic waves, temporal finite difference schemes would generally be unstable in media with absorption, in contrast to the quantum mechanical case. The reason is that the Hamiltonian in (9.2) is not anti-Hermitian. Consequently, convergence to the continuum solution would also be violated.

A general solution to (9.2) can be written in the form

$$\Psi_{n\Delta t} \ = \ \left(\mathcal{G}_{\Delta t}^{(+)}\right)^n \Psi_+ + \left(\mathcal{G}_{\Delta t}^{(-)}\right)^n \Psi_- \ , \tag{9.3}$$

$$\mathcal{G}_{\Delta t}^{(\pm)} \ = \ \mathcal{H}\Delta t \pm \sqrt{1+\mathcal{H}^2\Delta t^2} \ , \tag{9.4}$$

for some initial state vectors Ψ_0 and $\Psi_{\Delta t}$ (the vectors $\Psi_\pm$ are determined by them). Stability requires that there exists a positive constant C such that

$$|\Psi_{n\Delta t}| \le C\left(|\Psi_+| + |\Psi_-|\right) \ , \tag{9.5}$$

for all $0 \le n \le N$, $T = N\Delta t$ and $0 < \Delta t < \tau$. Note that in general a solution of (1.1) may have a legitimate exponential growth if the hermitian part of the Hamiltonian, $\mathcal{H}+\mathcal{H}^*$, is not negative semidefinite (see Lemma 7.2). For this reason, a typical stability criterion would be equivalent to the condition [16] that there exists some positive constant K_1 such that $\|\mathcal{G}_{\Delta t}^{(\pm)}\| \le 1 + K_1\Delta t$ uniformly for all parameters of $\mathcal{G}_{\Delta t}^{\pm}$ and for $0 < \Delta t < \tau$, which is clearly the case for (9.4) if $\mathcal{H}$ is bounded. The latter leads to

$$\left\|\left(\mathcal{G}_{\Delta t}^{(\pm)}\right)^n\right\| \le e^{K_1 T} \tag{9.6}$$

so that a legitimate exponential growth of the solution is allowed, i.e., $C \sim e^{K_1 T}$ in (9.5). For passive media, the Hamiltonian satisfies the conditions of Lemma 7.2 and, hence, no legitimate exponential growth should be present in a numerical solution in order to achieve convergence. However, as we shall see shortly, the scheme (9.2) always generates an exponentially growing solution for media with attenuation.

Let complex numbers $z = Re^{i\varphi}$ be eigenvalues of $\mathcal{H}\Delta t$. Since the spectral radius of $\mathcal{G}_{\Delta t}^{(\pm)}$ does not exceed its norm, the necessary (von Neumann) condition to suppress an exponential growth of the solution (9.3) reads

$$\rho(\mathcal{G}_{\Delta t}^{(\pm)}) = \max_{z \in D} \left| z \pm \sqrt{1+z^2} \right| \leq 1 \,. \tag{9.7}$$

The aim is to analyze the domain D of the complex plane for which (9.7) holds. Let $\eta = \sqrt{1+z^2}$ and $|\eta| = r$. The two inequalities in (9.7) require that for $z \in D$, $R^2 + r^2 \pm \xi \leq 1$, where $\xi = \bar{z}\eta + z\bar{\eta}$. By combining the latter inequalities, one gets $R^2 + r^2 \leq 1$ or $r^4 \leq (1-R^2)^2$. On the other hand, $r^4 = 1 + R^4 + 2R^2\cos(2\varphi)$. Hence, $\cos(2\varphi) \leq -1$ which is only possible if $\varphi = \pm\pi/2$ or $z = \pm iR$. The necessary condition (9.7) is satisfied if

$$\varphi = \pm\pi/2 \,, \qquad R^2 \leq 1 \,. \tag{9.8}$$

This does not yet guarantee that there is no norm growth. A norm growth, which is polynomial in time, can still occur.

Let us investigate general properties of the solution of (1.1) when the Hamiltonian satisfies the von Neumann condition (9.8). For any matrix $\mathcal{H}$ there exists a similarity transformation so that $\mathcal{S}^{-1}\mathcal{H}\mathcal{S}$ has the Jordan normal form. Let h_z be a block of the Jordan normal form corresponding to an eigenvalue z of $\mathcal{H}$. Any block h_k is a $q_z \times q_z$ bi-diagonal matrix, $q_z \geq 1$, with all the elements of the diagonal being equal to z and all the elements on the upper superdiagonal being equal to one. For $q_z = 1$, $h_z = z$ is just a complex number. The norm of any solution of (1.1) cannot grow faster than $\|\exp(t\mathcal{H})\|$. Let a q_z-dimensional vector ϕ_t satisfy the equation $\partial_t \phi_t = h_z \phi_t$. For a generic initial condition, the solution norm grows polynomially, $|\phi_t| = O(t^{q_z - 1})$ as $t \to \infty$. Using the similarity transformation $\mathcal{S}$, we define the corresponding μ-norm of state vectors and the corresponding matrix norm (cf. (6.5)) by setting $\mu = \mathcal{S}^{-1*}\mathcal{S}^{-1}$. From the equivalence of the norms $\|\cdot\|$ and $\|\cdot\|_\mu$ (see the proof of Theorem 7.3), the norm growth cannot be faster than

$$\|e^{t\mathcal{H}}\|_\mu = \|e^{t\mathcal{S}^{-1}\mathcal{H}\mathcal{S}}\| = \max_z \|e^{th_z}\| = O(t^{q-1}) \,, \qquad q = \max_z q_z \,, \quad t \to \infty \,, \tag{9.9}$$

provided $z = \pm iR$. However, a state vector norm growing polynomially with time is unacceptable from the physical point of view because in any passive medium there is no physical mechanism for such amplification of the field amplitudes in the large time limit. Consequently, we demand that any model Hamiltonian for a passive medium should be similar to a diagonal matrix (i.e., $\mathcal{H}$ is diagonalizable). In this latter case, the blocks h_z of the Jordan normal form of $\mathcal{H}$ are just complex numbers z. Hence $\|\exp(th_z)\| = |\exp(\pm itR)| = 1$ so that the μ-norm of any solution of (1.1) is conserved according to (9.9).

Two important conclusions about the leapfrog scheme (9.2) follow from our analysis. First, the von Neumann condition (9.8) is also sufficient for stability. Indeed, if (9.8) holds then $\|\mathcal{G}_{\Delta t}^{(\pm)}\|_\mu = \|\mathcal{S}\mathcal{G}_{\Delta t}^{(\pm)}\mathcal{S}^{-1}\| = \rho(\mathcal{G}_{\Delta t}^{(\pm)}) = 1$ and, hence, $\|(\mathcal{G}_{\Delta t}^{(\pm)})^n\|_\mu \le 1$ uniformly in $n \ge 0$. By the norm equivalence, $\|(\mathcal{G}_{\Delta t}^{(\pm)})^n\|$ is also bounded uniformly in $n \ge 0$. Second, reversing the argument, we conclude from the norm conservation of the stable leapfrog solution that no attenuation can be added to the Hamiltonian without destroying the stability and, consequently, the convergence to the continuum solution. Whenever the attenuation is added, the leapfrog solution would always contain an exponentially growing component, while this would not be so for a continuum solution (see Lemma 7.2).

Since $\mathcal{G}_{\Delta t}^{(+)}\mathcal{G}_{\Delta t}^{(-)} = 1$, only one of the two independent solutions in (9.3) would grow exponentially whenever the attenuation is added. Theoretically, for $\mathcal{H}+\mathcal{H}^* \le 0$ the exponentially growing solution can be eliminated by choosing the initial condition so that $\Psi_- = 0$ which is equivalent to the initial condition $\Psi_{\Delta t} = \mathcal{G}_{\Delta t}^{(+)}\Psi_0$. Practically, this is never possible due to rounding errors and/or numerical errors in computing $\mathcal{G}_{\Delta t}^{(+)}\Psi_0$. Even for a small $|\Psi_-|$ in (9.3) the growing part would eventually become comparable with the exponentially attenuating solution generated by Ψ_+. A reduction of the time step would not be helpful since the constant K_1 in (9.6) is independent of Δt while the simulation time T is fixed by the dimension of the simulation volume and the speed of light. One needs at least to modify the scheme so that there exists a constant K_p such that

$$\|\mathcal{G}_{\Delta t}^{(\pm)}\| \le 1 + K_p \Delta t^p \ , \quad p > 1 \ , \tag{9.10}$$

for $0 < \Delta t < \tau$. Indeed, it follows from (9.10) that $\|(\mathcal{G}_{\Delta t}^{(\pm)})^n\| \le \exp(K_p T \Delta t^{p-1}) = 1 + O(\Delta t^{p-1})$ for all $0 \le n \le N$ where $N\Delta t = T$. The norm growth could be reduced as much as desired by making the time step smaller. Next we show how to modify the leapfrog scheme to make (9.10) valid for at least $p = 3$ and, if the Hamiltonian is normal, an even stronger result holds, namely, $K_p = 0$.

Let $\mathcal{H} = \mathcal{H}_0 + \mathcal{V}$ where $\mathcal{V}^* + \mathcal{V} \le 0$ (negative semidefinite) and $\mathcal{H}_0^* = -\mathcal{H}_0$. In (1.1) we make a substitution $\Psi_t = \exp(t\mathcal{V})\Phi_t$. The new state vector Φ_t satisfies an equation with a time dependent Hamiltonian,

$$\partial_t \Phi_t = e^{-t\mathcal{V}}\mathcal{H}_0 e^{t\mathcal{V}}\Phi_t \equiv \mathcal{H}_t \Phi_t \ , \tag{9.11}$$

and with the same initial condition $\Phi_0 = \Psi_0$. Applying the leapfrog method to (9.11) we get $\Phi_{t+\Delta t} = \Phi_{t-\Delta t} + 2\Delta t \mathcal{H}_t \Phi_t$ valid up to $O(\Delta t^3)$. Returning to the initial variables, we arrive at the following recurrence relation

$$\Psi_{t+\Delta t} = \mathcal{L}_{2\Delta t}\Psi_{t-\Delta t} + 2\Delta t \mathcal{L}_{\Delta t}\mathcal{H}_0\Psi_t \ , \tag{9.12}$$

where $\mathcal{L}_{\Delta t} = \exp(\Delta t \mathcal{V})$. All the derivative operators are included into the anti-Hermitian part $\mathcal{H}_0$ of the Hamiltonian $\mathcal{H}$, while the attenuation operator $\mathcal{V}$ might even be independent of position and, hence, $\mathcal{L}_{\Delta t}$ has to be computed only once for given medium parameters and

time step. It can often be done analytically as, for example, in multiresonant Lorentz models (see Section 10). On the other hand, by Lemma 7.2, $\|\mathcal{L}_{\Delta t}\| \leq 1$ for any $\Delta t > 0$, and one might hope to stabilize the leapfrog scheme by satisfying the stability condition (9.8) for $\mathcal{H}_0$ only, that is, $1 + \mathcal{H}_0^2 \Delta t^2$ is positive semidefinite. This is indeed the case. The amplification matrix, $\Psi_{t+\Delta t} = \mathcal{G}_{\Delta t} \Psi_t$, for the recurrence (9.12), satisfies the equation

$$\mathcal{G}_{\Delta t} = \mathcal{L}_{2\Delta t} \mathcal{G}_{\Delta t}^{-1} + 2\Delta t \mathcal{L}_{\Delta t} \mathcal{H}_0 \, . \tag{9.13}$$

According to our analysis of the von Neumann stability condition (9.8), the anti-Hetmiticity condition of $\mathcal{H}_0$ in (9.12) and (9.13) can be weakened by demanding that $\mathcal{H}_0$ is related to an anti-Hermitian matrix by a similarity transformation. Some important properties of the amplification matrix obtained from (9.13) are stated in the following theorem.

Theorem 9.1. Suppose there exists a similarity transformation such that $\mathcal{S}^{-1}\mathcal{H}\mathcal{S} = \mathcal{H}_S + \mathcal{V}_S$ where $\mathcal{H}_S^* = -\mathcal{H}_S$, the Hermitian part of $\mathcal{V}_S$ is negative semidefinite, $\mathcal{V}_S^* + \mathcal{V}_S \leq 0$, and $\mathcal{H}_S$ also satisfies the von Neumann stability condition for the leapfrog scheme, $1 + \mathcal{H}_S^2 \Delta t^2 \geq 0$ (positive semidefinite). Consider the amplification matrix $\mathcal{G}_{\Delta t}$ of the modified leapfrog scheme (9.13) with $\mathcal{H}_0 = \mathcal{S}\mathcal{H}_S\mathcal{S}^{-1}$ and $\mathcal{V} = \mathcal{S}\mathcal{V}_S\mathcal{S}^{-1}$. Then there exists a norm $\|\cdot\|_\mu$ equivalent to $\|\cdot\|$ such that $\mathcal{G}_{\Delta t}$ has the following properties:

(*A*) if $[\mathcal{H}_0, \mathcal{V}] = 0$,

$$\|\mathcal{G}_{\Delta t}^n\|_\mu \leq 1 \tag{9.14}$$

uniformly in $n \geq 0$;

(*B*) if $[\mathcal{H}_0, \mathcal{V}] \neq 0$, there exists a non-negative constant K_3 such that

$$\|\mathcal{G}_{\Delta t}\|_\mu \leq 1 + K_3 \Delta t^3 \, , \tag{9.15}$$

for $0 < \Delta t < \tau$ and some positive τ.

Proof. Part (*A*). If $\mathcal{H}_0$ and $\mathcal{V}$ commute, the amplification matrix $\mathcal{G}_{\Delta t} = \mathcal{L}_{\Delta t}\mathcal{G}_{\Delta t}^0$ satisfies (9.13), provided $\mathcal{G}_{\Delta t}^0$ satisfies the same equation for $\mathcal{V} = 0$ (or $\mathcal{L}_{\Delta t} = 1$), which one can easily check by substituting the solution into (9.13). Consider the norm associated with the similarity transformation $\mathcal{S}$ of the Hamiltonian, $\|\mathcal{A}\|_\mu = \|\mathcal{S}^{-1}\mathcal{A}\mathcal{S}\|$. The norms $\|\cdot\|_\mu$ and $\|\cdot\|$ are equivalent (see the proof of Theorem 7.3). Since $\mathcal{H}_0$ satisfies the von Neumann stability condition and is anti-Hermitian relative to the μ scalar product, $\|\mathcal{G}_{\Delta t}^0\|_\mu = \rho(\mathcal{G}_{\Delta t}^0) = 1$ (according to the analysis after (9.7)). By Lemma 7.2, $\|\mathcal{L}_{\Delta t}\|_\mu \leq 1$, and we infer that $\|\mathcal{G}_{\Delta t}^n\|_\mu = \|(\mathcal{L}_{\Delta t}\mathcal{G}_{\Delta t}^0)^n\|_\mu \leq \|\mathcal{L}_{\Delta t}\|_\mu^n \leq 1$ uniformly for $n \geq 0$.

Part (*B*). Solving (9.13) by the perturbation theory in Δt, it is not hard to find that

$$\mathcal{G}_{\Delta t} - \mathcal{G}_{\Delta t}^V = \Delta t^3 \mathcal{K}_{\Delta t} \, , \quad \mathcal{G}_{\Delta t}^V = \mathcal{L}_{\Delta t/2}\mathcal{G}_{\Delta t}^0 \mathcal{L}_{\Delta t/2} \, , \tag{9.16}$$

where $\mathcal{K}_{\Delta t}$ is regular in the vicinity of $\Delta t = 0$ and vanishes whenever $\mathcal{H}_0$ and $\mathcal{V}$ commute. On the grid, $\mathcal{H}_0$ and $\mathcal{V}$ are bounded operators. Hence we can find a constant $K_3 = \sup_{\Delta t} \|\mathcal{K}_{\Delta t}\|_\mu$

for some open interval $0 < \Delta t < \tau$. Making use of the inequality $\|\mathcal{G}^V_{\Delta t}\|_\mu \le \|\mathcal{L}_{\Delta t/2}\|^2_\mu \le 1$, we find

$$\|\mathcal{G}_{\Delta t}\|_\mu = \|\mathcal{G}^V_{\Delta t} + \Delta t^3 \mathcal{K}_{\Delta t}\|_\mu \le 1 + \Delta t^3 K_3 \,, \tag{9.17}$$

which completes the proof.

The norm deviation of the solution generated by the modified leapfrog scheme (9.12) from the stable solution generated by $\mathcal{G}^V_{\Delta t}$ is of order $O(\Delta t^2)$ for the entire simulation time T and, hence, by reducing Δt a possible norm growth can be suppressed as much as desired. Indeed,

$$\begin{aligned} \left\|\mathcal{G}^n_{\Delta t} - (\mathcal{G}^V_{\Delta t})^n\right\|_\mu &= \|\sum_{k=1}^{n-1} \mathcal{G}^{n-k}_{\Delta t}(\mathcal{G}_{\Delta t} - \mathcal{G}^V_{\Delta t})(\mathcal{G}^V_{\Delta t})^k\|_\mu \\ &\le \Delta t^3 K \sum_{k=1}^{n-1} \|\mathcal{G}^{n-k}_{\Delta t}\|_\mu \le K_3 T \Delta t^2 e^{K_3 T \Delta t^2} = O(\Delta t^2) \,. \end{aligned}$$

Since in the continuum limit $\Delta t \to 0$, both the amplification matrices $\mathcal{G}^V_{\Delta t}$ and $\mathcal{G}_{\Delta t}$ generate the same solution and all the powers of the former are uniformly bounded by construction, a natural question to ask is whether one can find a recurrence relation for the function $\Psi^V_{n\Delta t} = (\mathcal{G}^V_{\Delta t})^n \Psi_0$ which could be used in place of (9.12). It is not difficult to derive an equation for $\mathcal{G}^V_{\Delta t}$ similar to (9.13), but, unfortunately, this equation cannot be converted into a simple recurrence relation for the wave function itself, like (9.12), suitable for numerical applications.

It should be noted that if the operator $\mathcal{L}_{\Delta t}$ in the modified leapfrog scheme (9.12) is replaced by another $\mathcal{L}^s_{\Delta t}$ such that $\mathcal{L}_{\Delta t} - \mathcal{L}^s_{\Delta t} = O(\Delta t^3)$ and $\|\mathcal{L}^s_{\Delta t}\|_\mu \le 1$, then the convergence is not violated because Part B of Theorem 9.1 still holds. This observation is useful for analytic computation of $\mathcal{L}_{\Delta t}$. For example, in the conditions of Theorem 9.1, put $\mathcal{S} = 1$. Let $\mathcal{V} = \mathcal{V}_1 + \mathcal{V}_2$ so that both $\mathcal{V}_{1,2}$ have their hermitian parts negative semidefinite. By using the split (4.2) we get

$$\mathcal{L}_{\Delta t} = e^{\Delta t \mathcal{V}} = e^{\Delta t \mathcal{V}_1/2} e^{\Delta t \mathcal{V}_2} e^{\Delta t \mathcal{V}_1/2} + O(\Delta t^3) = \mathcal{L}^s_{\Delta t} + O(\Delta t^3) \,. \tag{9.18}$$

By Lemma 7.2, $\|\mathcal{L}^s_{\Delta t}\| \le 1$ for $\Delta t \ge 0$. The operators $\mathcal{V}_{1,2}$ can be chosen so that their exponentials can be computed analytically.

10 Examples of the temporal leapfrog algorithm

There are many possibilities to split the original Hamiltonian $\mathcal{H}$ into two parts that satisfy the conditions of Theorem 9.1 and thereby to make the leapfrog scheme stable and convergent. Basic guide lines for doing that are as follows. The Hamiltonian $\mathcal{H}_0$ should contain all the derivative operators in $\mathcal{H}$ and, yet, the von Neumann condition is easy to establish for

$\mathcal{H}_0$. It would also be helpful to have an analytic expression for $\mathcal{L}_{\Delta t}$ at least up to order $O(\Delta t^3)$. As an illustration, we discuss multiresonant Lorentz models and geometric optics. To distinguish between the splits of the Hamiltonian in the split and leapfrog algorithms, we shall use an index l ("leapfrog") in the latter.

I Lorentz models

In the field representation of the Hamiltonian for multiresonant Lorentz models, we make the following decomposition

$$\mathcal{H}^F = \begin{pmatrix} \mathcal{H}_0 & \mathcal{V}_{FM} \\ \mathcal{V}_{MF} & 0 \end{pmatrix} + \begin{pmatrix} 0 & 0 \\ 0 & \mathcal{H}_M^F \end{pmatrix} \equiv \mathcal{H}_{0l}^F + \mathcal{V}_l^F \tag{10.1}$$

Thanks to (2.27) and $\mathcal{H}_0^* = -\mathcal{H}_0$, the operator $\mathcal{H}_{0l}^F$ is anti-Hermitian. From (2.28) it follows that the Hermitian part of $\mathcal{V}_l^F$ is negative semidefinite ($\gamma_a \geq 0$). The exponential of $\mathcal{V}_l^F$ is easily computed according to (5.14) and (5.15). Let ξ_t^a denote a six-component column whose three upper components coincide with $\boldsymbol{\xi}_t^{2a-1}$ and three lower components equal $\boldsymbol{\xi}_t^{2a}$ (see (2.9)–(2.11)). As a result we arrive at the following scheme

$$\psi_{t+\Delta t}^F = \psi_{t-\Delta t}^F + 2\Delta t \mathcal{H}_0 \psi^F + 2\Delta t \sum_a \mathcal{V}_{FMa} \xi_t^a \,, \tag{10.2}$$

$$\xi_{t+\Delta t}^a = e^{2\Delta t \mathcal{H}_{Ma}^F}\, \xi_{t-\Delta t}^a + 2\Delta t\, e^{\Delta t \mathcal{H}_{Ma}^F}\, \mathcal{V}_{MFa}\, \psi_t^F \,. \tag{10.3}$$

Stability is ensured if $\mathcal{H}_0^F$ satisfies the von Neumann condition (9.8). Eigenvalues of $\mathcal{H}_0^F$ satisfy the equation

$$\det(z - \mathcal{H}_{0l}^F) = z^q \det(z^2 - z\mathcal{H}_0 - \mathcal{V}_{FM}\mathcal{V}_{MF}) = 0 \tag{10.4}$$

where the non-negative integer q depends on the number of resonances in the Lorentz model. Non-zero eigenvalues satisfy the so-called pencil equation whose theory is well developed and might be useful for more general models [29]. Here we shall find a simpler (practical) criterion sufficient for (9.8) to hold. Since the plasma frequencies may depend on position, we apply the following general idea [30]. Suppose we have a finite difference scheme with variable coefficients in space. Consider a corresponding finite difference scheme with *frozen* coefficients. It is obtained from the original scheme by fixing the coefficients to particular values everywhere in space. A finite difference scheme with variable coefficients is stable if all the corresponding finite difference schemes with frozen coefficients are stable [30, 16]. So let us fix the plasma frequencies to particular values. The spatial dependence of the eigenfunctions for the pencil problem in (10.4) is given by a harmonic factor $\exp(i\mathbf{k}\cdot\mathbf{x})$ and the corresponding eigenvalues are $z = \pm i\sqrt{c^2\mathbf{k}^2 + \omega_p^2}$, where ω_p^2 is defined in (5.16). Let k_{max} be the maximal norm of all wave vectors of the initial wave packet and ω_p^{max} be the maximal value of ω_p as a function of position, then a sufficient criterion for stability reads

$$\Delta t \sqrt{c^2 k_{max}^2 + (\omega_p^{max})^2} \leq 1 \,. \tag{10.5}$$

The scheme (9.12) becomes especially simple in the case of small attenuation, $\gamma_a < \omega_a$. In the complex representation of the auxiliary fields (2.30) (cf. (2.12)) the matter Hamiltonians $\mathcal{H}^F_{Ma}$ are diagonal and the action of its exponential is reduced to multiplication by a complex number $e^{i\nu_a \Delta t}$ (see Section 5).

The stability condition (10.5) can be improved if one uses the induction representation arranging the split according to (4.11), that is, $\mathcal{H}^I_{0l} = \mathcal{H}^I_0$ and $\mathcal{V}^I_l = \mathcal{V}^I$. In this case the conditions of Theorem 9.1 are met if instead of (10.5) we demand a weaker condition

$$\Delta t c k_{max} \le 1 \,. \tag{10.6}$$

To prove this, we note first that by the similarity transformation defined in (2.22) we get

$$\mathcal{S}^{-1}\mathcal{H}^I\mathcal{S} = \begin{pmatrix} \mathcal{H}_0 & 0 \\ 0 & 0 \end{pmatrix} + \begin{pmatrix} 0 & \mathcal{V}_{FM} \\ \mathcal{V}_{MF} & \mathcal{H}^F_M \end{pmatrix} \equiv \mathcal{H}^I_S + \mathcal{V}^I_S \,. \tag{10.7}$$

Then (10.6) is obviously the von Neumann stability condition for $\mathcal{H}^I_S$, while the Hermitian part of $\mathcal{V}^I_S$ is negative semidefinite if $\gamma_a \ge 0$. The scheme is obtained from (9.12) by replacing $\Psi_t \to \Psi^I_t$, $\mathcal{H} \to \mathcal{H}^I_0$ and $\mathcal{V} \to \mathcal{V}^I$ as defined in (4.11). Since the left hand side of (10.7) coincides with $\mathcal{H}^F$, it can also be viewed as the leapfrog scheme in the field representation but with the split different from (10.1). This illustrates the point that the stability condition of the scheme (9.12) depends strongly on the choice of $\mathcal{H}_{0l}$. The price for a simpler stability condition in the induction representation is the lack of an explicit form of $\mathcal{L}_{\Delta t}$. However, this problem can be circumvented by making use of (9.18). Indeed, $\mathcal{V}^I_S = \mathcal{V}^F + \mathcal{V}^F_l$ where $\mathcal{V}^F$ is defined in (4.7). The exponentials of these operators are computed in Section 5. We also have $\|\exp(\Delta t \mathcal{V}^F)\| = 1$ because $\mathcal{V}^{F*} = -\mathcal{V}^F$ and $\|\exp(\Delta t \mathcal{V}^F_l)\| \le 1$ by Lemma 7.2 for a non-negative Δt. We set

$$\mathcal{L}^I_{\Delta t} = \mathcal{S} e^{\Delta t \mathcal{V}^F_l/2} e^{\Delta t \mathcal{V}^F} e^{\Delta t \mathcal{V}^F_l/2} \mathcal{S}^{-1} \tag{10.8}$$

so that $\|\mathcal{L}^I_{\Delta t}\|_\mu = \|\mathcal{S}^{-1}\mathcal{L}^I_{\Delta t}\mathcal{S}\| \le 1$. The operator (10.8) differs from $\mathcal{L}_{\Delta t} = \exp(\Delta t \mathcal{V}^I)$ $= \mathcal{S}\exp(\Delta t \mathcal{V}^I_S)\mathcal{S}^{-1}$ by terms of order $O(\Delta t^3)$ and, hence, according to (9.18), can be used in place of $\mathcal{L}_{\Delta t}$ in the leapfrog scheme without destroying its convergence and stability.

II Geometric optics

Another simple example is the case of geometric optics. For sake of simplicity we assume the medium to have no magnetic properties. A generalization is straightforward. Let $\varepsilon = \varepsilon(\mathbf{x})$ be the dielectric constant of the medium. If the medium is not isotropic, then ε is symmetric positive definite 3×3 matrix everywhere in space. We rewrite Maxwell's equations in the form

$$\partial_t \psi^I_t = \mathcal{H}_G \psi^I_t \,, \quad \mathcal{H}_G = \begin{pmatrix} 0 & c\boldsymbol{\nabla}\times \\ -c\boldsymbol{\nabla}\times(\varepsilon^{-1}\ ) & 0 \end{pmatrix} \,, \tag{10.9}$$

where the parentheses in (ε^{-1}) mean that the induction is first multiplied by ε^{-1} and then the curl of the resulting vector field is computed. Consider the scalar product

$$(\psi_1^I, \psi_2^I) = \int d\mathbf{r}\ \psi_1^{I*} \mu \psi_2^I\ , \quad \mu = \begin{pmatrix} \varepsilon^{-1} & 0 \\ 0 & 1 \end{pmatrix}\ . \tag{10.10}$$

In the grid representation of Section 3, the integral is replaced by the sum over grid points and $\mathcal{H}_G$ becomes a finite matrix. The Hamiltonian is anti-Hermitian with respect to this scalar product, $\mathcal{H}_G^* \mu = -\mu \mathcal{H}_G$. Therefore the corresponding μ norm is preserved in the time evolution generated by $\exp(t\mathcal{H}_G)$, that is, $(\psi_t^I, \psi_t^I) = (\psi_0^I, \psi_0^I)$. The electromagnetic energy of the wave packet is conserved because it is proportional to the μ norm of the initial state vector. Consequently, we expect that for a sufficiently small Δt the original leapfrog scheme (9.2),

$$\psi_{t+\Delta t}^I = \psi_{t-\Delta t}^I + 2\Delta t \mathcal{H}_G \psi_t^I\ , \tag{10.11}$$

becomes stable. To find a sufficient condition for stability, the same idea of finite difference schemes with frozen coefficients can be used. It obviously leads to a condition similar to (10.6),

$$\Delta t\, c\, k_{max}^{\varepsilon} \leq 1\ ,$$

where k_{max}^{ε} is the maximal norm of all wave vectors in the medium which can be estimated by $\sqrt{\rho(\varepsilon)} k_{max}$ with k_{max} being the maximal wave vector of the initial pulse in vacuum. The spectral radius $\rho(\varepsilon)$ is understood as the maximal spectral radius of $\varepsilon(\mathbf{x})$ over $\mathbf{x}$. If the Fourier basis is used to compute the derivatives, the algorithm does not violate the Gauss law. However, the algorithm would not conserve the μ norm (or energy), rather a quantity which, in many cases, approximates the energy. Multiplying (10.11) by ψ_t^I using the scalar product (10.10), we infer that

$$(\psi_{t+\Delta t}^I, \psi_t^I) = (\psi_t^I, \psi_{t-\Delta t}^I) = \cdots = (\psi_{\Delta t}^I, \psi_0^I)\ . \tag{10.12}$$

By expanding the exponential in $\psi_{t+\Delta t}^I = \exp(\Delta t \mathcal{H}_G)\psi_t^I$ into a Taylor series in both sides of (10.12) and making use of the anti-Hermiticity of $\mathcal{H}_G$, we find that the energy conservation violation is of order $O(\Delta t^2)$. Thus, it can be made as small as desired by reducing the time step.

11 Conclusions

The initial value problem in Maxwell theory for passive media has been reformulated in the Hamiltonian formalism. The path integral representation of the fundamental solution of the Hamiltonian evolution equation has been used to develop a time domain numerical algorithm for solving the initial value problem. The algorithm exhibits the main advantages of pseudospectral methods for solving differential equations such as an exponential convergence (and, hence, a greater accuracy), the absence of dispersive errors and numerical efficiency. In

addition, the algorithm is unitary, meaning that the energy of the initial pulse is conserved whenever the medium attenuation vanishes (Theorem 6.1). For widely used multiresonant Lorentz models, the algorithm is unconditionally stable (Theorems 7.1 and 7.3), and, for a generic passive medium, conditional stability can always be achieved (Theorem 7.4). As the time step Δt goes to zero, the algorithm accuracy is of order $O(\Delta t^2)$ (Theorem 8.1). It is possible to increase the convergence rate (accuracy) up to any desired order $O(\Delta t^n)$, $n \geq 2$. However, computational costs for increasing the accuracy in such a way are not necessarily lower than those for decreasing the time step in the original algorithm. An important advantage of the algorithm is that the Gauss law holds exactly in the process of numerical simulations with no extra computational cost (Theorem 8.2).

A drawback of the algorithm is related to well known problems of the fast Fourier method. Namely, a slower rate of convergence for non-smooth functions and aliasing. This might, perhaps, limit the advantages of the algorithm in some type of scattering problems with complex target geometries. Numerical tests are needed for a quantitative conclusion. There are several pseudospectral methods for approximating the fundamental solution of the Hamiltonian evolution equation that can help to circumvent this problem. We have analyzed one of them and formulated its stability criteria in the case of general passive media (Theorem 9.1). Other methods will be discussed elsewhere as well as the case when radiation sources (antennas) are included.

It is believed that the proposed algorithm would be useful in numerical studies of electromagnetic pulse propagation in passive media (e.g., foliage, soil, etc), photonic crystals and devices, and also in applications to scattering problems with targets made of dispersive materials.

Acknowledgments

I am grateful to Richard Albanese (Brooks, Air Force Base, TX) for suggesting this project and his continued support. I would like to thank John Klauder and Tim Olson (University of Florida) for useful discussions and encouragement. It is my pleasure to express my gratitude to LCAM (University of Paris-Sud) for the warm hospitality and support of this project, and my special thanks to Roger Azria and Victor Sidis of LCAM. I am deeply indebted to Andrei Borisov (LCAM, University of Paris-Sud) for numerous fruitful discussions and whose outstanding expertise in computational physics was invaluable for me. This work has been supported in part by US Air Force Grants F4920-03-1-0414 and F49620-01-1-0473.

12 Appendix

I Initial pulse configurations

In principle, any field configuration can serve as the initial configuration. However it is often desired to have an initial pulse with some specific properties (bandwidth, polarization, direction of propagation, etc). Yet, the initial wave packet should be built of radiation (propagating) electromagnetic fields. A simple method based on the fast Fourier transform algorithm is given below to obtain initial configurations made of radiation fields with designated properties.

A general solution of the Maxwell equations in vacuum can be written in the form

$$\mathbf{E}_t(\mathbf{r}) = \int d\mathbf{k} \left(\mathbf{C}_0^{(+)}(\mathbf{k})\, e^{i\mathbf{k}\cdot\mathbf{r}+ickt} + \mathbf{C}_0^{(-)}(\mathbf{k})\, e^{i\mathbf{k}\cdot\mathbf{r}-ickt} \right) \equiv \mathbf{C}_t^{(+)}(\mathbf{r}) + \mathbf{C}_t^{(-)}(\mathbf{r}) \quad (12.1)$$

$$\mathbf{B}_t(\mathbf{r}) = \frac{i}{\sqrt{-\Delta}} \boldsymbol{\nabla} \times \left(\mathbf{C}_t^{(+)}(\mathbf{r}) - \mathbf{C}_t^{(-)}(\mathbf{r}) \right) . \quad (12.2)$$

The representation (12.2) for the magnetic induction follows from the Maxwell equations and that the complex amplitudes $\mathbf{C}_t^{(\pm)}(\mathbf{k})$ satisfy the transversality and reality conditions which are, respectively,

$$\mathbf{k} \cdot \mathbf{C}_0^{(\pm)}(\mathbf{k}) = 0 , \quad \overline{\mathbf{C}}_0^{(\pm)}(\mathbf{k}) = \mathbf{C}_0^{(\mp)}(-\mathbf{k}) .$$

The representation (12.1) and (12.2) holds for any moment of time. Hence, we can set $t = 0$ to generate suitable initial conditions for an electromagnetic pulse propagating in empty space by choosing specific functions $\mathbf{C}_0^{(\pm)}(\mathbf{r})$.

Consider a few examples. Let there be translational invariance along the y axis. In this case the fields depend only on x and z, i.e., $\mathbf{r} = (x, 0, z)$. Accordingly, the wave vector has the form $\mathbf{k} = (k_x, 0, k_z)$ and $d\mathbf{k} = dk_x dk_z$. Let $\hat{\mathbf{e}}_2 = (0, 1, 0)$ be the unit vector along the y axis. Introduce

$$\mathbf{C}_0^{\pm}(\mathbf{r}) = \tfrac{1}{2}\hat{\mathbf{e}}_2\, A_0\, e^{-\kappa^2 r^2/2}\, e^{\mp i\mathbf{k}_0\cdot\mathbf{r}} \equiv \hat{\mathbf{e}}_2\, C_0^{\pm}(\mathbf{r}) , \quad (12.3)$$

where A_0 and κ are real constants, and $\mathbf{k}_0$ is a fixed wave vector. Note that the field $\mathbf{C}_0^{(\pm)}$ is automatically transversal. The corresponding fields determine suitable initial conditions to generate a pulse propagating in the direction of $\mathbf{k}_0$ whose frequency band is centered at $\omega_0 = ck_0$ and its width is proportional to $c\kappa$. The pulse is linearly polarized along the y axis:

$$\mathbf{E}_0 = \hat{\mathbf{e}}_2 E_0 , \quad E_0 = C_0^{(+)} + C_0^{(-)} , \quad (12.4)$$

$$\mathbf{B}_0 = \frac{i}{\sqrt{-\Delta}} \boldsymbol{\nabla} \times \hat{\mathbf{e}}_2 \left(C_0^{(+)} - C_0^{(-)} \right) . \quad (12.5)$$

The action of the differential operator is defined via the fast Fourier transform (see Section 3) on the grid fine enough to support the bandwidth limited function (12.3). In the Fourier basis, $i\boldsymbol{\nabla}/\sqrt{-\Delta} \to -\mathbf{k}/k$.

To obtain suitable initial conditions for a pulse propagating in the direction $\mathbf{k}_0$ and whose polarization lies in the xz-plane, we make use of the electromagnetic duality of Maxwell theory which states that the dynamics remains unchanged when electric and magnetic charges switch places and simultaneously $\mathbf{E}_t \to -\mathbf{B}_t$ and $\mathbf{B}_t \to \mathbf{E}_t$. According to the duality theorem, we can take

$$\mathbf{E}_0 = \frac{i}{\sqrt{-\Delta}} \boldsymbol{\nabla} \times \hat{\mathbf{e}}_2 \left(C_0^{(+)} - C_0^{(-)} \right) \tag{12.6}$$

$$\mathbf{B}_0 = -\hat{\mathbf{e}}_2 \left(C_0^{(+)} + C_0^{(-)} \right) . \tag{12.7}$$

Finally, suitable initial conditions for a pulse propagating in the direction $\mathbf{k}_0$ with a generic elliptic polarization are obtained by taking a linear combination of the above two initial conditions for two independent linear polarizations of the pulse. The amplitudes $\mathbf{C}_0^{(\pm)}(\mathbf{r})$ can also be set numerically from actual measurements of a particular pulse of interest.

II Conductivity and absorbing boundary conditions

In numerical simulations, the grid in coordinate space is of necessity finite. In scattering problems we are interested in the pulse shape and polarization which we wish to compute in the asymptotically large coordinate region. This requires that not only the leading edge of the reflected pulse should have reached the asymptotic region, but also the trailing edge should have done so as well. This is essential if the reflected pulse propagates in a highly dispersive medium, or the target has a complex shape, or both. A complication arises from the very nature of the fast Fourier transform method. The method is designed to describe periodic functions and, consequently, if the pulse has a finite amplitude at the edge of the grid, this finite value would appear back at the other edge, with totally disastrous results for the computation. In quantum computational physics this problem is often solved by using an optical potential that absorbs the signal as it reaches the grid boundary. A similar method can be developed for our treatment of Maxwell's theory. Before we do so let us point out that an absorbing boundary condition is not the only way to solve the problem. For instance, in the case of a complex target, an ancillary grid may be defined in one of the coordinates which extends to large distances. The pulse may be transferred in a gradual manner from the small grid (near the target) to this larger grid to prevent the pulse from ever reaching the edge of the small grid. This technique can also be applied to generate a pulse by an antenna of a complex construction. The dynamics of the portion of the pulse on the larger grid may be treated analytically (if dispersion properties of the medium are not too complex).

In quantum mechanics absorbing boundary conditions are made by adding an imaginary potential to the Hamiltonian with support near the grid edges. In the Maxwell theory, the same can be achieved by adding conductivity which gradually increases as the grid edges are

approached. An interaction of conducting media with electromagnetic radiation is described by Ohm's law,

$$\mathbf{J}_t = \sigma \mathbf{E}_t \,, \tag{12.8}$$

combined with Maxwell's equation (2.1), where the displacement current is amended as $\partial_t \mathbf{D}_t \to \partial_t \mathbf{D}_t + (4\pi\sigma/c)\mathbf{E}_t$ with $\sigma = \sigma(\mathbf{r})$ being the conductivity of the medium. Consider a linearly polarized plane wave moving along the z axis. Let $\tilde{E}_\omega$ be the Fourier transform of the only component of the electric field E_t. Disregarding for a moment any possible anomalous dispersion of the medium, we find that $\tilde{E}_\omega$ satisfies the equation

$$\partial_z^2 \tilde{E}_\omega(z) + \left[\frac{\omega^2}{c^2} - \frac{4\pi i\omega}{c}\sigma(z)\right] \tilde{E}_\omega(z) = 0 \,. \tag{12.9}$$

Equation (12.9) is identical to the stationary Schroedinger equation with an optical (absorbing) potential being proportional to $\sigma(z)$. In simulations of quantum wave packets it has been found that one of the optimal potentials has the form [17]

$$\sigma(z) = (n+1)^{-1}\,\sigma_n\,(z/L)^n \,, \quad n \geq 2 \,, \tag{12.10}$$

in the interval $z \in [0, L]$ and $\sigma(z) = 0$ otherwise. So, our next task is to find an optimal constant σ_n such that that the conducting layer would not reflect or transmit electromagnetic energy in some designated frequency band. Maxwell's equations in a conducting medium are form-invariant under the scaling transformations

$$\omega \to \beta\omega \,, \quad \sigma(\mathbf{r}) \to \beta\sigma(\beta\mathbf{r}) \,, \quad \tilde{\psi}^F_\omega(\mathbf{r}) \to \alpha\tilde{\psi}^F_\omega(\beta\mathbf{r}) \,, \tag{12.11}$$

where α and β are positive constants. If the conductivity $\sigma(\mathbf{r})$ was found optimal for a frequency ω and over a length L, then the optimal conductivity for a frequency $\beta\omega$ would be $\beta\sigma(\beta\mathbf{r})$ and the new length over which it is taken to act would be L/β.

Let us first study the reflectivity of the absorbing layer. Suppose, $\sigma(z) = \sigma_0\theta(z)$ where $\theta(z)$ is the Heaviside function. If a monochromatic linearly polarized wave coming from the negative z region has an amplitude one, then the reflected wave has the amplitude [19]

$$\eta_\omega = \frac{1-\nu_\omega}{1+\nu_\omega} \,, \qquad \nu_\omega^2 = 1 + \frac{4\pi i\sigma_0}{\omega} \equiv 1 + iq_\omega \,. \tag{12.12}$$

The energy of the reflected wave is

$$R_\omega = |\eta_\omega|^2 = q_\omega^2/4 + O(q_\omega^4) \,. \tag{12.13}$$

R_ω increases as the ratio q_ω gets higher and is small if $q_\omega^2/4 \ll 1$. Consider now $\sigma(z)$ which monotonically increases from $z = 0$ in the positive z direction. Let $k_\omega = k_\omega(z)$ be a local wave vector of the wave in the conducting medium,

$$k_\omega(z) = c^{-1}\omega\sqrt{1 + iq_\omega(z)} \,. \tag{12.14}$$

We shall argue that the reflection is negligibly small if the local wave vector does not significantly changes over a distance of order k_ω^{-1}, that is,

$$\left|\frac{k_\omega(z+\delta z)-k_\omega(z)}{k_\omega(z)}\right| \ll 1\,, \qquad \delta z \sim k_\omega^{-1}\,. \tag{12.15}$$

Making a linear approximation in (12.15), we infer that

$$|\partial_z q_\omega(z)| \ll (2c)^{-1}\,\omega\,\left(1+q_\omega^2(z)\right)^{3/4}\,, \tag{12.16}$$

which must be valid for all values of $q_\omega(z)$ including small ones when the reflection is small. Inequality (12.16) allows us to reverse the argument, that is, the reflection is small if $|\partial_z q_\omega(z)| \ll (2c)^{-1}\omega$. Let σ_L be an average conductivity over a layer of width L, $\sigma_L = L^{-1}\int_0^L dz\sigma(z)$. In particular, for (12.10), $\sigma_L = \sigma_n$. For a monotonically increasing function, the derivative can be approximated as $|\partial_z q_\omega(z)| \approx \sigma_L/L$. This leads to a necessary condition on conductivity to suppress the reflection, namely,

$$\sigma_L < \frac{\omega^2 L}{8\pi c}\,. \tag{12.17}$$

Our analysis is valid if the higher derivatives of $\sigma(z)$ are not large. This condition requires that the exponent n in (12.10) should not be less than two to insure a smooth behavior at $z=0$.

The transmission can be estimated as follows. Suppose the pulse occupies a compact region Ω. Let $\mathcal{E}_t^\Omega$ be the pulse energy. The pulse looses its energy as it propagates through a conducting medium according to Ohm's law, so that

$$c^{-1}\partial_t \mathcal{E}_t^\Omega = -(2c)^{-1}\int_\Omega d\mathbf{r}\;\sigma\;\mathbf{E}_t^2 \le -8\pi\sigma_\Omega \mathcal{E}_t^\Omega\,, \tag{12.18}$$

where $\sigma_\Omega = \max_\Omega \sigma$. Therefore the pulse energy decay can be bounded from above by

$$\mathcal{E}_t^\Omega \le e^{-8\pi t\sigma_\Omega}\,\mathcal{E}_0^\Omega\,. \tag{12.19}$$

In the one dimensional case (12.10), $\sigma_\Omega = \sigma_L/(n+1)$. For the time $t = L/c$ needed for a pulse to get through the layer of width L, the attenuation should be large, that is, $8\pi L\sigma_L/c(n+1) \gg 1$. Thus, the necessary conditions to suppress both transmission and reflection (that is, to ensure an almost total absorption) of the pulse are

$$\frac{(n+1)c}{8\pi L} < \sigma_L < \frac{\omega^2 L}{8\pi c}\,. \tag{12.20}$$

By changing the Hamiltonian $\mathcal{H}^Q$, the conducting layer can be included into the split or leapfrog algorithm. Since the conducting layer produces attenuation, the conductivity σ must be included into the operator $\mathcal{L}_{\Delta t}$ in the modified leapfrog scheme. It is also possible to create an absorbing and non-reflecting layer by using a passive medium (e.g. a Lorentz model). The analysis of the medium properties would be similar to that for a conducting layer. In fact, using a layer of a passive medium would offer more flexibility in solving the grid boundary problem.

References

[1] B. Fornberg, *A practical guide to pseudospectral methods*, Cambridge University Press, Cambridge, 1996;
J.P. Boyd, *Chebyshev and Fourier spectral methods*, Springer-Verlag, New York, 1989.

[2] C. Leforestier *et al*, J. Comput. Phys. 94 (1991) 59.

[3] A.G. Borisov and S.V. Shabanov, in preparation

[4] R.P. Feynman, Rev. Mod. Phys. 20 (1948) 367;
R.P. Feynman and A.R. Hibbs, *Quantum mechanics and path integrals*, McGraw-hill, New York, 1965.

[5] M. Pickering, *An introduction to fast Fourier transform methods for partial differential equations*, Research Study Press, John Wiley & Sons Inc., New York, 1986;
E.O. Brigham, *The fast Fourier transform and applications*, Prentice-Hall, Inc., Eglewood Cliffs, New Jersey, 1988.

[6] E. Nelson, J. Math. Phys. 5 (1964) 332.

[7] P.G. Petropoulos, IEEE Trans. Antennas Propagat., 42 (1994) 62;
S. A. Cummer. IEEE Trans. Antennas Propagat., 45 (1997) 392;
J.L. Yong, *et al*, IEEE Trans. Microwave Theory and Technique, 43 (1995) 1902.

[8] V.I. Arnold, *Mathematical methods of classical mechanics*, Springer-Verlag, Berlin, 1989.

[9] V.I. Arnold, V.V. Koslov and A.I. Neishtadt, *Mathematical aspects of classical mechanics* in: *Encyclopaedia of Mathematical Science, Vol. III, Dynamical Systems*, Springer-Verlag, Berlin, 1988.

[10] P.A.M. Dirac, *Lectures on Quantum Mechanics*, Yeshiva University, New York, 1964.

[11] I. Daubechies and J.R. Klauder, J. Math. Phys. 26 (1985) 2239.

[12] V.S. Buslaev, in: *Topics in Mathematical Physics* (Ed. M. Birman), Consultants Bureau, New York, 1968;
V.I. Klyatskin and V.I. Tatarskii, Sov. Phys. JETP, 30 (1970) 335;
R. Dashen, J. Math. Phys. 20 (1979) 894;
M. Eve, Proc.Roy.Soc. London, 347A (1976) 405;
I.M. Besieris, J. Opt. Soc. Amer. 2 (1985) 2095;
R.H. Hardin and F.D. Tappet, SIAM Rev. 15 (1973) 423;
R.D. Nevels, J.A. Miller and R.E. Miller, IEEE Trans. Antennas Propagat., 48 (2000) 565.

[13] G. Roepstorff, *Path integral approach to quantum physics: an introduction*, Springer-Verlag, Berlin, 1994;
L.S. Schulman, *Techniques and Applications of Path Integration*, Wiley, New York, 1981.

[14] S.V. Shabanov, Phys. Rept. 326 (2000) 1.

[15] A.G. Borisov, J.P. Gauyacq and S.V. Shabanov, Surf. Sci. 487 (2001) 243.

[16] R. Richtmyer and K. Morton, *Difference Methods for Initial-Value Problems*, Wiley, New York, 1967.

[17] D. Neuhauser and M. Baer, J. Chem. Phys. 90 (1989) 4351;
G.G. Balint-Kurti and Á. Vibók, in:*Numerical Grid Methods and Their Applications to Schrödinger's Equation*, (ed. C. Cerjan), Kluwer Academic Publisher, Netherlands, 1993, p.195.

[18] J.P. Bérenger, J. Comput. Phys. 114 (1994) 185; 127 (1996) 363;
P.G. Petropoulos, L. Zhao and Cangellaris, J. Comput. Phys. 139 (1998);
J.-L. Vay, J. Comput. Phys. 165 (2000) 511.

[19] L.D. Landau and E.M. Lifshitz, *Electrodynamics of continuous media, Theoretical Physics, Vol. VIII*, Oxford, Pergamon, New York, 1984.

[20] R.M. Joseph, S.C. Hagness, and A. Taflove, Opt. Lett. 16 (1991) 1412;
L.Gilles, S.C. Hagness, and L. Vázquez, J. Comput. Phys. 161 (2000) 379;
A. Taflove, *Advances in Computational Electrodynamics: The Finite-Difference Time-Domain Method*, Artech House, Norwood, MA, 1998.

[21] M.D. Feit, J.A. Fleck Jr. and A. Steiger, J. Comput. Phys. 47 (1982) 418.

[22] H. De Raedt, Comput. Phys. Rep. 7 (1987) 1.

[23] H.O. Kriess, Nordisk Tidskr. Informations-Behandlung, 2 (1962) 153.

[24] L.W. Kantorovich, Uspekhi Math. Nauk, USSR, 3 (1948) 89.

[25] T. Ichinose and H. Tamura, Proc. Indian Acad. Sci. (Math. Sci.) 112 (2002) 99.

[26] C. Lanczos, J. Res. Nat. Bur. Stand. 45 (1950) 255;
T.J. Park and J.C. Light, J. Chem. Phys. 85 (1986) 5870.

[27] A.G. Borisov and S.V. Shabanov, Chem. Phys. Lett. 361 (2002) 15.

[28] E. Fattal, R. Baer and R. Kosloff, Phys. Rev. E 53 (1996) 1217;
D. Lemoine, Chem. Phys. Lett. 320 (2000) 492.

[29] D. Inman, *Vibration and Control, Measurement and Stability*, Prentice Hall, 1989.

[30] H. Shintani and K. Tomoeda, Hiroshima Math. J., 7 (1977) 309.

FINANCIAL STATUS REPORT

(Long Form)

PLEASE DO NOT RETURN YOUR COMPLETED FORM TO THE OFFICE OF MANAGEMENT AND BUDGET.

Please type or print legibly. The following general instructions explain how to use the form itself. You may need additional information to complete certain items correctly, or to decide whether a specific item is applicable to this award. Usually, such information will be found in the Federal agency's grant regulations or in the terms and conditions of the award (e.g., how to calculate the Federal share, the permissible uses of program income, the value of in-kind contributions, etc.). You may also contact the Federal agency directly.

Item	Entry
1, 2 and 3.	Self-explanatory.
4.	Enter the Employer Identification Number (EIN) assigned by the U.S. Internal Revenue Service.
5.	Space reserved for an account number or other identifying number assigned by the recipient.
6.	Check *yes* only if this is the last report for the period shown in item 8.
7.	Self-explanatory.
8.	Unless you have received other instructions from the awarding agency, enter the beginning and ending dates of the current funding period. If this is a multi-year program, the Federal agency might require cumulative reporting through consecutive funding periods. In that case, enter the beginning and ending dates of the grant period, and in the rest of these instructions, substitute the term "grant period" for "funding period."
9.	Self-explanatory.
10.	The purpose of columns, I, II, and III is to show the effect of this reporting period's transactions on cumulative financial status. The amounts entered in column I will normally be the same as those in column III of the previous report *in the same funding period*. If this is the first or only report of the funding period, leave columns I and II blank. If you need to adjust amounts entered on previous reports, footnote the column I entry on this report and attach an explanation.
10a.	Enter total gross program outlays. Include disbursements of cash realized as program income if that income will also be shown on lines 10c or 10g. Do not include program income that will be shown on lines 10r or 10s. For reports prepared on a cash basis, outlays are the sum of actual cash disbursements for direct costs for goods and services, the amount of indirect expense charged, the value of in-kind contributions applied, and the amount of cash advances and payments made to subrecipients. For reports prepared on an accrual basis, outlays are the sum of actual cash disbursements for direct charges for goods and services, the amount of indirect expense incurred, the value of in-kind contributions applied, and the net increase or decrease in the amounts owed by the recipient for goods and other property received, for services performed by employees, contractors, subgrantees and other payees, and other amounts becoming owed under programs for which no current services or performances are required, such as annuities, insurance claims, and other benefit payments.
10b.	Enter any receipts related to outlays reported on the form that are being treated as a reduction of expenditure rather than income, and were not already netted out of the amount shown as outlays on line 10a.
10c.	Enter the amount of program income that was used in accordance with the deduction alternative.
Note:	Program income used in accordance with other alternatives is entered on lines q, r, and s. Recipients reporting on a cash basis should enter the amount of cash income received; on an accrual basis, enter the program income earned. Program income may or may not have been included in an application budget and/or a budget on the award document. If actual income is from a different source or is significantly different in amount, attach an explanation or use the remarks section.
10d,	e, f, g, h, i and j. Self-explanatory.
10k.	Enter the total amount of unliquidated obligations, including unliquidated obligations to subgrantees and contractors. Unliquidated obligations on a cash basis are obligations incurred, but not yet paid. On an accrual basis, they are obligations incurred, but for which an outlay has not yet been recorded. Do not include any amounts on line 10k that have been included on lines 10a and 10j. On the final report, line 10k must be zero.
10l.	Self-explanatory.
10m.	On the final report, line 10m must also be zero.
10n,	o, p, q, r, s and t. Self-explanatory.
11a.	Self-explanatory.
11b.	Enter the indirect cost rate in effect during the reporting period.
11c.	Enter the amount of the base against which the rate was applied.
11d.	Enter the total amount of indirect costs charged during the report period.
11e.	Enter the Federal share of the amount in 11d.
Note:	If more than one rate was in effect during the period shown in item 8, attach a schedule showing the bases against which the different rates were applied, the respective rates, the calendar periods they were in effect, amounts of indirect expense charged to the project, and the Federal share of indirect expense charged to the project to date.

Signal Transmission in Passive Media

John R. Klauder *
Departments of Physics and Mathematics
University of Florida
Gainesville, FL 32611

Abstract

Under rather general assumptions, and in a relatively simple and straightforward manner, it is shown that the characteristics of signals which travel through homogeneous, as well as inhomogenous, passive media have the principal features usually associated with the phenomena of precursors, as generally follows from more elaborate studies. The simplicity of the present arguments permit analytic studies to be made for a greater variety of media than is normally the case.

Introduction

The propagation of electromagnetic signals through passive media, i.e., media exhibiting both dispersive and absorptive properties, of many different kinds is a problem of interest in many applications. For simplicity of analysis, we model such problems in relatively economical but fairly general terms. Let $f_0(t)$ denote the temporal dependence of the initial signal at some initial depth level $z = 0$ inside, or at the surface, of some medium. We presume the medium to be homogeneous at this stage and that its response characteristics are stationary. We denote by $f_z(t)$ the temporal dependence of the signal after traveling a distance $z > 0$ through the passive medium. The relation between the input and output signals is that of a standard filtration which

*Electronic mail: klauder@phys.ufl.edu

may be presented in several different forms. One such form is given by convolution with the medium impulse response function $m_z(t)$, and takes the form

$$f_z(t) = \int m_z(t-s)\, f_0(s)\, ds\,. \tag{1}$$

Note that all integrals with unspecified limits are assumed to extend over the whole real line. As a convolution, these functions have a multiplicative relation in frequency space given by

$$F_z(\omega) = M_z(\omega)\, F_0(\omega)\,, \tag{2}$$

where

$$F_z(\omega) = \int e^{i\omega t}\, f_z(t)\, dt\,, \tag{3}$$

$$M_z(\omega) = \int e^{i\omega t}\, m_z(t)\, dt\,. \tag{4}$$

As a causal phenomena (no signal out before a signal in), it follows that $m_z(t) \equiv 0$, $t < 0$, a property that means that $M_z(\omega)$ has no poles in the upper half complex ω plane, i.e., no poles for $\omega = \omega_r + i\omega_i$ with $\omega_i > 0$. These few properties are standard for causal signal transmission [1].

Let us now take up an elementary property of $M_z(\omega)$ regarding its dependence on the depth parameter z. Clearly,

$$\begin{aligned} F_{z_1+z_2}(\omega) &= M_{z_1}(\omega)\, F_{z_2}(\omega) \\ &= M_{z_1}(\omega)\, M_{z_2}(\omega)\, F_0(\omega) \\ &= M_{z_1+z_2}(\omega)\, F_0(\omega)\,. \end{aligned} \tag{5}$$

Since $F_0(\omega)$ is arbitrary in this expression, it follows that

$$M_{z_1+z_2}(\omega) = M_{z_1}(\omega)\, M_{z_2}(\omega) \tag{6}$$

holds for all nonnegative z_1 and z_2. In particular, it follows that

$$M_0(\omega) = M_0(\omega)^2 \tag{7}$$

implying that either $M_0(\omega) = 1$ or $M_0(\omega) = 0$. If there are frequency bands that $F_0(\omega)$ will never possess, then it is possible to choose $M_0(\omega) = 0$ in that

band, but for simplicity we may as well assume that $M_0(\omega) = 1$ for all ω since the final answer will be unchanged. Moreover, on physical grounds it is natural to assume, for each ω, that $M_z(\omega)$ is a continuous function of z. In that case, a standard argument asserts that the only function that fulfills (6) necessarily has the functional form

$$M_z(\omega) = e^{-z\,A(\omega)} \,. \tag{8}$$

Let us recall that argument.

To establish the stated form for $M_z(\omega)$, we first observe that

$$M_z(\omega) = [M_{z/n}(\omega)]^n \tag{9}$$

for an arbitrary positive integer n. Since $M_z(\omega)$ is assumed to be continuous and $M_0(\omega) = 1$, it follows that $M_{z/n}(\omega) \neq 0$ for large enough n, and so $M_z(\omega) \neq 0$ for any z. Next, let $R_z(\omega) \equiv \ln(M_z(\omega))$, which is well defined for all z and ω; furthermore, (6) leads to $R_{z_1+z_2}(\omega) = R_{z_1}(\omega) + R_{z_2}(\omega)$. This relation implies that $R_{nz}(\omega) = nR_z(\omega)$ as well as $R_{z/m}(\omega) = (1/m)R_z(\omega)$, for arbitrary positive integers n and m. Consequently,

$$R_{nz/m}(\omega) = (n/m)R_z(\omega) \,. \tag{10}$$

Now let $z = 1$ so that $R_{n/m}(\omega) = (n/m)R_1(\omega)$; then take a limit such that $(n/m) \to z$, an arbitrary positive number. By the assumption of continuity, this limit converges and we learn that

$$R_z(\omega) = z\,R_1(\omega) \equiv -z\,A(\omega) \,. \tag{11}$$

This concludes the proof of (8).

As the transfer function of a passive medium it is necessary that $|M_z(\omega)| \leq 1$ in which case we also find that $\mathrm{Re}\,A(\omega) \geq 0$. To simplify notation, we let

$$A(\omega) = B(\omega) + iC(\omega) \,, \tag{12}$$

where $B(\omega) = \mathrm{Re}\,A(\omega)$ and $C(\omega) = \mathrm{Im}\,A(\omega)$. Thus we require that

$$B(\omega) \geq 0 \,. \tag{13}$$

By causality, $B(\omega)$ and $C(\omega)$ are related by Hilbert transforms, while $C(\omega)$ is undetermined by this procedure up to the contribution of a so-called Blaschke

factor. We also note that for real functions $f_z(t)$ for all z and any initial signal $f_0(t)$, it necessarily follows that the impulse response function $m_z(t)$ is a real function. Consequently, $M_z(-\omega) = M_z(\omega)^*$, which implies that

$$B(-\omega) = B(\omega)\,, \tag{14}$$

$$C(-\omega) = -C(\omega)\,. \tag{15}$$

Since $B(\omega) \geq 0$ it follows that the function $B(\omega)$ has special properties at and near any frequency, say ω', for which $B(\omega') = 0$. Assuming on physical grounds that $B(\omega)$ is continuous in ω, and even has a few derivatives [e.g., $B(\omega) \in C^2$], then the behavior of B in the vicinity of ω' is given by

$$B(\omega) = \tfrac{1}{2}a^{-1}(\omega - \omega')^2\,, \qquad (\omega - \omega')^2 \ll 1\,. \tag{16}$$

where $a > 0$ has the units of acceleration (e.g., m/s^2).

Let us focus on the behavior of $A(\omega)$ in the vicinity of $\omega = 0$. In that case, and to sufficient accuracy, we have

$$B(\omega) = L^{-1} + \tfrac{1}{2}a^{-1}\omega^2\,, \tag{17}$$

$$C(\omega) = -v^{-1}\omega\,, \tag{18}$$

where L, v, and a denote constants with the dimensions of length, velocity, and acceleration, respectively. The behavior at $\omega = 0$ forces $L^{-1} \geq 0$. Moreover when $B(0) = L^{-1} = 0$, it follows that $a^{-1} \geq 0$; in that case, we shall adopt the generic form and assume that $a > 0$.

It is natural to ask the question: Under what circumstances does it follow that $B(0) = 0$? A common model of a passive medium is based on the Lorentz model [2]. The physical principle behind this model is the response of a damped harmonic oscillator to a driving force. The physical model in this case is given by

$$m\ddot{q}(t) + b\dot{q}(t) + kq(t) = h(t)\,, \tag{19}$$

where $m > 0$, $b \geq 0$, and $k > 0$ denote the inertial, damping, and restorative parameters, $q(t)$ denotes the oscillator amplitude, and $h(t)$ denotes the applied force. Assuming that any transients have decayed away, let us focus on the steady state solution. If $h(t) = U\cos(\omega t)$, then $q(t) =$

$V\cos(\omega t) + W\sin(\omega t)$, where

$$V = \frac{(k - m\omega^2)U}{(k - m\omega^2)^2 + (b\omega)^2}\,, \tag{20}$$

$$W = \frac{b\omega U}{(k - m\omega^2)^2 + (b\omega)^2}\,. \tag{21}$$

If the driving frequency $\omega = 0$ for this model it follows that $V = U/k$ and $W = 0$. Since this result is entirely independent of the dissipation coefficient b, it holds even when $b = 0$, namely, it holds in the case there is no loss whatsoever. Consequently, for such a model it follows that at $\omega = 0$ there can be *no* loss and so $B(0) = 0$. Of course, such an argument does not apply to a metal, but it does hold for a broad spectrum of materials.

Although we have argued that $B(0) = 0$ for a specialized model, it is quite plausible that such a result holds for a wide class of models as well. One such more general model would be of the form

$$m_i\ddot{q}_i(t) + b_i\dot{q}_i(t) + \Sigma_{j=1}^{J} k_{ij}\, q_j(t) = h(t)\,, \qquad 1 \le i \le J\,, \tag{22}$$

which corresponds to a situation where $h(t)$ acts as the driving force on a collection of coupled damped harmonic oscillators. Again we may consider the steady state response when $h(t) = U\cos(\omega t)$. In particular, if $\omega = 0$ the solution is totally independent of any dissipation parameters. Consequently, it follows that $B(0) = 0$ in this case as well. It is not difficult to imagine other, more complicated situations for which the same result holds. Therefore, on the basis of a wide class of physically plausible models, we are encouraged to consider the consequences of the assumption that $B(\omega) = \frac{1}{2}a^{-1}\omega^2$, $a > 0$, when ω is small.

We now examine the signal behavior as a function of z that follows from the foregoing discussion. In particular, we first focus on the impulse response function

$$m_z(t) = \frac{1}{2\pi}\int e^{-i\omega t}\, e^{iv^{-1}z\omega - za^{-1}\omega^2/2 - z\tilde{A}(\omega)}\, d\omega\,, \tag{23}$$

where $\tilde{A}(\omega) \equiv \tilde{B}(\omega) + i\tilde{C}(\omega)$, and $\tilde{B}(\omega) = O(\omega^4)$ while $\tilde{C}(\omega) = O(\omega^3)$. To simplify matters, let us further assume that $\tilde{B}(\omega)$ is bounded away from 0 for nonzero values of ω. In that case, for large z, we observe that the integrand

tends to be strongly suppressed for ω away from zero. To sufficient accuracy it follows that we may set

$$m_z(t) = \frac{1}{2\pi}\int e^{-i\omega(t-v^{-1}z)}\, e^{-za^{-1}\omega^2/2}\, d\omega$$
$$= \sqrt{\frac{a}{2\pi z}}\, \exp\Big(-\frac{a(t-v^{-1}z)^2}{2z}\Big)\,. \tag{24}$$

Consequently, for large z values we learn that

$$f_z(t) = \int m_z(t-s)\, f_0(s)\, ds$$
$$= \sqrt{\frac{a}{2\pi z}}\int \exp\Big(-\frac{a(t-s-v^{-1}z)^2}{2z}\Big)\, f_0(s)\, ds$$
$$= \sqrt{\frac{a}{2\pi z}}\int e^{-as^2/2z}\, f_0(s+t-v^{-1}z)\, ds\,. \tag{25}$$

There are two characteristic features of this resultant behavior that are worth emphasizing:

1. According to the square root prefactor, it follows that the amplitude decays proportional to $z^{-1/2}$.

2. According to the integral factor, the result has a temporal dependence determined by the form of the original signal centered at a temporal value of $t-v^{-1}z$, and then integrated over that region weighted by a Gaussian of increasing width.

Approximate causality

Before passing to several examples of (25) it is important to observe that the medium impulse response function (24) is *not* causal since it does not vanish for $t < 0$. In point of fact, the expressions (17) and (18) do *not* make a strictly causal impulse function. However, they make an *approximate* causal function provided that $az \gg v^2$ since in that case the impulse function is extremely small for $t < 0$. Let us examine this situation more closely.

In order for the medium function $A(\omega)$ to correspond to a causal function it should be represented in the form

$$A(\omega) = \int_0^\infty [1 - e^{i\omega s}]\, k(s)\, ds\,, \tag{26}$$

where $A(0) = 0$, and in order that $\mathrm{Re}A(\omega) = B(\omega) \geq 0$ it is sufficient that the weight function $k(s) \geq 0$. Observe, by this representation, that $A(\omega)$ is analytic in the upper half plane, which is a necessary and sufficient condition for the impulse function to be causal. Now, as an example, consider $k(s) = K'e^{-Ks}$, where K' and K are positive parameters to be determined. In that case

$$B(\omega) = K' \int_0^\infty [1 - \cos(\omega s)]\, e^{-Ks}\, ds\,, \tag{27}$$

$$C(\omega) = -K' \int_0^\infty \sin(\omega s)\, e^{-Ks}\, ds\,. \tag{28}$$

We are intested in a large value for both K and K' such that, to some approximation, $k(v)$ acts rather like a delta function in the integrand focusing on values of v near zero. Thus, to a certain approximation,

$$B(\omega) = \tfrac{1}{2} K'\omega^2 \textstyle\int_0^\infty s^2 e^{-Ks}\, ds + \cdots\,, \tag{29}$$

$$C(\omega) = -K'\omega \int_0^\infty s\, e^{-Ks}\, ds + \cdots\,. \tag{30}$$

On comparison with (17) and (18) we see that

$$a^{-1} = K' \int_0^\infty s^2 e^{-Ks}\, ds = 2K'/K^3\,, \tag{31}$$

$$v^{-1} = K' \int_0^\infty s\, e^{-Ks}\, ds = K'/K^2\,. \tag{32}$$

Thus $a = \frac{1}{2} Kv$. Provided $K \gg 1$, this approximation is satisfactory from a practical viewpoint; otherwise some of the additional terms in (29) and (30) need to be taken into account. Unfortunately, introducing additional terms makes the medium impulse response function no longer analytically tractable, generally speaking.

Specific examples

Let us illustrate the resultant signal (25) in two important examples. First we consider an analytically simple case, namely a Gaussian initial pulse. Thus, let

$$f_0(t) = e^{-t^2/2T^2} \cos(\omega_o t)\,, \tag{33}$$

where we refer to T as the pulse width. In this case, (25) reads

$$f_z(t) = \sqrt{\frac{a}{2\pi z}} \int e^{-a(s-t+v^{-1}z)^2/2z} e^{-s^2/2T^2} \cos(\omega_o s)\, ds\,. \tag{34}$$

An elementary integration leads to

$$f_z(t) = \frac{1}{\sqrt{1+z/aT^2}} \times \exp\Big(-\frac{[(a/z)(t-v^{-1}z)^2+\omega_o T^2]}{2(1+aT^2/z)}\Big) \cos\Big(\frac{\omega_o(t-v^{-1}z)}{1+z/aT^2}\Big)\,. \tag{35}$$

If we assume that $z \gg aT^2$, then in effect (35) reduces to

$$f_z(t) = \sqrt{\frac{aT^2}{z}} \exp\Big[-\frac{a(t-v^{-1}z)^2}{2z} - \frac{(\omega_o T)^2}{2}\Big]\,. \tag{36}$$

The peak amplitude of the resultant pulse $f_z(t)$ occurs when $z = vt$, or stated otherwise when $t = v^{-1}z$. At that point in z (or at that moment in time t), the amplitude has been reduced from its initial maximum of unity by a factor proportional to $z^{-1/2}$. The resultant pulse shape in the present case is still Gaussian, but it is substantially broadened since the pulse width T of the input Gaussian has been replaced by $\sqrt{z/a} \gg T$. If we assume the energy (or power) in a given pulse $f_z(t)$ is proportional to $\int |f_z(t)|^2\, dt$, then it follows, for $z \gg aT^2$, that the normalized signal energy is given by

$$\frac{\int |f_z(t)|^2\, dt}{\int |f_0(t)|^2\, dt} = \sqrt{\frac{aT^2}{z}}\, e^{-(\omega_o T)^2}\,. \tag{37}$$

As anticipated, this ratio decreases as z increases, but thanks to the pulse broadening, it decreases only as $z^{-1/2}$ rather than z^{-1}, as may have been expected.

As a second example, we suppose that

$$f_0(t) = \mathrm{rect}(t/T)\cos(\omega_o t)\,, \tag{38}$$

which leads to the output signal

$$f_z(t) = \sqrt{\frac{a}{2\pi z}} \int_{-T/2}^{T/2} e^{-a(s-t+v^{-1}z)^2/2z} \cos(\omega_o s)\, ds\,. \tag{39}$$

This integral depends on z in a moderately involved way, and for convenience we only evaluate (39) in the case that $z \gg aT^2$. Then we find

$$f_z(t) = \sqrt{\frac{a}{2\pi z}} \int_{-T/2}^{T/2} e^{-a(t-v^{-1}z)^2/2z} \cos(\omega_o s)\, ds$$
$$= \sqrt{\frac{aT^2}{2\pi z}} \left[\frac{\sin(\omega_o T/2)}{(\omega_o T/2)}\right] e^{-a(t-v^{-1}z)^2/2z} . \tag{40}$$

Again, the result is that of a traveling pulse moving essentially at the speed v, the amplitude of which falls off with distance like $z^{-1/2}$, provided of course that $\sin(\omega_o T/2) \neq 0$. For the case that $\sin(\omega_o T/2) = 0$, $\omega_o T \neq 0$, see below.

More general inputs

Apart from an unimportant factor, observe that the amplitude factor from $f_0(t)$ in (36), i.e., $\exp[-\omega_o^2 T^2/2]$, is basically $F_0(0) = \int f_0(s)\, ds$, and the amplitude factor in (40), i.e., $\sin(\omega_o T/2)/(\omega_o T/2)$ is essentially just $F_0(0) = \int f_0(s) ds$. We can understand and generalize this result as follows. Since

$$f_z(t) = \int m_z(t-s) f_0(s)\, ds\ , \tag{41}$$

it follows, for an initial signal which is much narrower in the temporal domain than the medium response function, that we can make a Taylor series expansion of the medium response function. In particular, we have

$$f_z(t) = \int [m_z(t) f_0(s) - m_z'(t) s f_0(s) + \tfrac{1}{2} m_z''(t) s^2 f_0(s) + \cdots]\, ds$$
$$= m_z(t) \int f_0(s)\, ds - m_z'(t) \int s f_0(s)\, ds + \tfrac{1}{2} m_z''(t) \int s^2 f_0(s)\, ds + \cdots . \tag{42}$$

When $m_z(t)$ is sufficiently broad in time, then its time derivatives are typically much smaller, and the indicated sum involves terms that are rapidly diminishing relative to the former terms.

As an example of the application of (42), suppose that $\omega_o T = 2n\pi$, $n \in \{1, 2, 3, \ldots\}$, then (40) vanishes because $\int f_0(s)\, ds = 0$. Moreover, since $f_0(t)$ in (38) is an even function, it also follows that $\int s f_0(s)\, ds = 0$. Thus according to (42), we find to leading order that

$$f_z(t) = \tfrac{1}{2} m_z''(t) \int s^2 f_0(s)\, ds\ , \tag{43}$$

namely,

$$f_z(t) = (-1)^n \frac{T^2}{(n\pi)^2} \sqrt{\frac{a}{2\pi z}} \frac{1}{z^2} \Big[a(t - z/v)^2 - z \Big] \, e^{-a(t-z/v)^2/2z} \,, \qquad (44)$$

where the amplitude has been evaluated when $\omega_o T = 2n\pi$.

Commentary

Observe, that although the original Gaussian and the rectangular envelopes are fundamentally different, the pulses that result after a long propagation distance $z \gg aT^2$ are essentially the same, differing only in their respective amplitudes. Those amplitudes effectively measure the spectral content of the original pulse at zero frequency where the narrow window of transmission exists, and for the Gaussian envelope that content is much smaller than is available with the rectangular envelope. This result is entirely consistent with the concept that the output selects its preferred signal shape consistent with the frequency window allowed by the medium. Ultimately, this means that the transmitted signal is Gaussian in character with an ever increasing pulse width in accord with the ever narrowing Gaussian pass band as z increases. This kind of temporal behavior is essentially the kind of behavior typically ascribed to the so-called Brillouin precursor [2]. It is paradoxical, but true, that Brillouin precursors require pulse envelopes with *high* frequency content. Sharp edges in pulse envelopes significantly enhance the high frequency content as compared to smooth envelopes, and this situation is clearly illustrated in Eqs. (36) and (40).

However, sharp edges in pulse envelopes are not the only way to raise the high frequency content.

Chirp Signals

As an initial signal consider the linearly chirped signal [3]

$$f_0(t) = e(t) \cos(\omega_o t + \tfrac{1}{2}\alpha t^2) \,, \qquad (45)$$

where the signal envelope $e(t)$ has a pulse width of T and we assume that $\alpha T^2 \gg 1$. The Fourier transform of (45) may be approximately given by

$$F_0(\omega) = \frac{1}{2} \sqrt{\frac{2\pi}{i\alpha}} e((\omega - \omega_o)/\alpha) e^{i(\omega-\omega_o)^2/2\alpha}$$

$$+\frac{1}{2}\sqrt{\frac{2\pi i}{\alpha}}e(-(\omega+\omega_o)/\alpha)e^{-i(\omega+\omega_o)^2/2\alpha}\,. \tag{46}$$

The frequency content at $\omega = 0$ is then given by

$$F_0(0) = \frac{1}{2}\sqrt{\frac{2\pi}{i\alpha}}e(-\omega_o/\alpha)e^{i\omega_o^2/2\alpha} + \frac{1}{2}\sqrt{\frac{2\pi i}{\alpha}}e(-\omega_o/\alpha)e^{-i\omega_o^2/2\alpha}\,. \tag{47}$$

As an illustration, consider $e(t) = \exp(-t^2/2T^2)$. In this case,

$$F_0(0) = \sqrt{\frac{\pi}{\alpha}}\exp\Big[-\frac{(\omega_o T)^2}{2\alpha^2 T^4}\Big]\Big[\cos\Big(\frac{(\omega_o T)^2}{\alpha T^2}\Big) + \sin\Big(\frac{(\omega_o T)^2}{\alpha T^2}\Big)\Big]\,. \tag{48}$$

As noted above this factor essentially dictates the amplitude for the output Gaussian in (24).

The main point to observe in this calculation is the significant enhancement of the overall amplitude of the signal that will emerge. In particular, the primary change has been that the factor $\exp[-(\omega_o T)^2/2]$ in (36) has been replaced by $\exp[-(\omega_o T)^2/2\alpha^2 T^4]$, where $\alpha T^2 \gg 1$. This model calculation strongly suggests that combining chirp signals with envelopes having sharp or nearly sharp edges should lead to signals with relatively significant precursor content.

Composite Media

Up to this point we have assumed that the signal propagates through a single, homogenous medium, the properties of which are characterized by the complex medium function $A(\omega)$. Suppose instead we deal with a composite media made up from J layers each of thickness $l_1 = z_1,\ l_2 = z_2 - z_1, \ldots, l_J = z_J - z_{J-1}$. To each layer we attribute a medium function $A_j(\omega)$, $1 \le j \le J$. If we assume that $z_j \le z \le z_{j+1}$, for example, then

$$M_z(\omega) = \exp[-(z - z_j)\,A_{j+1}(\omega) - \Sigma_{k=1}^{j}\, l_k A_k(\omega)]\,. \tag{49}$$

A more convenient expression for such media is given by

$$M_z(\omega) = \exp[-\textstyle\int_0^z A_u(\omega)\,du]\,, \tag{50}$$

which applies for piecewise constant functions $A_u(\omega)$. It is plausible that such an expression applies as well for slowly varying media functions $A_u(\omega)$.

As was previously the case, it is useful to separate $A_u(\omega)$ into real and imaginary parts, i.e.,

$$M_z(\omega) = \exp[-\textstyle\int_0^z B_u(\omega)\,du - i\int_0^z C_u(\omega)\,du]\,. \tag{51}$$

Under suitable conditions we may set

$$B_u(\omega) = \tfrac{1}{2}a^{-1}(u)\omega^2\,, \qquad C_u(\omega) = -v^{-1}(u)\omega\,, \tag{52}$$

in which case we are led to

$$M_z(\omega) = \exp[-\tfrac{1}{2}\textstyle\int_0^z a^{-1}(u)\omega^2\,du + i\int_0^z v^{-1}(u)\omega\,du]\,. \tag{53}$$

Equations (51) and (53) apply to various situations.

As a simple example of how these equations may be applied let us consider a signal that penetrates a passive medium with a finite thickness of ℓ and otherwise propagates in free space. Therefore, in this case $B_u(\omega) > 0$ for $0 < u < \ell$, while for $u > \ell$, $B_u(\omega) = 0$. This example pertains to a radar signal that penetrates a canopy of foliage or some other absorbing and dispersive medium. Even a comparatively thin passive medium may be well approximated by (53) when $A_u(\omega)$ is sufficiently large for $\omega \neq 0$. Under the stated conditions it follows, when $z > \ell$, that

$$M_z(\omega) = \exp\{-\ell\omega^2/2\tilde{a} + i[(z-\ell)\omega/c + \ell\omega/\tilde{v}]\}\,, \tag{54}$$

where c is the speed of light in vacuum, and

$$\begin{aligned} \tilde{a} &\equiv \ell\,[\textstyle\int_0^\ell a(u)^{-1}\,du]^{-1}\,, \\ \tilde{v} &\equiv \ell\,[\textstyle\int_0^\ell v(u)^{-1}\,du]^{-1}\,. \end{aligned} \tag{55}$$

Since $v(u) \leq c$, it follows that $\tilde{v} \leq c$. For simplicity in our example, let us assume that $\tilde{v} \simeq c$. Finally, when $\ell/\tilde{a}$ is sufficiently large, we are led to

$$f_z(t) = \sqrt{\tilde{a}/\ell}\; e^{-\tilde{a}(t-z/c)^2/2\ell} \textstyle\int f_0(s)\,ds\,, \tag{56}$$

defined for $z > \ell$. If $F_0(0) = 0$, then appeal can be made to (42).

This equation should be compared with Eq. (36) that corresponds to propagation within a single, homogeneous passive medium. The temporal signal in both cases is Gaussian and apart from the overall amplitude, the shape is principally determined by the passive medium. This result holds whenever the medium acts as a low pass filter for an initial signal that, comparatively speaking, has a broad spectral content including $\omega = 0$.

Stochastic Media

Under certain cimcumstances, it is appropriate to regard the passive medium as a stochastic variable and to define the output signal as the ensemble average of a stochastic output. A description of this kind may arise if the output signal is the superposition of multiple signals from a rapidly changing collection of media profiles. More specifically, such a situation may arise in the case of a coherent superposition of multiple radar pulse returns that have traversed a rapidly fluctuating medium. While details of the fluctuating medium may be too difficult to describe, certain overall features – stochastic invariants – may provide gross characteristics with which selected signal properties may be analyzed.

Let us focus on propagation through a stochastic but otherwise homogeneous medium. In mathematical terms this means that $M_z(\omega)$ and thereby $A(\omega)$ are regarded as suitable stochastic variables. The observed signal $f_z^o(t)$ is determined by the expression

$$f_z^o(t) = \frac{1}{2\pi}\int e^{-i\omega t}\,\langle e^{-zA(\omega)}\rangle\, F_0(\omega)\,d\omega\,, \tag{57}$$

where $\langle(\cdot)\rangle$ denotes an ensemble average. Let us illustrate the kind of behavior that may occur. For that purpose we again suppose that

$$A(\omega) = \tfrac{1}{2}a^{-1}\omega^2 - iv^{-1}\omega \tag{58}$$

and we assume that a is the only random variable. As an example we suppose that the variable a, which can only be positive, is distributed according to a probability density given by

$$p(a^{-1}) = \frac{b}{m!}(ba^{-1})^m e^{-ba^{-1}}\,, \qquad 0 < a^{-1} < \infty\,, \tag{59}$$

where b is a parameter which essentially sets the scale. In particular, the mean value of a^{-1} is given by

$$\int_0^\infty a^{-1}p(a^{-1})\,da^{-1} = \frac{m+1}{b}\,. \tag{60}$$

As a consequence, we find that

$$f_z^o(t) = \frac{1}{2\pi}\int e^{-i\omega(t-z/v)}\frac{F_0(\omega)}{(1+z\omega^2/b)^{m+1}}\,d\omega\,. \tag{61}$$

Even without evaluating the Fourier transform it is clear that our stochastic example has led to a dramatically enhanced pass band at low frequencies. This result is due, of course, to the nonvanishing probability that arbitrarily small values of a^{-1} are present in the ensemble, despite the fact that the probability that $a^{-1} = 0$ is strictly zero for any $m \geq 1$.

As outlined in (42), the leading behavior of (61) is given by

$$f_z^o(t) = m_z^o(t) \int f_0(s)\, ds\,, \tag{62}$$

where

$$m_z^o(t) = \frac{1}{2\pi} \int \frac{e^{-i\omega t}}{(1 + z\omega^2/b)^{m+1}}\, d\omega\,. \tag{63}$$

This expression may be evaluated in the following form:

$$m_z^o(t) = \frac{1}{2^{m+1}} \frac{1}{m!} \sqrt{b/z} \left\{ \sum_{l=0}^{m} C_l^{(m)} \left(\sqrt{b/z}\, |t - z/v| \right)^l \right\} e^{-\sqrt{b/z}\,|t - z/v|}\,, \tag{64}$$

where the $C_l^{(m)}$ coefficients, for $0 \leq l \leq m$ and $1 \leq m$, are determined by the recursion relation

$$\begin{aligned} C_m^{(m)} &= 1 \\ C_0^{(m)} &= (2m-1)!! \\ C_l^{(m)} &= (2m-1-l) C_l^{(m-1)} + C_{l-1}^{(m-1)}, \quad 1 \leq l \leq m-1\,. \end{aligned} \tag{65}$$

Conclusions

Traditional radar applications involve signal generation, transmission, and reception, with little or no spectral modification save for a possible spectral shift (or dilation) due to relative motion. By contrast, radar signals, or electromagnetic waves more generally, that traverse passive media with normal absorptive and dispersive properties, typically suffer significant spectral distortion. For example, over a large spectral domain, an exponential attenuation effectively removes any signal energy. An exception to exponential attenuation occurs at zero frequency when attenuation is frequently absent. On the basis of generally applicable arguments, and under a wide

set of circumstances, it has been clearly demonstrated in this paper that the amplitude of the transmitted signal decays as the inverse square root of the distance traveled rather than exponetially. Such behavior is exactly that characteristic of so-called Brillouin percursors [1, 2]. While such phenomena are frequently discussed in terms of more advanced mathematical techniques, it is demonstrated in the present work that they can be largely understood in terms of fairly simple pass band arguments.[1]

The simplicity of the present discussion has enabled us to determine the form of signals that have traversed inhomogeneous or stochastic media as well. The robustness of the characteristic precursor decay rate has also been established for these more general media.

Acknowledgments

Thanks are expressed to T. Olson and S.V. Shabanov for their interest and their comments. This work has been partially supported by AFOSR Grant F49620-01-1-0473.

References

[1] J.D. Jackson, *Classical Electrodynamics*, (Wiley & Sons, New York, 1975).

[2] See, e.g., K.E. Oughstun and G.C. Sherman, *Propagation of Electromagnetic Pulses in a Linear Dispersive Medium with Absorption* (Springer-Verlag, Heidelberg, 1994).

[3] J.R. Klauder, A.C. Price, S. Darlington and W.J. Albersheim, "The Theory and Design of Chirp Radars", Bell System Technical Journal **39**, 745-808 (1960).

[1] It is noteworthy that my colleague Tim Olson has devised quite another explanation for precusor behavior. See his forthcoming paper "Derivation of Precursors via Finite Toeplitz Forms".

Applications of the wave packet method to resonant transmission and reflection gratings

Andrei G. Borisov [a,1] and Sergei V. Shabanov [b,2]

[a] *Laboratory of Atomic and Molecular Collisions, University of Paris-Sud, Orsay, France*

[b] *Department of Mathematics, University of Florida, Gainesville, FL 32611, USA*

Abstract

Maxwell's theory for an electromagnetic pulse propagating in passive linear media is reformulated in the Hamiltonian formalism so that the time evolution is governed by the first-order equation, $\partial\Psi/\partial t = \mathcal{H}\Psi$, where $\mathcal{H}$ is a linear differential operator (Hamiltonian) acting on a multi-dimensional vector Ψ built of the electromagnetic inductions and auxiliary matter fields describing the medium response. The initial value problem is then solved by means of the time leapfrog method in combination with the Fourier pseudospectral method, leading to a time domain algorithm for numerical simulations of wide-band electromagnetic wave packet propagation and scattering. The algorithm is applied to scattering of a femtosecond laser pulse on resonant transmission and reflection gratings made of dispersive (Drude metals) and dielectric materials.

[1]email: borisov@lcam.u-psud.fr

[2]email: shabanov@phys.ufl.edu

1 Lorentz models in the Hamiltonian formalism

Propagation of an electromagnetic wave packet in passive (dispersive and absorbing) media in the absence of external radiating sources is described by the following set of equations [1]

$$\partial_t \mathbf{D}_t = c\nabla \times \mathbf{H}_t \,, \quad \partial_t \mathbf{B}_t = -c\nabla \times \mathbf{E}_t \,, \tag{1.1}$$

$$\mathbf{D}_t = \mathbf{E}_t + \mathbf{P}_t \,, \quad \mathbf{B}_t = \mathbf{H}_t + \mathbf{M}_t \,, \tag{1.2}$$

$$\nabla \cdot \mathbf{D}_t = \nabla \cdot \mathbf{B}_t = 0 \,, \tag{1.3}$$

where $\mathbf{E}_t$ and $\mathbf{H}_t$ are electric and magnetic fields, respectively, $\mathbf{D}_t$ and $\mathbf{B}_t$ are the corresponding inductions, $\mathbf{P}_t$ and $\mathbf{M}_t$ are the medium polarization and magnetization vectors, c is the speed of light, ∂_t stands for the partial derivative with respect to time t, boldface letters denotes three-vector fields in $\mathbb{R}^3$ whose spatial argument, denoted below by $\mathbf{r}$, is suppressed, and the time dependence is indicated by a subscript. The time evolution of the medium response is usually described in the framework of a particular microscopic medium model. In the present study, multiresonant Lorentz models are considered. A general case within the formalism being developed can be found in [2]. In the Lorentz model, the medium magnetization is zero, while the medium polarization is described by a set of decoupled second-order differential equations [1]

$$\partial_t^2 \mathbf{P}_t^a + 2\gamma_a \partial_t \mathbf{P}_t^a + \omega_a^2 \mathbf{P}_t^a = \omega_{pa}^2 \mathbf{E}_t \,, \qquad \mathbf{P}_t = \sum_{a=1}^{N} \mathbf{P}_t^a \,. \tag{1.4}$$

where ω_a are resonant frequencies, γ_a are the damping coefficients, and ω_{pa} are the so called plasma frequencies.

In our approach no boundary conditions are imposed on electromagnetic fields at medium and/or target interfaces. The latter are modeled by spatially dependent couplings of media to electromagnetic fields, $\omega_{pa} = \omega_{pa}(\mathbf{r})$. At any interface, the couplings are allowed to have discontinuities, or, from the physical point of view, they remain smooth but change rapidly, $\lambda_w |\nabla \omega_p| / \omega_p \gg 1$, at the interface, where λ_w is a typical wave length of the incoming wave packet. The conventional boundary conditions are automatically generated by the dynamics [1].

The initial value problem is solved in the space of square integrable functions for every component of the medium polarization and electromagnetic fields. This implies that the energy of the propagating wave packet remains finite (in contrast to the scattering matrix approach based on plane wave solutions). The initial conditions imposed are $\mathbf{P}_{t=0} = \partial_t \mathbf{P}_{t=0} = 0$ and the electromagnetic fields form an initial wave packet built of radiation electromagnetic fields.

The best way to solve the initial value problem for a system of differential equations is to find its fundamental solution. The latter problem is often studied by means of the Hamiltonian formalism [3]. In the framework of the Hamiltonian formalism, an original system of differential equations is transformed to an equivalent system of first-oder (in time) differential equations by expanding the original configuration space, that is, by going over to a generalized phase space

where all time derivatives, save for the one of highest order, become independent variables [3]. A generic linear homogeneous first-order system can be written in the form

$$\partial_t \Psi_t = \mathcal{H}\Psi_t \,, \qquad \Psi_{t=0} = \Psi_0 \,, \tag{1.5}$$

where a linear operator $\mathcal{H}$ is called Hamiltonian, while Ψ_t is called a state vector (or wave function). It is an element of the generalized phase space of the system and viewed a collection (column) of the original variables and their time derivatives. The generalized phase space is equipped with an inner product and becomes a Hilbert space. State vectors are typically vector-valued functions, and the Hamiltonian is a differential operator. The choice of the inner product depends on the problem on hands. One usually requires that components of Ψ_t are elements of the space of square integrable functions.

The advantage of the Hamiltonian formalism is evident because the fundamental solution can be written as the exponential of the Hamiltonian,

$$\Psi_t = \exp(t\mathcal{H})\,\Psi_0 \equiv \mathcal{U}_t\Psi_0 \,, \quad t \geq 0 \,, \tag{1.6}$$

assuming, of course, that the exponential of $\mathcal{H}$ exists. In numerical studies, the exponential representation of the fundamental solution yields a rather natural time domain algorithm, $\Psi_{t+\Delta t} = \mathcal{U}_{\Delta t}\Psi_t$. The amplification matrix $\mathcal{U}_{\Delta t}$ can effectively be computed by means of the Kato-Trotter product formula in combinations with pseudospectral methods [2].

The Hamiltonian formalism has been used in [4] to develop a finite differencing algorithm to study an electromagnetic pulse propagation in Lorentz media. Consider $2N$ real vector fields, $\boldsymbol{\xi}_t^j$, $j = 1, 2, ..., 2N$, such that

$$\mathbf{P}_t^a = (\omega_{pa}/\omega_a)\,\boldsymbol{\xi}_t^{2a-1} \,, \tag{1.7}$$

$$\partial_t \boldsymbol{\xi}_t^{2a-1} = \omega_a \boldsymbol{\xi}_t^{2a} \,, \quad \partial_t \boldsymbol{\xi}_t^{2a} = -2\gamma_a \boldsymbol{\xi}_t^{2a} - \omega_a \boldsymbol{\xi}_t^{2a-1} + \omega_{pa}\mathbf{E}_t \,. \tag{1.8}$$

Thus, the original system of second order equations has been converted into the first order system. Another convenient way to introduce the Hamiltonian formalism is to use N complex vector fields $\boldsymbol{\zeta}_t^a$ which satisfy the first order differential equation

$$\partial_t \boldsymbol{\zeta}_t^a = \lambda_a \boldsymbol{\zeta}_t^a - i\omega_{pa}\mathbf{E}_t \,, \quad \mathbf{P}_t^a = \frac{\omega_{pa}}{2\nu_a}\left(\boldsymbol{\zeta}_t^a + \bar{\boldsymbol{\zeta}}_t^a\right) \,, \tag{1.9}$$

where $\lambda_a = -\gamma_a + i\nu_a$ and $\nu_a = \sqrt{\omega_a^2 - \gamma_a^2}$. This representation is defined only if $\gamma_a < \omega_a$ (i.e., the attenuation is not high). From the numerical point of view, solving a *decoupled* system of N first order differential equation and taking complex conjugation (denoted here by an over bar) is less expensive than solving an original system of differential equations to compute the medium polarization.

Define

$$\Psi_t^F = \begin{pmatrix} \psi_t^F \\ \xi_t \end{pmatrix} \,, \quad \Psi_t^I = \begin{pmatrix} \psi_t^I \\ \xi_t \end{pmatrix} \,, \tag{1.10}$$

where the vector ξ_t is composed of ξ_t^a, and

$$\psi_t^F = \begin{pmatrix} \mathbf{E}_t \\ \mathbf{H}_t \end{pmatrix} , \quad \psi_t^I = \begin{pmatrix} \mathbf{D}_t \\ \mathbf{B}_t \end{pmatrix} , \quad \xi_t^a = \begin{pmatrix} \xi_t^{2a-1} \\ \xi_t^{2a} \end{pmatrix} .$$

The wave function Ψ_t^F satisfies the Schrödinger equation

$$\partial_t \Psi_t^F = \mathcal{H}^F \Psi_t^F , \quad \mathcal{H}^F = \begin{pmatrix} \mathcal{H}_0 & \mathcal{V}_{FM} \\ \mathcal{V}_{MF} & \mathcal{H}_M^F \end{pmatrix} , \tag{1.11}$$

where

$$\mathcal{H}_0 = \begin{pmatrix} 0 & c\boldsymbol{\nabla}\times \\ -c\boldsymbol{\nabla}\times & 0 \end{pmatrix} , \tag{1.12}$$

$$\mathcal{V}_{FM} = (\mathcal{V}_{FM1}, \mathcal{V}_{FM2}, \cdots, \mathcal{V}_{FMN}) , \quad \mathcal{V}_{FMa} = \begin{pmatrix} 0 & -\omega_{pa} \\ 0 & 0 \end{pmatrix} , \tag{1.13}$$

$$\mathcal{V}_{MF} = -\mathcal{V}_{FM}^* , \tag{1.14}$$

$$\mathcal{H}_M^F = \mathsf{diag}\ (\mathcal{H}_{M1}^F, \mathcal{H}_{M2}^F, \cdots, \mathcal{H}_{MN}^F) , \quad \mathcal{H}_{Ma}^F = \begin{pmatrix} 0 & \omega_a \\ -\omega_a & -2\gamma_a \end{pmatrix} , \tag{1.15}$$

where diag indicates that the corresponding matrix is block-diagonal with blocks listed in the order from the upper left to lower right corners. Note that the matrices $\mathcal{V}_{FMa}$ and $\mathcal{H}_{FMa}$ act on a six-dimensional column ξ^a. Therefore they should be understood as composed of 3×3 blocks. Each block is obtained by multiplying the unit matrix by the number indicated in place of the block in (1.13) and (1.15). We shall refer to (1.11) as to the theory in the field representation.

If the inductions are used as independent electromagnetic degrees of freedom, this is, Ψ_t^I, the corresponding evolution equation can be obtained by the similarity transformation. Let $\mathcal{R}$ be an operator that maps the auxiliary matter field ξ_t onto the actual medium polarization vector, $\mathbf{P}_t = \mathcal{R}\xi_t$. Its explicit form is not hard to deduce. Then

$$\Psi_t^I = \mathcal{S}\Psi_t^F , \quad \mathcal{S} = \begin{pmatrix} 1 & \mathcal{R} \\ 0 & 1 \end{pmatrix} , \quad \mathcal{S}^{-1} = \begin{pmatrix} 1 & -\mathcal{R} \\ 0 & 1 \end{pmatrix} , \tag{1.16}$$

Hence,

$$\partial_t \Psi_t^I = \mathcal{H}^I \Psi_t^I , \quad \mathcal{H}^I = \mathcal{S}\mathcal{H}^F\mathcal{S}^{-1} . \tag{1.17}$$

The corresponding blocks of $\mathcal{H}^I$ have the form

$$\mathcal{H}_I = \mathcal{H}_0 , \quad \mathcal{V}_{MI} = \mathcal{V}_{MF} , \tag{1.18}$$

$$\mathcal{V}_{IM} = \mathcal{V}_{FM} + \mathcal{R}\mathcal{H}_M - \mathcal{H}_0\mathcal{R} = -\mathcal{H}_0\mathcal{R} , \tag{1.19}$$

$$\mathcal{H}_M^I = \mathcal{H}_M^F - \mathcal{V}_{MF}\mathcal{R} . \tag{1.20}$$

In what follows we shall use Ψ_t^Q where Q indicates the representation, F or I.

Our final remark concerns a change of basis in the space of auxiliary fields (canonical transformations in the Hamiltonian formalism). There is a freedom of making general complex nonsingular linear transformations

$$\xi_t \to \mathcal{S}_M \xi_t \,, \quad \det \mathcal{S}_M \neq 0 \,. \tag{1.21}$$

If the infinitesimal evolution operator $\mathcal{U}^Q_{\Delta t} = \exp(\Delta t \mathcal{H}^Q)$ is computed with one choice of the auxiliary fields, a simple similarity transformation, like the one in (1.17), would allow us to compute it in any other basis of auxiliary fields. This is an important observation because the auxiliary field basis can be chosen in a way that facilitates computation of the evolution operator (e.g., to improve the convergence rate or speed up simulations). For instance, in the complex representation (1.9) of the auxiliary fields in the Lorentz model, the matter Hamiltonian $\mathcal{H}^F_M$ is diagonal. The corresponding transformation of the auxiliary fields is given by

$$\begin{pmatrix} \xi_t^{2a-1} \\ \xi_t^{2a} \end{pmatrix} = \frac{1}{2\nu_a} \begin{pmatrix} \omega_a & \omega_a \\ \lambda_a & \bar{\lambda}_a \end{pmatrix} \begin{pmatrix} \zeta_t^a \\ \bar{\zeta}_t^a \end{pmatrix} \equiv \mathcal{S}_M \begin{pmatrix} \zeta_t^a \\ \bar{\zeta}_t^a \end{pmatrix} \,. \tag{1.22}$$

To transform the whole system into this representation, the Hamiltonian $\mathcal{H}^F$ is replaced by $\mathcal{S}^{-1}\mathcal{H}^F\mathcal{S}$ and the wave function Ψ^F_t by $\mathcal{S}\Psi^F_t$ where $\mathcal{S}$ is block-diagonal with the unit matrix in the upper left (field) corner and with $\mathcal{S}_M$ in the lower right (matter) corner.

2 Energy and the norm of state vectors

Let us discuss the choice of a norm in the space spanned by state vectors Ψ^Q_t. Consider multi-resonant Lorentz models with no attenuation $\gamma_a = 0$. The field and matter evolution equations can be obtained from the variational principle for the action

$$S = \int dt L = \int dt \int d\mathbf{r} \left[\frac{1}{2} \left(\mathbf{E}_t^2 - \mathbf{B}_t^2 \right) + \frac{1}{2} \sum_a \left((\partial_t \boldsymbol{\vartheta}_t^a)^2 - \omega_a^2 \boldsymbol{\vartheta}_t^{a2} \right) + \sum_a \omega_{pa} \boldsymbol{\vartheta}_t^a \cdot \mathbf{E}_t \right] \,, \tag{2.1}$$

where electromagnetic degrees of freedom are described by the vector and scalar potentials, respectively, $\mathbf{A}_t$ and φ_t, so that $\mathbf{E}_t = \boldsymbol{\nabla}\varphi_t - \partial_t \mathbf{A}_t$ and $\mathbf{B}_t = \boldsymbol{\nabla} \times \mathbf{A}_t$. The units are chosen in this Section so that $c = 1$. The polarization of the medium is expressed via the matter fields as $\mathbf{P}_t = \sum_a \omega_{pa} \boldsymbol{\vartheta}_t^a$. The least action principle for the scalar potential φ_t leads to the Gauss law, $\boldsymbol{\nabla} \cdot \mathbf{D}_t = 0$, for the vector potential $\mathbf{A}_t$ to the Maxwell's equation, $\partial_t \mathbf{D}_t = \boldsymbol{\nabla} \times \mathbf{B}_t$, and for the matter field $\boldsymbol{\vartheta}_t^a$ to the medium polarization evolution equation of the Lorentz model with no attenuation, $\gamma_a = 0$. The second Maxwell's equation and the Gauss law for the magnetic field follows from the relation $\mathbf{B}_t = \boldsymbol{\nabla} \times \mathbf{A}_t$ by taking its time derivative and divergence, respectively. The energy of the system coincides with the canonical Hamiltonian which is obtained by the Legendre transformation [3] of the Lagrangian L for the velocities $\partial_t \mathbf{A}_t$ and $\partial_t \boldsymbol{\vartheta}_t^a$. Doing the Legendre transform, we find the canonical Hamiltonian (energy) of the system

$$E_t = \frac{1}{2} \int d\mathbf{r} \left[\mathbf{E}_t^2 + \mathbf{B}_t^2 + \sum_a \left(\boldsymbol{\pi}_t^{a2} + \omega_a^2 \boldsymbol{\vartheta}_t^{a2} \right) \right] \,, \tag{2.2}$$

where $\boldsymbol{\pi}_t^a = \delta L/\delta(\partial_t \boldsymbol{\vartheta}^a)$ are canonical momenta of the matter fields. The energy conservation follows directly from the Noether theorem [3] applied to the time translation symmetry of the action (2.1), $\partial_t E_t = 0$. Equation (2.2) becomes the conventional expression for the electromagnetic energy in a passive medium [1] when $\boldsymbol{\pi}_t^a$ and $\boldsymbol{\vartheta}_t^a$ are replaced by the corresponding solutions of the equations of motion with initial conditions $\boldsymbol{\pi}_0^a = \boldsymbol{\vartheta}_0^a = 0$.

An important observation is that the Noether integral of motion (2.2) coincides with the norm squared of the corresponding state vector [2]

$$E_t = \frac{1}{2}\int d\mathbf{r}\, \Psi_t^{F*}\Psi_t^F \equiv (\Psi_t^F, \Psi_t^F) = (\Psi_t^I, \mu\Psi_t^I)\,, \tag{2.3}$$

where $\mu = \mathcal{S}^{-1*}\mathcal{S}^{-1}$. This is proved by observing that $\boldsymbol{\xi}_t^{2a} = \boldsymbol{\pi}_t^a$ and $\boldsymbol{\xi}_t^{2a-1} = \omega_a \boldsymbol{\vartheta}_t^a$ which follow from comparison of the canonical Hamiltonian equations of motion [3] for the canonically conjugated variables $\boldsymbol{\vartheta}_t^a$ and $\boldsymbol{\pi}_t^a$ and Eqs. (1.8) with $\gamma_a = 0$. Note that the canonical momentum conjugated to the vector potential $\mathbf{A}_t$ coincides with $-\mathbf{D}_t = -\mathbf{E}_t - \mathbf{P}_t$, not $-\mathbf{E}_t$ in this system. Therefore, the coupling between the electromagnetic and matter degrees of freedom is included into the term $\mathbf{E}_t^2 = (\mathbf{D}_t - \mathbf{P}_t)^2$ of the canonical Hamiltonian (2.2).

Thus, in the absence of attenuation, the norm of the state vector is proportional to the wave packet electromagnetic energy and, hence, is conserved. The norm conservation follows also from the skew-symmetry of the Hamiltonian $\mathcal{H}^{F*} = -\mathcal{H}^F$ if $\gamma_a = 0$, while (2.3) establishes a relation between the electromagnetic energy and the norm. In the induction representation, the norm in the measure space, defined by the operator μ in (2.3), is also conserved by construction. Consequently, the Hamiltonian is skew-symmetric relative to the measure space scalar product, $\mathcal{H}^{I*}\mu = -\mu\mathcal{H}^I$.

The norm (energy) conservation can be used to control numerical convergence, especially when the aliasing problem in the fast Fourier transform is present, e.g., when parameters of the medium are discontinuous functions in space. In a properly designed algorithm the loss of energy (norm) due to attenuation should be controlled by the symmetric part of the Hamiltonian operator

$$\partial_t E_t = -\sum_a \gamma_a |\boldsymbol{\xi}_t^{2a}|^2 \equiv \frac{1}{2}(\Psi_t^Q, \mathcal{V}_\gamma^Q \Psi_t^Q) \le 0\,, \tag{2.4}$$

where $\mathcal{V}_\gamma^{Q*} = \mathcal{V}_\gamma^Q = (\mathcal{H}^{Q*} + \mathcal{H}^Q)/2 \le 0$ (a negative semidefinite operator) which is, in this case, a diagonal matrix with nonpositive elements.

If the medium in question does not have dispersion and absorption, the formalism is simplified. Let $\varepsilon = \varepsilon(\mathbf{x})$ be the dielectric constant of the medium. If the medium is not isotropic, then ε is symmetric positive definite 3×3 matrix everywhere in space. We rewrite Maxwell's equations in the form

$$\partial_t \psi_t^I = \mathcal{H}_G \psi_t^I\,, \quad \mathcal{H}_G = \begin{pmatrix} 0 & c\boldsymbol{\nabla}\times \\ -c\boldsymbol{\nabla}\times(\varepsilon^{-1}\ ) & 0 \end{pmatrix}\,, \tag{2.5}$$

where the brackets in (ε^{-1}) mean that the induction is first multiplied by ε^{-1} and then the curl of the resulting vector field is computed. Consider the scalar product

$$(\psi_1^I, \mu_\varepsilon \psi_2^I) = \int d\mathbf{r}\ \psi_1^{I*} \mu_\varepsilon \psi_2^I\ , \quad \mu_\varepsilon = \begin{pmatrix} \varepsilon^{-1} & 0 \\ 0 & 1 \end{pmatrix} . \tag{2.6}$$

The Hamiltonian is anti-Hermitian with respect to this scalar product, $\mathcal{H}_G^* \mu_\varepsilon = -\mu_\varepsilon \mathcal{H}_G$. Therefore the corresponding μ norm is preserved in the time evolution generated by $\exp(t\mathcal{H}_G)$, that is, $(\psi_t^I, \mu_\varepsilon \psi_t^I) = (\psi_0^I, \mu_\varepsilon \psi_0^I)$. The electromagnetic energy of the wave packet is conserved because it is proportional to the μ norm of the initial state vector.

3 The algorithm

Consider an equidistantly spaced finite grid with periodic boundary conditions. Let Δr be the grid step and $\mathbf{n}$ be a vector with integer valued components. Then the dynamical variables are projected onto the grid by taking their values at grid points $\mathbf{r} = \mathbf{n}\Delta r$, that is, $\Psi_t^Q(\mathbf{r}) \to \Psi_t^Q(\mathbf{n}\Delta r)$. A cubic grid is assumed. Consider a discrete Fourier transformation associated with the grid, $\tilde{\Psi}_t^Q(\mathbf{n}k_0) = \sum_{\mathbf{n}'} \mathcal{F}_{\mathbf{n}\mathbf{n}'} \Psi_t^Q(\mathbf{n}'\Delta r)$, where $\mathcal{F}^*\mathcal{F} = \mathcal{F}\mathcal{F}^* = 1$. The dual lattice step is $k_0 = 2\pi/\Delta r$. The grid spatial size L and step Δr must be chosen so that the Fourier transform of the initial wavepacket has support within the region $k \in [k_{min}, k_{max}]$ where $k = |\mathbf{k}|$, $k_{max} = k_0$ and $k_{min} = 2\pi/L$. The Hamiltonian $\mathcal{H}^Q$ is split into a sum $\mathcal{H}^Q = \mathcal{H}_0^Q + \mathcal{V}^Q$, where all the spatial derivatives are included into $\mathcal{H}_0^Q$ and $\mathcal{V}^Q$ contains multiplications by position dependent functions. The operator $\mathcal{V}^Q$ is projected naturally

$$\mathcal{V}^Q(\mathbf{r})\Psi_t^Q(\mathbf{r}) \to \mathcal{V}^Q(\mathbf{n}\Delta r)\Psi_t^Q(\mathbf{n}\Delta r)\ . \tag{3.1}$$

Consider $\mathcal{H}_0^Q$ in the Fourier basis, $\mathcal{H}_0^Q(\boldsymbol{\nabla}) \to \mathcal{H}_0^Q(i\mathbf{k})$. The projection is then done via the discrete Fourier transform

$$\mathcal{H}_0^Q(\boldsymbol{\nabla})\Psi_t^Q(\mathbf{r})\Big|_{\mathbf{r}=\mathbf{n}\Delta r} \to \sum_{\mathbf{n}'} (\mathcal{F}^*)_{\mathbf{n}\mathbf{n}'}\, \mathcal{H}_0^Q(i\mathbf{n}'k_0)\tilde{\Psi}_t^Q(\mathbf{n}'k_0)\ . \tag{3.2}$$

The projection (3.2) as well as any action of $\mathcal{H}_0^Q$ on state vectors is performed by the fast Fourier method.

In what follows, the rules (3.1) and (3.2) *define* the action of the operators $\mathcal{V}^Q$ and $\mathcal{H}_0^Q$ and their functions on any state vector. The action of a product of $\mathcal{V}^Q$ and $\mathcal{H}_0^Q$ on any state vector is understood as consecutive actions of these operators according to the rules (3.1) and (3.2) in the order specified in the product. The main advantage of using the Fourier basis is the exponential convergence (versus the polynomial one in finite differencing schemes) [5] as the grid size increases.

The time evolution on the grid is simulated by the time leapfrog method for the Schrödinger equation (1.5) in both the cases, the Lorentz model and the geometric optic case,

$$\Psi_{t+\Delta t} = \Psi_{t-\Delta t} + 2\Delta t \mathcal{H}\Psi_t\ . \tag{3.3}$$

As is well known from the Fourier analysis, the convergence rate can be affected for functions which have discontinuities [6]. The latter is, unfortunately, the case in electromagnetic scattering problems. Suppose there is an interface between two media. It can be deduced from the Maxwell's equations that the components of the electric and magnetic fields, $\mathbf{E}_t$ and $\mathbf{H}_t$, tangential to the interface must be continuous, provided there is no surface electric current on the interface. From the Gauss law it follows that the components of the inductions, $\mathbf{D}_t$ and $\mathbf{B}_t$, normal to the interface must be continuous, provided there is no surface charge on the interface. In contrast, the normal components of the fields and the tangential components of the inductions can be discontinuous. Their discontinuities are proportional to discontinuities of medium parameters (e.g., discontinuities in plasma frequencies in Lorentz models). Therefore, in either the induction or field representation, there are components which suffer discontinuities at the interface. The only way to cope with the problem, while keeping the use of the Fourier basis, is to make the grid finer. This would lead to a substantial waste of computational resources because the sampling efficiency should only be increased in the neighborhood of medium interfaces. The use of wavelet bases might be efficient for such a task [7]. Here we retain the Fourier basis, and increase the sampling efficiency by a change of variables.

Consider a change of variables $\mathbf{y} = \mathbf{y}(\mathbf{x})$. A uniform grid in the new variables $\mathbf{y}$ would generate a non-uniform grid in the original Euclidean (physical) coordinates $\mathbf{x}$. A desired local density of grid points in the physical space, to enhance the sampling efficiency in designated regions, can be achieved by an appropriate choice of the functions $\mathbf{y}(\mathbf{x})$ [8]. The fast Fourier transform algorithm is applied to the auxiliary uniform grid according to the rule $\boldsymbol{\nabla}_{\mathbf{x}} = \mathcal{A}(\mathbf{y})\boldsymbol{\nabla}_{\mathbf{y}}$, where the product of the derivative and multiplication operators is treated by the rules (3.2) and (3.1).

Let us introduce the amplification matrix for the leapfrog algorithm, $\Psi_{t+\Delta t} = \mathcal{G}_{\Delta t}\Psi_t$. It satisfies the equation $\mathcal{G}_{\Delta t}^2 - 2\Delta t\mathcal{H}\mathcal{G}_{\Delta t} - 1 = 0$ which has two solutions

$$\mathcal{G}_{\Delta t}^{(\pm)} = \mathcal{H}\Delta t \pm \sqrt{1 + \mathcal{H}^2\Delta t^2}\ . \tag{3.4}$$

The stability of the algorithm requires that the energy norm of both the solutions $(\mathcal{G}_{\Delta t}^{(\pm)})^n\Psi_0$ must be bounded. The necessary condition (but not sufficient) is the von Neumann condition that the spectral radius of the amplification matrix does not exceed 1. If $Re^{i\varphi}$ is an eigenvalue of $\Delta t\mathcal{H}$, then the von Neumann condition leads to $\varphi = \pm\pi/2$ and $R^2 \leq 1$. In other words, the eigenvalues must be imaginary and their magnitude should not exceed 1. So, the Hamiltonian should, at least, be anti-Hermitian, and therefore the von Neumann criterion becomes also sufficient for the stability because anti-Hermitian operators are also normal.

In the geometric optic case, the Hamiltonian is anti-Hermitian, and the von Neumann condition is fulfilled if

$$\Delta t\, c\, k_{max}^{\varepsilon} \leq 1\ ,$$

where k_{max}^{ε} the maximal norm of all wave vectors in the medium which can be estimated by $\sqrt{\rho(\varepsilon)}k_{max}$ with k_{max} being the maximal wave vector of the initial pulse in vacuum and $\rho(\varepsilon)$

the maximal spectral radius of the symmetric matrix $\varepsilon(\mathbf{x})$ over $\mathbf{x}$ (or simply the maximum of $\varepsilon(\mathbf{x})$ if the medium is isotropic). This can be understood from the following principle [9]. A finite difference scheme with variable coefficients is stable if all the corresponding schemes with frozen (i.e., fixed to a particular value everywhere in space) coefficients are stable.

The von Neumann condition cannot be met for Lorentz models if absorption is present, $\gamma_a \neq 0$. To circumvent this difficulty, the leapfrog scheme is modified in the following way [2]. Let $\mathcal{H} = \mathcal{H}_0 + \mathcal{V}$ where $\mathcal{H}_0 = -\mathcal{H}_0^*$ is such that the von Neumann condition is satisfied for it, while $\mathcal{V}$ is negative semidefinite, that is, for any Ψ, $(\Psi, \mathcal{V}\Psi) \leq 0$. In Lorentz models this is easily achieved by taking, for instance, $\mathcal{H}_0 = \mathcal{H}|_{\gamma_a=0}$. Then $\mathcal{V}$ is diagonal with matrix elements being zeros and $-2\gamma_a$. Another possibility is to identify $\mathcal{H}_0$ with the Hamiltonian in the vacuum, then it is straightforward to show that $\mathcal{V} = \mathcal{H} - \mathcal{H}_0$ is negative semidefinite. In (1.5) we make a substitution $\Psi_t = \exp(t\mathcal{V})\Phi_t$. The new state vector Φ_t satisfies the equation with a time dependent Hamiltonian

$$\partial_t \Phi_t = e^{-t\mathcal{V}} \mathcal{H}_0 e^{t\mathcal{V}} \Phi_t \equiv \mathcal{H}_t \Phi_t \ , \tag{3.5}$$

and with the same initial condition $\Phi_0 = \Psi_0$. Applying the leapfrog method to (3.5) we get $\Phi_{t+\Delta t} = \Phi_{t-\Delta t} + 2\Delta t \mathcal{H}_t \Phi_t$ valid up to $O(\Delta t^3)$. Returning to the initial variables, we arrive at the following recurrence relation

$$\Psi_{t+\Delta t} = \mathcal{L}_{2\Delta t} \Psi_{t-\Delta t} + 2\Delta t \mathcal{L}_{\Delta t} \mathcal{H}_0 \Psi_t \ , \tag{3.6}$$

where $\mathcal{L}_{\Delta t} = \exp(\Delta t \mathcal{V})$. The amplification matrix, $\Psi_{t+\Delta t} = \mathcal{G}_{\Delta t} \Psi_t$, for the recurrence (3.6) satisfies the equation

$$\mathcal{G}_{\Delta t} = \mathcal{L}_{2\Delta t} \mathcal{G}_{\Delta t}^{-1} + 2\Delta t \mathcal{L}_{\Delta t} \mathcal{H}_0 \ . \tag{3.7}$$

According to Theorem 7 of [2] the deviation of the approximate solution $\mathcal{G}_{\Delta t}^n \Psi_0$ from the exact solution relative to the energy norm is of order Δt^2 for any n. Thus, a possible exponential norm growth can be suppressed as much as desired by making the time step small enough. Mathematical details of the proof are omitted here. However, its basic idea can be understood from the following observation. Solving (3.7) by perturbation theory in Δt, it is not hard to find that

$$\mathcal{G}_{\Delta t} - \mathcal{G}_{\Delta t}^V = \Delta t^3 \mathcal{K}_{\Delta t} \ , \quad \mathcal{G}_{\Delta t}^V = \mathcal{L}_{\Delta t/2} \mathcal{G}_{\Delta t}^0 \mathcal{L}_{\Delta t/2} \ , \tag{3.8}$$

where $\mathcal{K}_{\Delta t}$ is regular in the vicinity of $\Delta t = 0$ and vanishes whenever $\mathcal{H}_0$ and $\mathcal{V}$ commute, and $\mathcal{G}_{\Delta t}^0$ is the amplification matrix when $\mathcal{V}$ is set to zero. The von Neumann condition is satisfied for $\mathcal{G}_{\Delta t}^0$ (or, it is always possible to find $\Delta t > 0$ to satisfy it). Hence the powers of $\mathcal{G}_{\Delta t}^0$ applied to Ψ_0 do not produce the exponential norm growth. The powers of $\mathcal{G}_{\Delta t}^V$ differs from those of $\mathcal{G}_{\Delta t}^0$ by factors $e^{\Delta t \mathcal{V}}$ which can only produce the exponential attenuation of the amplitude. Indeed, let $\Psi_t^V = e^{t\mathcal{V}} \Psi_0$. Then $\partial_t (\Psi_t^V, \Psi_t^V) = 2(\Psi_t^V, \mathcal{V}\Psi_t^V) \leq 0$ since $\mathcal{V}$ is negative semidefinite. Thus, the solution produced by the amplification matrix $\mathcal{G}_{\Delta t}^V$ has no exponential growth, while differing, relative to the energy norm, from that produced by $\mathcal{G}_{\Delta t}$ by order of $O(\Delta t^2)$. Since both the solutions differ from the exact one by order of $O(\Delta t^2)$, we conclude that the modified leapfrog scheme can be made as accurate as desired by reducing the time step. Here is an example.

In the field representation of the Hamiltonian for multiresonant Lorentz models, we make the following decomposition

$$\mathcal{H}^F = \begin{pmatrix} \mathcal{H}_0 & \mathcal{V}_{FM} \\ \mathcal{V}_{MF} & 0 \end{pmatrix} + \begin{pmatrix} 0 & 0 \\ 0 & \mathcal{H}_M^F \end{pmatrix} \equiv \mathcal{H}_0^F + \mathcal{V}^F \ . \tag{3.9}$$

As a result we arrive at the following scheme

$$\psi^F_{t+\Delta t} = \psi^F_{t-\Delta t} + 2\Delta t \mathcal{H}_0 \psi^F + 2\Delta t \sum_a \mathcal{V}_{FMa} \xi^a_t \ , \tag{3.10}$$

$$\xi^a_{t+\Delta t} = e^{2\Delta t \mathcal{H}^F_{Ma}} \, \xi^a_{t-\Delta t} + 2\Delta t \, e^{\Delta t \mathcal{H}^F_{Ma}} \, \mathcal{V}_{MFa} \, \psi^F_t \ , \tag{3.11}$$

$$e^{t\mathcal{H}^F_{Ma}} = e^{-\gamma_a t} \left[\cosh \tilde{\nu}_a t + \frac{\sinh \tilde{\nu}_a t}{\tilde{\nu}_a} \left(\mathcal{H}^F_{Ma} + \gamma_a \right) \right] \ , \tag{3.12}$$

where $\tilde{\nu}_a = (\gamma_a^2 - \omega_a^2)^{1/2}$. The exponential (3.12) is easy to compute by expanding $\mathcal{H}^F_{Ma}$ in the Pauli matrix basis, which is also a basis for the Lie algebra $su(2)$, and then by using the well known formula for the exponential of a linear combination of Pauli matrices. For small attenuation, $\gamma_a < \omega_a$, we get $\tilde{\nu}_a = i\nu_a$. The hyperbolic functions in (3.12) become the trigonometric ones and $\tilde{\nu}_a$ is replaced by ν_a. The eigenvalues of the matter Hamiltonian are $\lambda_a = -\gamma_a \pm \tilde{\nu}_a$. Hence, $\mathrm{Re}\,\lambda_a < 0$ and amplitudes of the matter fields are always exponentially attenuated as $t \to \infty$, unless $\gamma_a = 0$ leading to $\mathrm{Re}\,\lambda_a = 0$.

The stability is ensured if $\mathcal{H}_0^F$ satisfies the von Neumann condition. Let k_{max} be the maximal norm of all wave vectors of the initial wave packet and ω_p^{max} be the maximal value of $\omega_p = (\sum_a \omega_{pa}^2)^{1/2}$ as a function of position, then a sufficient criterion for stability reads

$$\Delta t \sqrt{c^2 k_{max}^2 + (\omega_p^{max})^2} \leq 1 \ . \tag{3.13}$$

Here the idea of the frozen coefficients has been used again. The scheme (3.6) becomes especially simple in the case of small attenuation $\gamma_a < \omega_a$. In the complex representation of the auxiliary fields (1.22) (cf. (1.9)) the matter Hamiltonians $\mathcal{H}^F_{Ma}$ are diagonal and the action of its exponential is reduced to multiplication by a complex number $e^{i\nu_a \Delta t}$.

Finally, it should be mentioned that, by rearranging operators in the split, namely, by moving $\mathcal{V}_{FM}$ and $\mathcal{V}_{MF}$ to $\mathcal{V}^F$ in (3.9), the stability condition (3.13) can be weakened to $\Delta t c k_{max} \leq 1$. This would come at the price of having a more complicated expression for $\mathcal{L}_{\Delta t}$. In the case of the Lorentz model it can still be computed analytically. The new split can also be viewed as the use of the induction representation in the modified leapfrog scheme, $\mathcal{H}^I = \mathcal{H}_0^I + \mathcal{V}^I$ where $\mathcal{H}_0^I$ contains only the blocks of $\mathcal{H}^I$ with the derivative operator ∇. The proof of the weaker stability condition can be found in [2].

References

[1] L.D. Landau and E.M. Lifshitz, *Electrodynamics of continuous media, Theoretical Physics, Vol. VIII*, Oxford, Pergamon, New York, 1984.

[2] S.V. Shabanov, *Electromagnetic pulse propagation in passive media by path integral methods*, a technical report and UF preprint, 2003

[3] V.I. Arnold, *Mathematical methods of classical mechanics*, Springer-Verlag, Berlin, 1989.

[4] R.M. Joseph, S.C. Hagness, and A. Taflove, Opt. Lett. 16 (1991) 1412;
L.Gilles, S.C. Hagness, and L. Vázquez, J. Comput. Phys. 161 (2000) 379.

[5] B. Fornberg, *A practical guide to pseudospectral methods*, Cambridge University Press, Cambridge, 1996;
J.P. Boyd, *Chebyshev and Fourier spectral methods*, Springer-Verlag, New York, 1989.

[6] M. Pickering, *An introduction to fast Fourier transform methods for partial differential equations*, Research Study Press, John Wiley & Sons Inc., New York, 1986;
E.O. Brigham, *The fast Fourier transform and applications*, Prentice-Hall, Inc., Eglewood Cliffs, New Jersey, 1988.

[7] A.G. Borisov and S.V. Shabanov, Chem. Phys. Lett. 361 (2002) 15.

[8] E. Fattal, R. Baer and R. Kosloff, Phys. Rev. E 53 (1996) 1217;
D. Lemoine, Chem. Phys. Lett. 320 (2000) 492.

[9] H. Shintani and K. Tomoeda, Hiroshima Math. J., 7 (1977) 309.

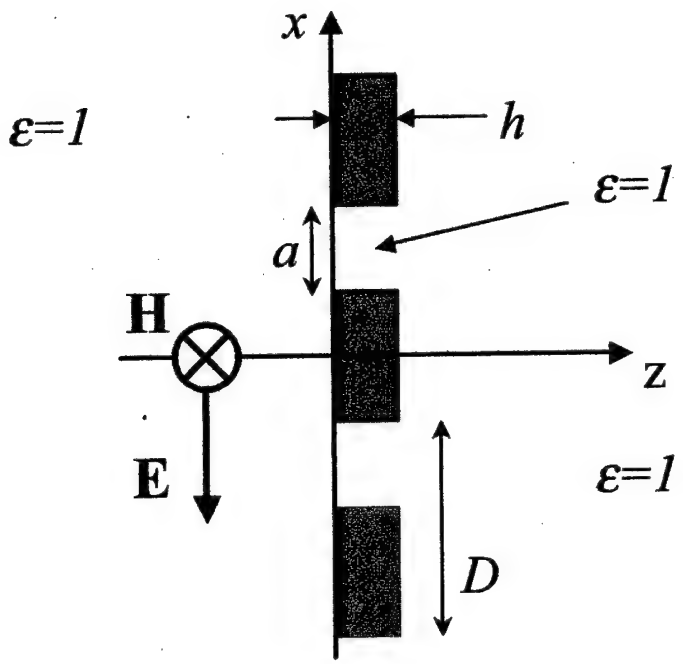

Figure 1

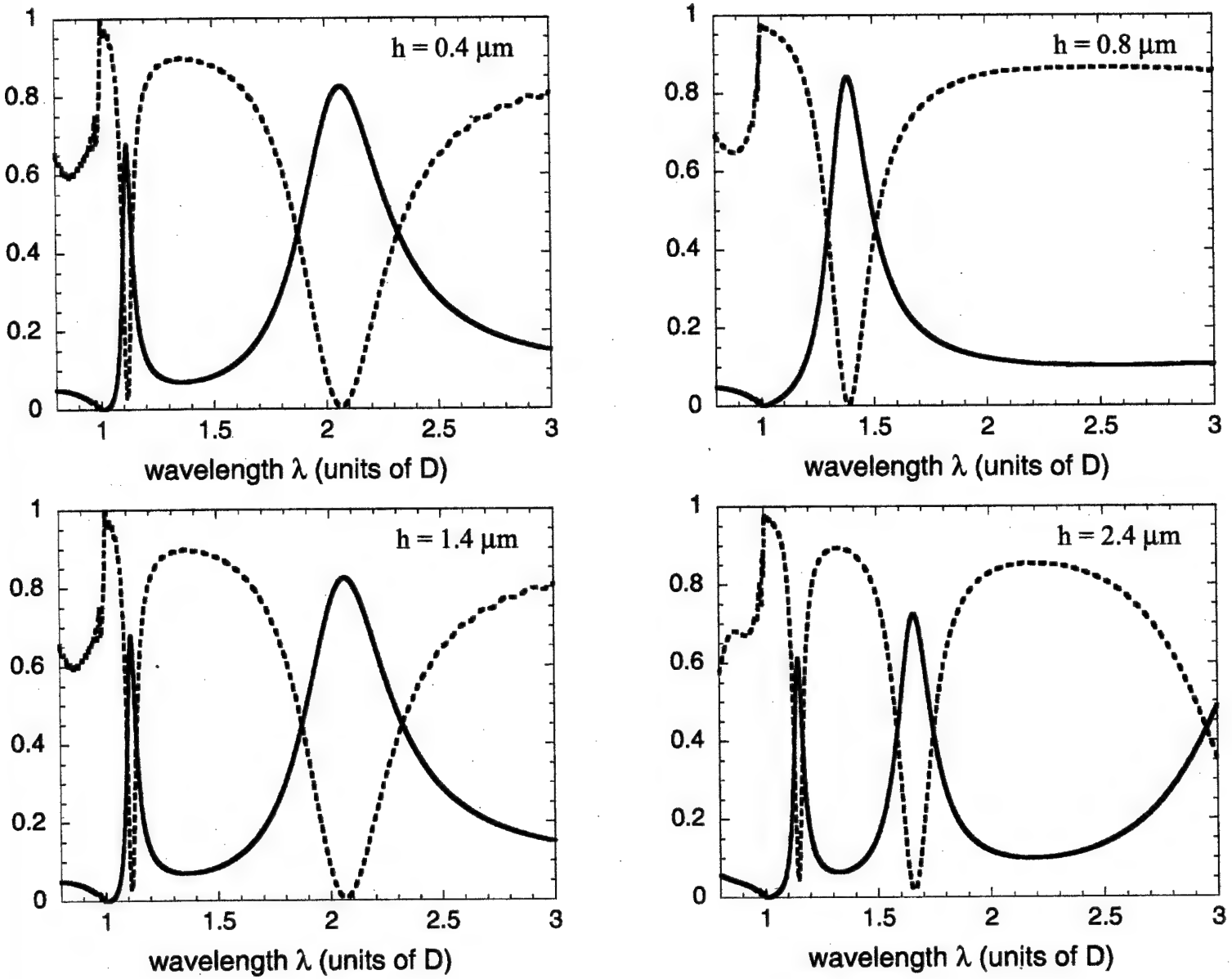
h = 0.4 μm
h = 0.8 μm
h = 1.4 μm
h = 2.4 μm
wavelength λ (units of D)
wavelength λ (units of D)
wavelength λ (units of D)
wavelength λ (units of D)

Figure 2

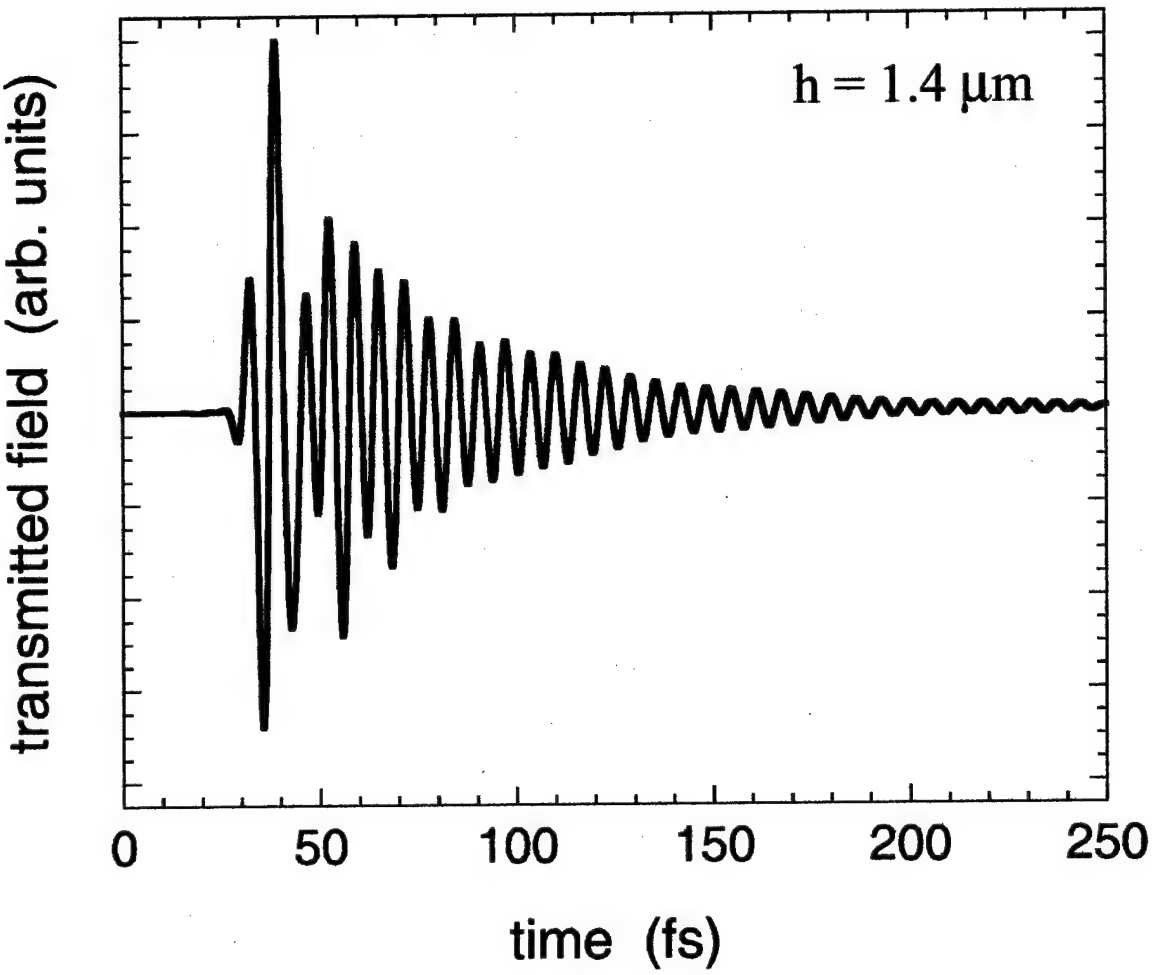
h = 1.4 μm
transmitted field (arb. units)
0
50
100
150
200
250
time (fs)

Figure 3.

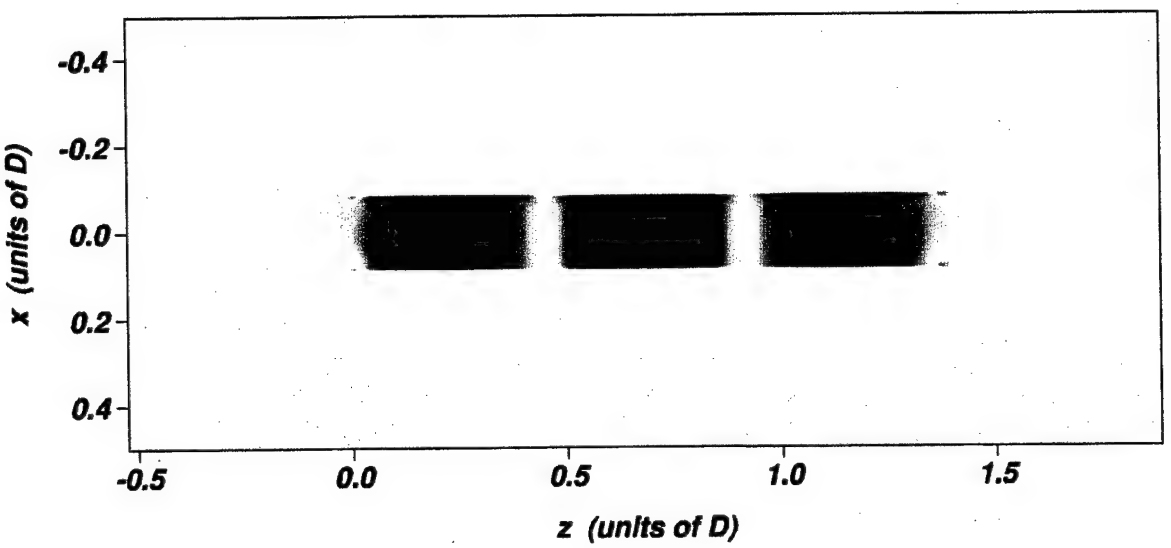

Figure 4.

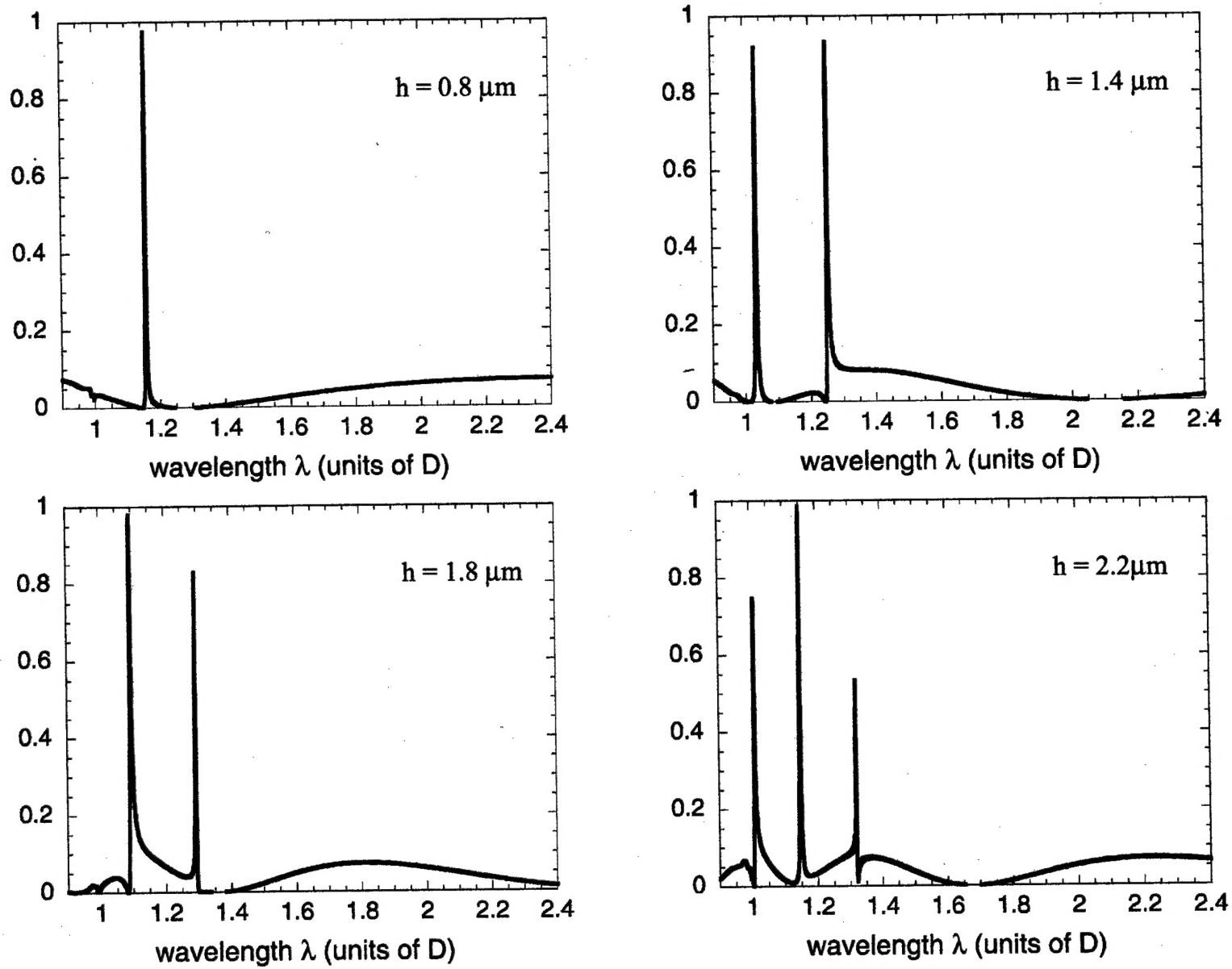
h = 0.8 μm
h = 1.4 μm
h = 1.8 μm
h = 2.2μm
wavelength λ (units of D)
wavelength λ (units of D)
wavelength λ (units of D)
wavelength λ (units of D)

Figure 5.

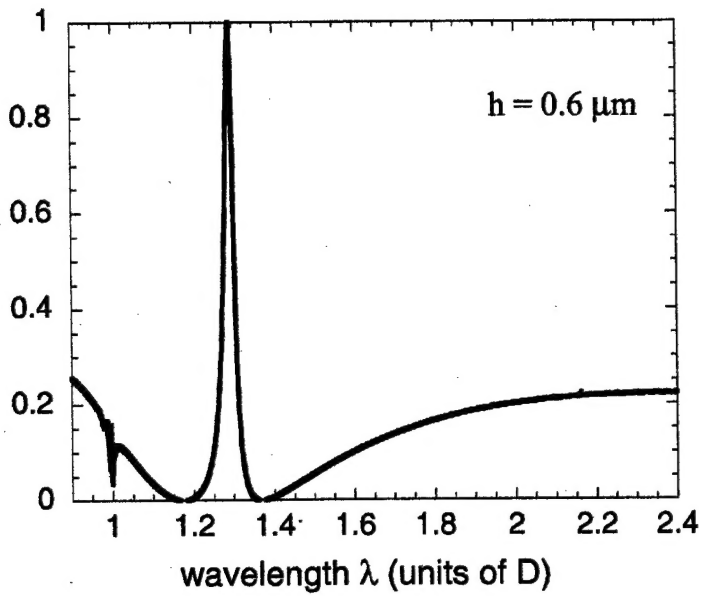
h = 0.6 μm
wavelength λ (units of D)

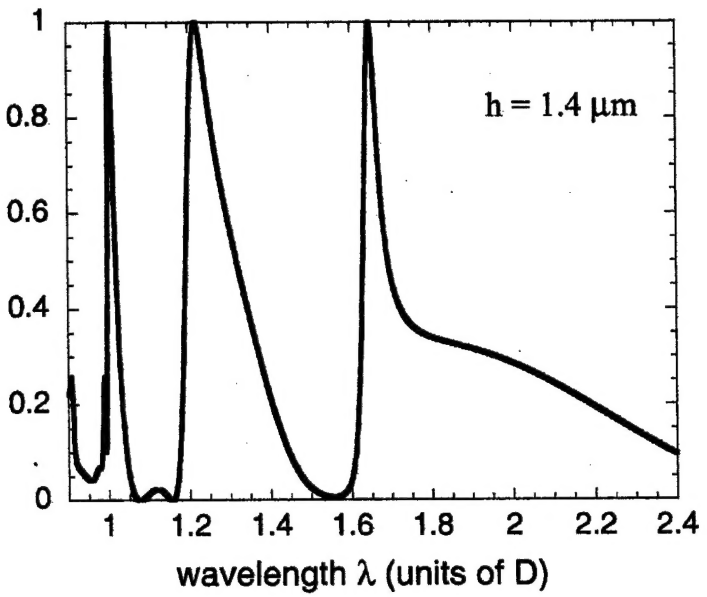
h = 1.4 μm
wavelength λ (units of D)

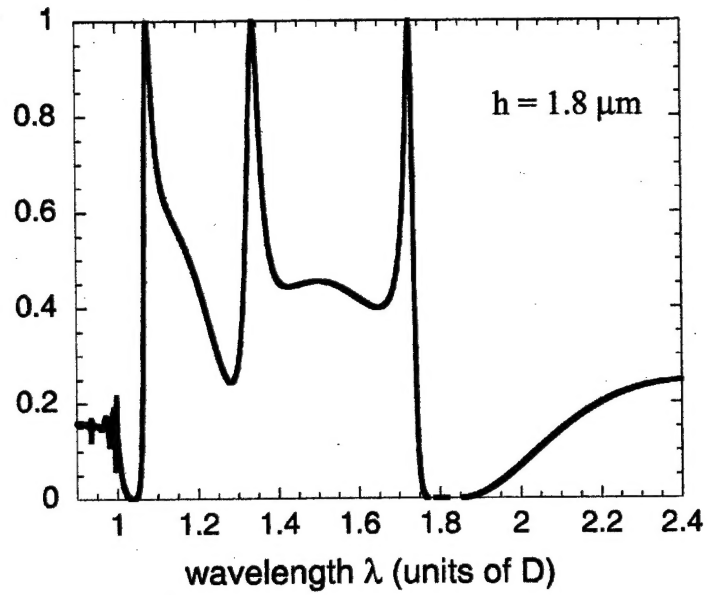
h = 1.8 μm
wavelength λ (units of D)

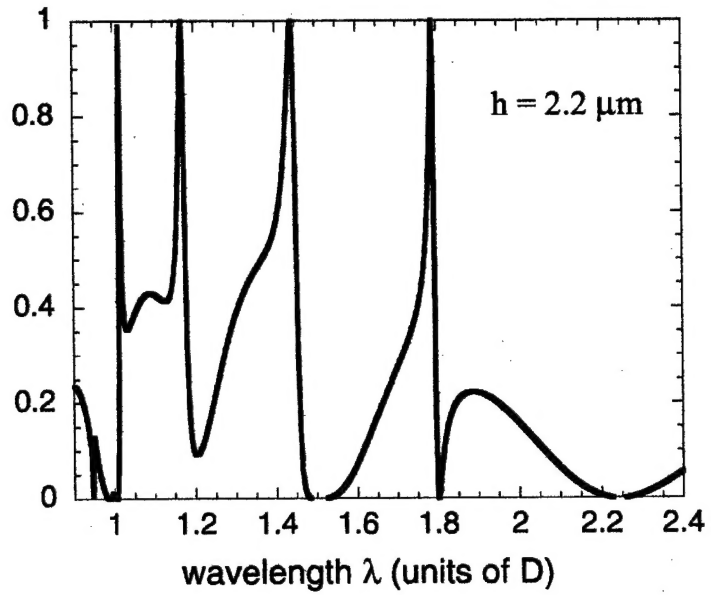
h = 2.2 μm
wavelength λ (units of D)

Figure 6.

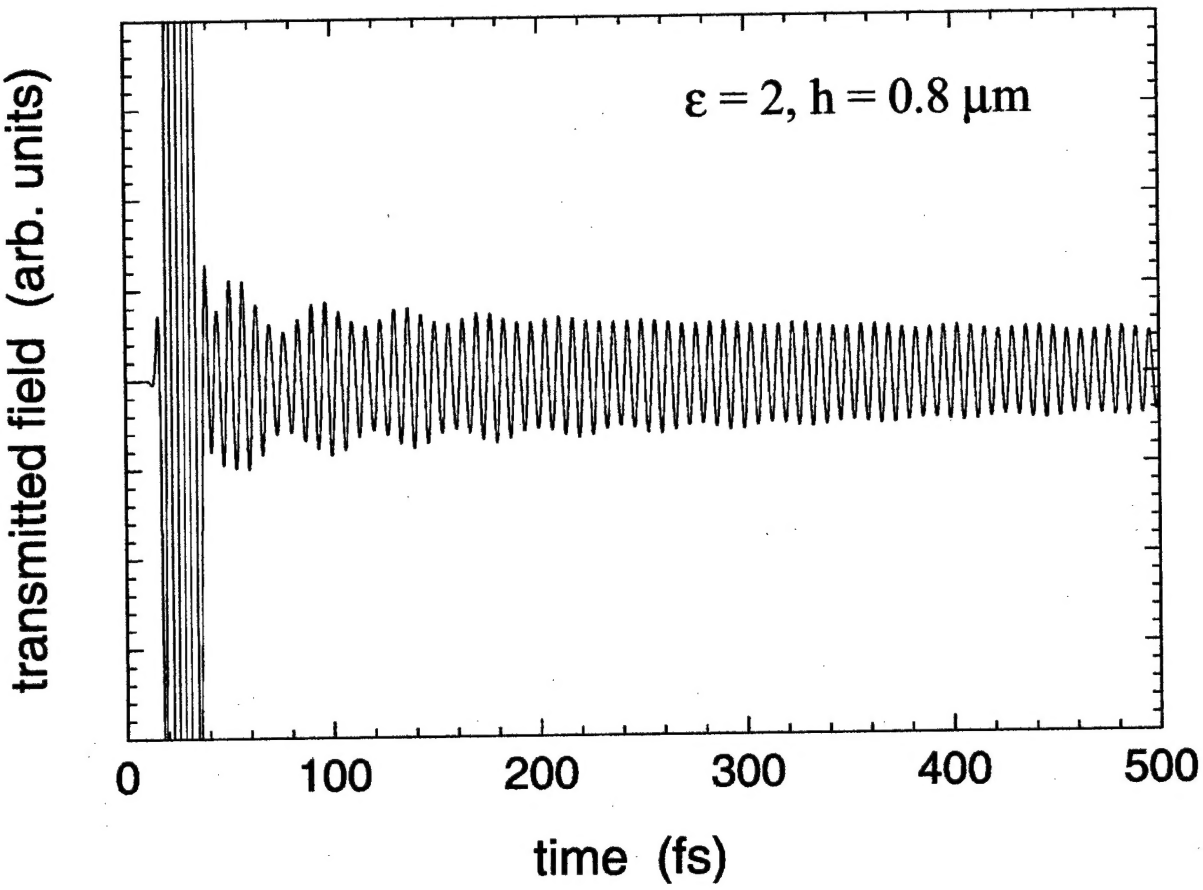
ε = 2, h = 0.8 μm
transmitted field (arb. units)
0
100
200
300
400
500
time (fs)

Figure 7.

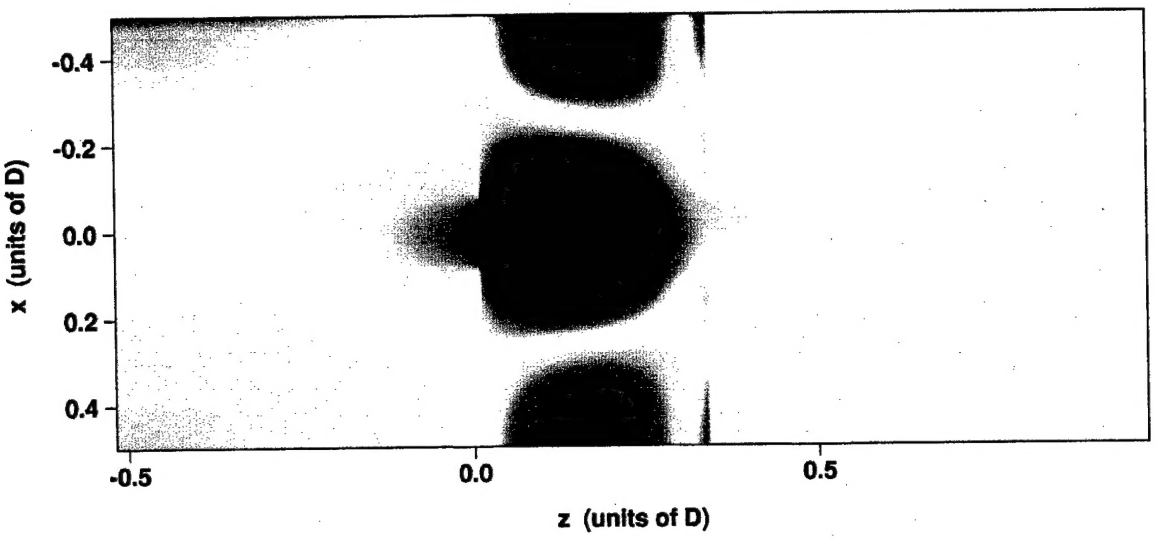

Figure 8.